INFORMATION TO USERS

This reproduction was made from a copy of a document sent to us for microfilming. While the most advanced technology has been used to photograph and reproduce this document, the quality of the reproduction is heavily dependent upon the quality of the material submitted.

The following explanation of techniques is provided to help clarify markings or notations which may appear on this reproduction.

1. The sign or "target" for pages apparently lacking from the document photographed is "Missing Page(s)". If it was possible to obtain the missing page(s) or section, they are spliced into the film along with adjacent pages. This may have necessitated cutting through an image and duplicating adjacent pages to assure complete continuity.

2. When an image on the film is obliterated with a round black mark, it is an indication of either blurred copy because of movement during exposure, duplicate copy, or copyrighted materials that should not have been filmed. For blurred pages, a good image of the page can be found in the adjacent frame. If copyrighted materials were deleted, a target note will appear listing the pages in the adjacent frame.

3. When a map, drawing or chart, etc., is part of the material being photographed, a definite method of "sectioning" the material has been followed. It is customary to begin filming at the upper left hand corner of a large sheet and to continue from left to right in equal sections with small overlaps. If necessary, sectioning is continued again–beginning below the first row and continuing on until complete.

4. For illustrations that cannot be satisfactorily reproduced by xerographic means, photographic prints can be purchased at additional cost and inserted into your xerographic copy. These prints are available upon request from the Dissertations Customer Services Department.

5. Some pages in any document may have indistinct print. In all cases the best available copy has been filmed.

University Microfilms International
300 N. Zeeb Road
Ann Arbor, MI 48106

Hill, John Milton

MULTIPLE OBJECT SPECTROSCOPY: THE MX SPECTROMETER DESIGN

The University of Arizona PH.D. 1984

PLEASE NOTE:

In all cases this material has been filmed in the best possible way from the available copy. Problems encountered with this document have been identified here with a check mark ___✓___.

1. Glossy photographs or pages ___✓___
2. Colored illustrations, paper or print _____
3. Photographs with dark background ___✓___
4. Illustrations are poor copy _____
5. Pages with black marks, not original copy _____
6. Print shows through as there is text on both sides of page _____
7. Indistinct, broken or small print on several pages _____
8. Print exceeds margin requirements _____
9. Tightly bound copy with print lost in spine _____
10. Computer printout pages with indistinct print _____
11. Page(s) _____ lacking when material received, and not available from school or author.
12. Page(s) _____ seem to be missing in numbering only as text follows.
13. Two pages numbered _____. Text follows.
14. Curling and wrinkled pages _____
15. Other _____

MULTIPLE OBJECT SPECTROSCOPY: THE MX SPECTROMETER DESIGN

by

John Milton Hill

A Dissertation Submitted to the Faculty of the

DEPARTMENT OF ASTRONOMY

In Partial Fulfillment of the Requirements
For the Degree of

DOCTOR OF PHILOSOPHY

In the Graduate College

THE UNIVERSITY OF ARIZONA

1 9 8 4

THE UNIVERSITY OF ARIZONA
GRADUATE COLLEGE

As members of the Final Examination Committee, we certify that we have read the dissertation prepared by John Milton Hill

entitled Multiple Object Spectroscopy:
The MX Spectrometer Design

and recommend that it be accepted as fulfilling the dissertation requirement for the Degree of Doctor of Philosophy.

Marcia J. Rieke	4/6/84 Date
John T. McGraw	4/6/84 Date
P. A. Strittmatter	4/6/84 Date
J. N. Pacy	4/6/84 Date
	Date

Final approval and acceptance of this dissertation is contingent upon the candidate's submission of the final copy of the dissertation to the Graduate College.

I hereby certify that I have read this dissertation prepared under my direction and recommend that it be accepted as fulfilling the dissertation requirement.

J. N. Pacy	4/27/84
Dissertation Director	Date

STATEMENT BY THE AUTHOR

This dissertation has been submitted in partial fulfillment of requirements for an advanced degree at the University of Arizona and is deposited in the University Library to be made available to borrowers under the rules of the Library.

Brief quotations from this dissertation are allowable without special permission, provided that accurate acknowledge of source is made. Requests for permission for extended quotation from or reproduction of this manuscript in whole or in part may be granted by the head of the major department or the Dean of the Graduate College when in his judgement the proposed use of the material is in the interests of scholarship. In all other instances, however, permission must be obtained from the author.

Signed: John M. Hill

DEDICATION AND ACKNOWLEDGEMENTS

Dedication

I would like to dedicate this work to Howard Milton Hill, July 1, 1924 to December 12, 1970, a father who shared his love of science and instrumentation with me; and to Daniel John Frederick, February 19, 1957 to April 13, 1977, a friend who stimulated my interest in astronomy and building telescopes.

> For he delivered us from the domain of darkness, and transferred us to the kingdom of His beloved Son, in whom we have redemption, the forgiveness of sins. And He is the image of the invisible God, the first-born of all creation. For in Him all things were created, both in heaven and on earth, visible and invisible, whether thrones or dominions or rulers or authorities -- all things have been created through Him and for Him. And he is before all things, and in Him all things hold together.
>
> Colossians 1:13-17 NASV

Acknowledgements

I would like to thank the gang of three advisors who have guided the development of the Medusa and the MX. Roger Angel has been a never ending source of inspiration and great ideas. Perhaps this dissertation should have been titled "Extraction of Ideas from an Angel with High Efficiency". John Scott has been a great source of scientific and personal motivation. Creative proposal writing while bass fishing is an art every astronomer should master. John pointed out years ago and still believes that the MX will produce "big science". Pete Stockman provided an operational CCD camera and has been a continuous reminder

never to sacrifice the quantum efficiency. My other collaborators and friends, Paul Hintzen, Del Lindley, Mike Wenz, Dave Silva, and Jon Eisenhamer should also be credited for doing much of the work required to successfully measure redshifts of galaxies in clusters. I express my gratitude to the members of my preliminary (R. Angel, D. Dearborn, A. Pacholczyk, R. Williams, and N. Woolf) and doctoral (R. Angel, J. McGraw, M. Rieke, and P. Strittmatter) examination committees for their thoughtful comments and advice.

I would also like to thank the Steward Observatory scientific and technical staff for their efforts toward making many of these ideas reality. Specific thanks to R. Allen, R. Cromwell, J. Fletchall, R. Goff, D. Harvey, G. Hagedon, K. Johnson, A. Koski, R. Leach, C. Lynn, B. McClendon, G. McGlaughlin, R. Miller, M. Miller, S. Mileski, D. Mitchell, C. Poland, D. Sackenheim, V. Schiano, D. Skillman, L. Steen, J. Stocke, W. Stone, S. Tumia, L. Ulrickson, L. Wilson, R. Young, and others. Not to be forgotten are my fellow graduate students the "Not Ready for Dark Time Players", past and present, who have made it all bearable and sometimes even fun. No names will be mentioned to avoid recriminations. You know who you are! And perhaps most important, Shirley Hill and Alice Hill, my mother and sister who have baked countless dozen cookies to keep me going through long hours of research.

The development and use of the Medusa spectrograph has been supported by NASA grants NAGW-121 and NAGW-124. The MX Spectrometer is being constructed under grant AST-8116965 from the National Science Foundation. I would like to acknowledge support from the University of Arizona Summer Research Support Program. I would also like to thank the

Quartz Products Corporation for their assistance in providing information and fiber samples. I would also like to thank J. R. Powell of the Royal Greenwich Observatory for permission to reproduce his fiber measurements.

TABLE OF CONTENTS

TABLE OF CONTENTS -- Continued

TABLE OF CONTENTS -- Continued

TABLE OF CONTENTS -- Continued

LIST OF ILLUSTRATIONS

LIST OF TABLES

ABSTRACT

This dissertation describes the techniques involved in using a fiber optic coupled spectrometer to do multiple object spectroscopy of astronomical objects. The Medusa spectrograph, with optical fibers fixed in a focal plane aperture plate, was used to study clusters of galaxies via velocity distributions. Some relevant problems in the study of the structure and dynamics of clusters of galaxies are outlined as motivation for building a multiple fiber spectrometer. The history of fiber optic spectroscopy in astronomy is presented along with an outlook for the future. The results and experience gained from the Medusa spectrograph are used to design a second generation instrument. The MX Spectrometer uses optical fibers which are positioned remotely under computer control. These fibers are optically matched to the telescope and spectrograph optics to achieve optimum performance. The transmission, flexibility, and image scrambling properties of step-index silica fibers allow efficient reformatting of multiple objects into the spectrometer entrance aperture. By allowing spectra of 32 objects to be obtained simultaneously, the MX Spectrometer will make an order of magnitude increase in the quantity of spectroscopic data that can be recorded with a large telescope. Mechanical, control, and optical elements of the MX design are discussed. Telescope and fiber parameters influencing the design of the fishermen-around-the-pond mobile fiber head are detailed. Results of testing the stepper motor driven fiber positioner probes are described. The algorithm for controlling the

motion of 32 positioners in the telescope focal plane without collisions is outlined. Detector performance and spectrometer efficiency are considered for both the Medusa and MX systems. The use of a Charge Coupled Device (CCD) array detector provides increased quantum efficiency, dynamic range, and stability, as well as allowing digital sky subtraction. Microlenses and their use in correctly coupling optical fibers to the telescope and spectrograph are discussed. In particular, the pupil-imaging technique for microlens matching to fibers is introduced.

CHAPTER 1

INTRODUCTION TO MULTIPLE OBJECT FIBER OPTIC SPECTROSCOPY

Since the early 1900's, astronomers have devoted a substantial fraction of their resources to obtaining spectra of stars and galaxies. The spectra are used to investigate the apparent velocity, chemical composition, and physical state of the objects under study. Astronomers show remarkable perserverance when collecting spectroscopic data. V. M. Slipher (1921) exposed a spectrogram from the end of December to the middle of January to measure the radial velocity of a galaxy. Modern equipment and observing techniques have improved the situation by many orders of magnitude, but the need for spectroscopic information continues. Approximately 70% of the observing time on the large University of Arizona telescopes (MMT, 2.3m) is used for spectroscopic observations. Spectroscopic exposures over 30 hours in length are very rare, but are still used for the study of galaxies at high redshifts. Spinrad, Stauffer, and Butcher (1981) used an integration time of 40 hours to determine the redshift of 3C427.1, a radio galaxy at $z = 1.175$. The ability to collect spectra of many objects in the field of view greatly enhances the scientific productivity of a telescope. This dissertation describes the design and development of a multiple object fiber optic spectrometer. The multiple fiber spectrometer collects many spectra simultaneously, and therefore, allows the astronomer to study more objects by collecting more photons.

Photons for Spectroscopy

Telescopes

There are many ways to collect more photons for astronomical use. The most straightforward is to build a larger telescope to increase the collecting aperture. This is a rather time consuming and expensive way to go. Since the mid-nineteenth century it has taken roughly 15 years and 20 - 100 million 1980 dollars to add two magnitudes to the light gathering capability of the largest telescopes. Improvements in technology have allowed the construction of generations of successively larger telescopes at roughly the same level of real cost. For actual statistics on the costs of large telescopes see Meinel (1979). Despite the cost in money and other resources, each new generation of large telescopes has opened exciting new areas of scientific study.

Another way to increase the quantity of photons or the amount of data collected is to build many small telescopes rather than ever larger single telescopes. This helps to minimize design and structure cost at the possible risk of increased support cost. This approach is unfavorable in the infrared, since the diffraction limited image of a large telescope with a single detector or array of detectors will give better signal-to-noise and/or resolution than an equivalent-area array of smaller telescopes. The UAO/SAO Multiple Mirror Telescope is an example of a new instrument which successfully combined the economics of several smaller telescopes with the performance of a single large telescope. Additional details on telescope design and concepts for larger telescopes may be found in the proceedings of "Optical and

Infrared Telescopes for the 1990's" (ed. Hewitt 1980), and in "Advanced Technology Optical Telescopes I&II" (eds. Burbidge and Barr 1982, Barr and Mack 1983).

A third way to improve the performance of a telescope is to remove it from the Earth's atmosphere. This allows study of objects in electromagnetic windows which were blocked by atmospheric absorption or emission. Working in space also removes the turbulence of the atmosphere to give sharper images. Longair and Warner (1979) in "Scientific Research with the Space Telescope", and Hall (1982) in "The Space Telescope Observatory", provide additional details on the Space Telescope and describe some of the science to be done in space at visible wavelengths. Like building a larger telescope on the ground, putting a telescope in space is very expensive and time consuming. As technological advances make it economically feasible, most new large telescopes will eventually be built in space because of the improved performance which is possible. At the present time, ground-based telescopes are an order of magnitude less expensive than similar instruments in space. Space missions are used for observations which cannot be made through the atmosphere. Because of the new wavelengths available, the impact of satellite observations at the x-ray, ultraviolet, and infrared wavelengths has dramatically changed observational astronomy in the past two decades.

Technology advances can also allow sharper images containing more information, if not more photons, to be obtained on the ground. Angel (1982a) describes some of the improvements to be made with large ground-based telescopes. Improvements in optical design, materials, and

fabrication will allow telescope optics to give sharper images over wider fields of view. Atmospheric seeing is the limiting factor in the quality of ground-based images. Since it consist of components caused high in the atmosphere and components caused by the local telescope environment, the seeing can be improved by proper site selection and telescope design. Angel and Hill (1982), Angel and Woolf (1983), Hill and Angel (1983), and Angel and Hill (1983) discuss the use of honeycomb mirror blanks to improve local seeing and reduce the cost and mass of a large telescope. Lightweight primary mirrors reduce the weight, and therefore, the cost of the entire telescope. Honeycomb blanks also reduce the thermal equilibration time of the optics for better images and less telescope-induced seeing. Telescopes with lightweight, monolithic, 8m, honeycomb mirrors and arrays of these mirrors should be available by the end of the decade. Astronomical seeing is discussed in detail by Woolf (1982). Even with active optical control and other improvements, the size of the seeing-limited image is unlikely to decrease below 0.1 arcsecond. Interferometric techniques such as speckle interferometry (Beckers, Hege, and Murphy, 1983; and Labeyrie, 1970), and the work of Labeyrie (1978) and his colleagues on two-telescope interferometry show the possibility of increasing the resolution beyond the atmospheric limit for some classes of observations.

Detectors

During the last century, the largest performance gain in optical astronomy has not come from larger or higher quality telescopes, but

from improvements in the detectors used at these telescopes. Astronomy has seen the transition from the human eye to the photographic plate to today's electronic detectors. Silicon-based detectors, ie. CCDs, with their high quantum efficiency (up to 80%), have vastly increased the output of large telescopes like the Hale 200-inch (5m), built during the first half of this century when the photographic plate, with 1-3% quantum efficiency, was the dominant detector. While large gains in quantum efficiency have nearly ended, there is still much work to be done with regard to the size and quality of today's detectors. The photographic plate remains useful for wide-field imaging because of its ability to collect and store large quantities of data. A 14 by 14 inch photographic plate can record image information in $4x10^8$ pixels compared to only $6x10^5$ pixels for single CCD devices with much higher quantum efficiency. Angel (1983) has suggested the use of arrays of hundreds of CCD chips to compete with photographic plates for wide-field imaging.

Multiplex Advantage

By collecting of all available information in the field of view of a telescope, the astronomer may claim that he is practicing conservation of photons. It is certainly easier and less expensive to make use of more of the photons in the focal plane than to build a whole new telescope to deliver more photons from one on-axis object. The goal of the work described here was to take advantage of what might be called spatial multiplexing to greatly enhance the amount of scientific data produced in a given period of time. It has become possible to exploit this spatial multiplex advantage with the advent of modern wide-field

optical designs such as the Ritchey-Chrètien telescope (Ritchey, 1928) and the Paul-Baker two-mirror corrector (Angel, Woolf, and Epps, 1982). Classical Newtonian and Cassegrain designs have much narrower fields. The possibility of wide-field multiple object spectroscopy has led to the development of optical designs for 8m telescopes which have very high quality images over one-degree fields-of-view (Angel, 1983; Arganbright, 1984).

The following chapters of this dissertation will be devoted to the spectroscopic rather than imaging aspects of the spatial multiplex advantage. Specifically applicable are those programs which require statistical data on large numbers of similar objects or those programs which must observe many objects simultaneously in order to obtain sufficient telescope time to study extremely faint sources. In no way should it be construed that multiple object spectroscopy is the only technique which makes use of the multiplex advantage. Other powerful tools of current research include automatic plate measuring machines (Kibblewhite, 1983). Current research on measuring machines such as COSMOS and APM is described in the Proceedings of the Workshop on Astronomical Measuring Machines 1982 (eds. Stobie and McInnes, 1982). These machines combine the data collecting capability of the photographic plate with the data processing capability of modern computers to obtain the maximum amount of useful information from each image. In addition to photometric surveys, such a plate measuring machine may be used to identify objects for spectroscopic study, or to obtain rough redshifts from objective prism plates. Other instruments, such as the Steward Observatory CCD Transit Instrument (CTI) built by

McGraw, et al. (1982), combine array detectors and computer technology to obtain real time (sidereal) observations of large areas of the sky. With both image and time variability data, this survey telescope will be very useful for identifying objects for further spectroscopic and photometric study. Another device which complements the spatial multiplex spectrometer is the SPIV (simultaneous photometry infrared visual) multichannel photometer developed by Eisenhardt (1982,1984). By obtaining simultaneous colors in four broad bands, this instrument uses wavelength multiplexing to study sources which are too faint to be studied in detail with conventional spectroscopic or photometric techniques.

Overview of Multiple Fiber Spectroscopy

Due to the pressure for observing time on large optical telescopes, my colleagues and I have developed an instrument to obtain simultaneous spectra of up to 32 objects. By simultaneously obtaining spectra of many objects in the field-of-view, rather than one at a time, we have greatly increased the data-taking capacity of the Steward Observatory 2.3m and other telescopes. By using short lengths of optical fiber to bring the light from galaxies throughout the field of the telescope into a row of images at the spectrograph slit, the wide-field imaging potential of the Ritchey-Chrétien telescope is realized for spectroscopy. The fibers cause objects spread at random over the telescope field to appear to be neatly arranged in a row at the spectrograph slit.

Major factors in the development of fiber spectroscopy have been the production of extremely transparent, inexpensive, optical fibers for the communications industry, and the development of high-efficiency array detectors such as Charge Coupled Devices (CCDs). Quartz optical fibers 200 microns in diameter can be used in 10m lengths without significant transmission losses at wavelengths longer than 380 nm. The spectrograph must have a two-dimensional array detector to record the individual spectra derived from the fiber outputs. The spectrograph can be mounted on the telescope, or on the observing floor, or in a controlled environment instrument room, depending on the length of the fibers used.

Multiple object fiber optic spectroscopy is most valuable in studies of faint, clustered objects where long observations are required. I am particularly interested in clusters of galaxies where large statistical samples are required. Many radial velocities or redshifts (>100) must be measured to determine accurately the dynamical properties of a cluster of galaxies. Careful mapping of the velocity dispersion profiles of clusters is needed if we are to learn anything about the distribution of the "missing mass". Clusters of galaxies are rarely smooth, spherical distributions of galaxies. Study of the structure in clusters on all scales may provide insight into the formation of galaxies and clusters. Other applications where multiple object capability is valuable include "deep surveys" to probe the structure and evolution of objects at the limit of observability, and spectroscopic identification of sources detected at other wavelengths such as radio, x-ray, or gamma ray. Because 30 or more objects can be

observed simultaneously, longer exposures can be obtained on each set of objects to allow the study of sources fainter than those normally detectable. Spectroscopic surveys of faint quasi-stellar objects allow us to probe the limits of the observable universe. Chapter 2, which might be subtitled "Why do we need all those spectra anyway?", will provide more detail on the many problems in astronomy requiring large numbers of spectra. Chapter 3 will discuss some of the scientific results of our observations of clusters of galaxies with the Medusa spectrograph.

Chapter 4 will provide a brief history of the development of fibers for astronomical instrumentation, and a summary of instruments currently in use. Chapter 4 will also describe the operation of our prototype, multiple fiber, aperture plate instrument dubbed the Medusa spectrograph. The Medusa is now producing spectra of about 100 galaxies per clear night down to apparent magnitude V=17.5.

The following four chapters (5,6,7,8) describe in detail the design and construction of the MX Spectrometer. The MX is a mobile fiber multiple object spectrograph designed to eliminate the drawbacks of the Medusa aperture plate system. 32 stepper motor driven probes are used to position the fibers at the locations of galaxies. Significant improvements which are being made with the MX include: better optical matching to the spectrograph; the use of computer-positioned fibers in the focal plane to replace the aperture plates used in the Medusa; and the use of a bare Charge Coupled Device as the spectrograph detector. The CCD allows sky subtraction, gives increased dynamic range, and provides more accurate wavelength calibration compared to a photographic

plate behind an image tube. The combination of simultaneous multiple object spectroscopy and improved two-dimensional detectors has increased, by a factor of 100 over what was possible a few years ago, the rate at which velocities of faint galaxies can be measured.

Chapter 5 describes the design and construction of the mobile fiber probes which position the fibers in the focal plane. The fiber probes are arranged in the "fishermen-around-the-pond" configuration for maximum focal plane access. Procedures for alignment of the probes on target objects are also discussed in chapter 5. The philosophy and the components of the computer control system for the fiber probes is discussed in chapter 6. An intersecting line algorithm is used to avoid collisions between fiber probes. Chapter 7 discusses the performance of the intensified CCD detector used with Medusa, as well as the optical efficiency of the overall spectrometer system. Chapter 7 also outlines the two-dimensional data reduction procedures used with multiple fiber data. Chapter 8 discusses the matching of fibers to optical systems with particular emphasis on the use of microlenses. "Multiple object" and "multiple fiber" will be replaced in the rest of this dissertation by "multiobject" and "multifiber". This transition has occurred to many words now in common usage, ie. basket ball, basket-ball, basketball.

CHAPTER 2

STATISTICAL AND DYNAMICAL PROBLEMS IN ASTRONOMY

The astronomical objects which offer the most potential for study via multiobject spectroscopy are those which cluster naturally on the sky. Clusters of galaxies and stars are well-suited to simultaneous spectroscopy and photometry, because from several objects up to thousands of related objects often appear within the same telescopic field. The photographic plate has allowed simultaneous photometry to be done for most of this century. Large scale spectroscopic surveys provide detailed statistical information on populations of sparsely distributed objects.

Clusters of Galaxies

Many problems in astronomy require large statistical samples for effective study. The study of clusters of galaxies has been the principal motivation behind this work on multiple object spectroscopy. Until recently the dynamics of galaxies in clusters (other than Virgo and Coma) and superclusters were studied only as bulk properties of the cluster. This approach was forced by the lack of available velocity data. Large amounts of telescope time are required to measure redshifts of faint galaxies one at a time. Noonan (1981) lists only seven clusters with more than 50 measured redshifts (see also Sarazin, Rood, and Struble, 1982). Much effort has been devoted to collecting redshifts in recent years. Chincarini (1983) estimates that redshifts

of 12,000 - 14,000 galaxies may now be known. Many of these are from the CFA Redshift Survey (Huchra, et al., 1983; and Davis, et al., 1982) of bright nearby galaxies which are not generally cluster members. Even in the well-studied clusters, with several hundred redshifts, the small-number statistics of galaxies in spatial and velocity coordinates make quantitative study of the cluster dynamics very difficult. Nature is able to work with only a few galaxies interacting in the cluster potential. The astronomer is forced to work with projected velocities and positions; therefore, he requires many more sample points to deduce accurately the existing gravitational potential. In addition to this "resolution" problem caused by small number statistics of observable galaxies, there are contamination effects from dynamically unrelated foreground and background galaxies.

Clusters of galaxies present two major problems relating to their dynamics. These problems involve the so-called "missing mass" and the recently observed "structure" within clusters. The solution or resolution of these two problems is of major importance in our understanding of the universe beyond our own Galaxy. Galaxy clusters represent the largest objects in the universe which can reasonably be assumed to be near gravitational equilibrium. Astronomers can use their observed properties to study the laws of physics on the largest of scales. Reviews of the observations, theories, and problems in clusters have been given by Bahcall (1977), Faber and Gallagher (1979), Van den Bergh (1977), and Oort (1983). Forman and Jones (1982), and Jones and Forman (1984) review the X-ray observations of clusters. Gregory and Thompson (1982) give a more popular review of supercluster structure.

Dynamics

This section provides an overview of the observational problems encountered in studying the dynamics of clusters of galaxies. The missing mass, velocity dispersion profiles, and the formation of cD galaxies, are currently receiving much observational and theoretical attention.

Missing Mass. The ratio of inferred mass to light emitted from astronomical objects is observed to increase as one expands the region of measurement from the local solar neighborhood out to objects as large as clusters of galaxies. The increase in mass-to-light ratio is frequently attributed to some non-luminous form of matter distributed on large scales. It is presumed that the radial dependence of the gravitational potential may be determined from a study of the distribution of galaxy velocity dispersion in clusters. The radial dependence of the potential is then modelled to find the distribution of the unseen or "missing" mass. This assumes, of course, that clusters actually contain some form of non-luminous matter to account for the observed increase in mass-to-light ratios (M/L). Smith, et al. (1980) point out the potential difficulty of determining the distribution of the missing mass with this technique. The missing mass could account for up to 90% of the total mass in the universe. Accurate measurements of the mass distribution in clusters of galaxies should constrain models which account for the unseen matter and its distribution.

Velocity Dispersion Profiles. Fuchs and Materne (1982) and Materne and Fuchs (1982) discuss the dynamics of two well-studied clusters, Coma and Hydra I. More velocity data would be useful in

determining the correlation, or lack thereof, of the velocity dispersion with the spatial density of the galaxies in these clusters. A lack of correlation of velocity dispersion with the galaxy distribution would imply that cluster dynamics are dominated by a mass component other than galaxies. 200 or more redshifts per cluster will be needed for detailed dynamical study. Compare this to the 20 redshifts now used to measure the velocity dispersion of a cluster. This critical need for data is discussed by Capelato, et al. (1982). They consider the inversion of the line-of-sight radial velocity data to obtain the spatial velocity dispersion profile. The observed velocity dispersion profile can be affected by a non-symmetric dispersion tensor as well as stream velocity fields in the outer regions of the cluster which have not yet virialized. The previously mentioned studies deal primarily with the inner regions of rich clusters which are assumed to be "virialized and in hydrostatic equilibrium". Rivolo and Yahil (1983) present a model for nonlinear evolution of clusters and their surroundings as the collapse of a density perturbation. Their model predicts a virialized cluster core surrounded by a larger region of infalling galaxies which has not yet reached equilibrium. The boundary between these two regions should occur at a secondary maximum in the local galaxy density and should exhibit a significant drop in the local velocity dispersion. Such a model appears consistent with present observations where the secondary maximum has been seen, but, as Rivolo and Yahil point out, much more detailed velocity studies in the outer regions of rich clusters are needed to assess properly the true situation. When clusters at redshifts greater than 0.5 are observed in detail, velocity

data will be important in the study of cluster evolution. Silk and Wilson (1979a,b) discuss density and velocity distributions around clusters as a possible probe of primordial density perturbations. Density distributions of many clusters will be necessary to sort out the problem.

cD Galaxies with their characteristic halos are often seen at the center of clusters of galaxies. Study of these giant galaxies may shed some light on the evolution of galaxies in clusters. Suggested methods of forming cDs include: cannibalism or mergers of galaxies caused by dynamical friction in the clusters, accumulation of debris resulting from tidal stripping of galaxies with orbits passing near the center of the cluster, and star formation in a cooling accretion flow in the cluster or galaxy potential. Merritt (1984) has calculated dynamical friction timescales for the mergers of galaxies to form cD galaxies in the cores of rich clusters. He concludes that cD galaxies or subclusters from which they evolve must have formed prior to cluster collapse and relaxation. Merritt argues that tidal stripping of galaxy halos during cluster collapse prevents more than a small percentage of the total cluster mass being attached to galaxies. Predictions of the dependence of cluster velocity dispersion versus radius and versus galaxy luminosity made by this type of model can be tested, or at least constrained, if sufficient galaxy velocities can be measured. This may involve measuring the velocities of numerous intergalactic globular clusters and dwarf galaxies for nearby clusters such as Coma, because the sample of bright galaxies near the center is too small to give an accurate velocity dispersion. Loss of orbital energy by dynamical

friction may also account for the multiple nuclei frequently observed in cD galaxies. Beers and Geller (1983) find that D and cD galaxies are preferentially located in regions of local density maxima, regardless of the location of the center of the cluster. Again, many velocities are needed to study the dynamics of the environments of these giant galaxies. After carrying out Monte Carlo simulations of cluster evolution, Malumuth and Richstone (1984) find that roughly 25% of all clusters form cD galaxies. Their models indicate that the core of the cD is formed by mergers independent of cluster richness, while the extended halo is made of debris from tidal stripping. The strong dependence of stripping on cluster richness leads to the prediction that rich clusters without central cDs should still have a component of intracluster light previously associated with the cD halo. Dressler (1984) provides an excellent review of current observational problems related to cDs and their formation.

Structure

In addition to dynamical studies, complementary studies of the spatial structure of clusters of galaxies are needed. Structure in galaxy clusters is observed on size scales from small groups of galaxies to superclusters. The more closely clusters are examined, the more complicated they appear. There are few, if any, examples of clusters which are relaxed to a state of virial equilibrium or have potentials that can be modelled by smooth spherical distributions of matter. Consider, for example, the secondary maxima in the galaxian density distribution around rich clusters reported by Oemler (1974) and others.

Binary Clusters. One of the most interesting recent results on structure in clusters of galaxies is the discovery of the binary x-ray clusters by Forman, et al. (1981) and Henry, et al. (1981). Preliminary studies by Beers, Huchra, and Geller (1983) indicate that the optically observed galaxies form a binary structure similar to the x-ray gas and that this structure appears to be dynamical in origin. Beers, Geller, and Huchra (1982) find evidence that the two clumps in Abell 98 are bound. Computer models of evolving clusters by White (1976) seem to show structures that are similar in appearance. Additional study in the x-ray and optical will be necessary to see how these binary clusters are formed. Particularly large numbers of redshifts will be needed to study the galaxy motions in such clusters. Beers, Huchra, and Geller (1983) conclude their paper by pointing out the need for more redshifts. I reproduce that paragraph here as independent justification of the need for a high-throughput redshift device like the MX spectrometer.

> One lesson of this study is that a larger number of individual redshift measurements is required to obtain even preliminary estimates of dynamical parameters for a cluster at high redshift than for clusters at low redshift. At a redshift as large as 0.2, foreground contamination, not at all serious at low redshifts, is a considerable problem. At least one-third of our galaxies with measured redshifts are not in the cluster! At redshifts as high as 0.5, this problem will be even worse, and improper treatment will lead to incorrect results in studies of cluster morphology and galaxy color distributions (Mathieu and Spinrad 1981).
>
> Geller and Beers (1982) pointed out that clusters of galaxies are probably not, in general, well characterized by a single scale parameter and velocity dispersion. A115 serves as a case in point, whereby a blind adoption of a cluster scale and dispersion including all galaxies within $\pm$ 3 sigma_{los} of the cluster mean would lead to a considerable overestimation of the cluster dynamical parameters.

Dressler and Gunn (1983) have demonstrated the importance of spectroscopic follow-up to photometric studies of distant clusters of galaxies by showing that the excess of blue galaxies in the cluster around 3C295 found by Butcher and Oemler (1978) was due to a foreground cluster and not an evolutionary effect. The same spectroscopic data revealed in the cluster a very large fraction of galaxies with active nuclei, which could be another evolutionary effect. Butcher and Oemler (1984) claim that the results of Dressler and Gunn are consistent with their previously observed excess of blue galaxies in the 3C295 cluster. They also report on the results of photometry of 33 clusters with redshifts up to $z=0.54$, and find that the evidence for recent strong evolution of spirals in most compact clusters remains. Clearly, more galaxy spectra are needed to resolve this controversial issue. Redshifts can eliminate the largest source of error in these photometric studies, which is contamination by foreground and background objects. Verification of cluster membership by velocity measurement is of great importance when determining the luminosity functions of these distant clusters.

Subclustering. Clumps have also been reported on smaller scales inside rich clusters of galaxies by Dressler (1980a,b). Dressler finds that galaxy morphology depends on local galaxy density rather than the density of the cluster as a whole. Postman and Geller (1984) have extended Dressler's work to groups of galaxies so the morphology - density relation extends over six orders of magnitude in galaxy space density. This may mean that clumps of galaxies have retained their identity since the epoch of cluster formation. Redshifts of the members

of the clumps are needed to determine if these clumps are gravitationally bound independently of the the overall cluster or are only statistical fluctuations. Lindley (1983) discusses the statistics of observations of clumps in clusters. Hintzen, et al. (1982) reported some velocities of galaxies in clumps in the cluster Abell 576, but have not yet obtained statistically significant results. Bothun, et al. (1983) have recently shown via redshifts and galaxy counts that the Cancer cluster is not a well-behaved sphere, but is composed of several fairly distinct subclumps of galaxies. Perhaps a regular cluster of galaxies does not exist, and the impression of smoothness is only caused by our lack of resolution. (After all, "A cow to first-order is a sphere." to quote a distinguished astronomer, formerly at Kitt Peak, in a 1982 colloquium). Struble and Rood (1981) point out a class of clusters with an apparent excess of binary galaxies. In all these examples, neither surface density counts, nor velocities, nor x-ray maps are alone sufficient to untangle the actual structure of the cluster. Both velocities and projected positions are needed to untangle the projection effects if any hope is given to understanding the three-dimensional structure of clusters on both large and small scales.

Superclusters

Distributions of galaxies also show structure on scales much larger than individual clusters. Many people in recent years have found significant structure on supercluster scales. Clustering of galaxies on scales of 10 Mpc or less is firmly established, but may extend to scales of order 100 Mpc before the universe becomes homogeneous. Batuski and

Burns (1984), and N. Bahcall (1984) have used Abell clusters as tracers to map supercluster structure. The observation of bridges of galaxies between superclusters and large voids may mean that all of the matter in the universe occurs in a cellular or spongelike structure. As much as 90% of the matter (galaxies) may occupy only 10% of the volume of the universe. Multiobject spectroscopy has great potential in studying supercluster dynamics and structure. The five rich superclusters with substantial dynamical data available include Coma/A1367, Hercules/A2197, Perseus, 1451+22, and 1615+43. The term "substantial data" is here used loosely to mean more data than elsewhere in the sky. Current studies are mostly based on redshifts of only a few galaxies in each of the individual clusters in the supercluster. Almost no data exist on the supercluster galaxies which lie outside the rich clusters. Each of these five superclusters appears to be a filamentary or pancake structure lying in or near the plane of the sky. Additional velocity studies of these and other superclusters are needed to distinguish whether the flattened shapes are real, with the velocity dispersion caused by the unperturbed Hubble flow, or whether the gravitational interaction of the clusters has perturbed the Hubble flow near the superclusters. Additional discussion of superclusters and references may be found in Ciardullo, et al. (1983). Multiple object studies will greatly increase the quantity of data that can be obtained in studies of objects like these which stretch over several degrees on the sky. The problem encountered in supercluster studies is that limited telescope time for single object observations usually requires rather sparsely distributed sample points in the supercluster region. Tifft and a host

of collaborators have measured hundreds of redshifts in order to define several superclusters (see Tarenghi, et al., 1979; Tifft and Gregory, 1976; and Thompson and Gregory, 1983). With so few velocities, it is difficult to measure the supercluster velocity dispersion of a few hundred km s^{-1}, which is superimposed on the much larger dispersion of individual rich clusters.

Kirshner, Oemler, Schecter, and Shectman (1981,1983) have discovered the infamous "hole in space" which might be considered an anti-supercluster occupying a volume of 10^6 Mpc^3. Many redshifts and galaxy counts are needed to produce meaningful quantitative results in this type of study, since the sample needs to have a scale greater than the size of the observed structures. Miller (1983) and others have carried out n-body simulations of clustering of galaxies which reproduce the clumps and filamentary structures which are observed on supercluster scales. Miller finds the "holes or voids" between groupings of galaxies to be the dominant structures in the universe and to be extremely empty due to the departure of galaxies in the clumps. The other possibility is that the holes are areas of marginally lower overall density which did not form galaxies or clusters. The statistical problems in the study of large "nothings" are clearly greater than in the study of clusters, but a spectroscopic survey of some voids could test the results of Miller's models. Shanks, et al. (1983) describe the results of the AAT Redshift Survey. They use the redshifts and positions of 340 galaxies in five fields to estimate the spatial two-point correlation function. The redshift information is needed to eliminate confusion which occurs in projected catalogs when

the correlation function is studied on large scales . In addition to clustering information, this type of survey also provides valuable data on the galaxy luminosity function. Ellis (1983) discusses plans to extend the survey over larger spatial scales with the AAT multiple object spectrograph (FOCAP) described in chapter 4.

Clusters of Stars

As you may have noticed by now, the MX was motivated by the local interest in clusters of galaxies. There are, however, some very interesting stellar observations that can be made with this type of device. It should be noted that the multifiber technique is not limited to the low dispersion spectroscopy typically used on clusters of galaxies. The multifiber coupled spectrograph is very well suited to high resolution, high signal-to-noise, stellar spectroscopy. I briefly mention in the following paragraphs some interesting work from the recent literature that would benefit from multiobject fiber spectroscopy.

As with galaxies, stars are often studied in clusters - a domain well suited for multiobject spectroscopy. With the Medusa we have obtained (but not yet reduced) some spectra of pre-main sequence, low mass stars in the open cluster NGC 2264. These stars were predicted to be hydrogen alpha emission stars by Adams (1981) based on his multicolor photographic photometry of that cluster. An initial look at our observations demonstrates that obtaining spectra of 20th magnitude stars in the middle of an HII region is not a trivial problem and truly will test our sky subtraction abilities.

Globular clusters of stars present several interesting possibilities for studies using multiple object spectroscopy. Gustafsson (1983) describes the ongoing controversy over abundances in metal-rich globular clusters. Pilachowski, et al. (1983) point out that cluster metallicities are best studied with high resolution spectra of individual cluster members. Their data argue against the existence of a metallicity gradient in the Galaxy. A data base of uniformly high quality spectra in a number of clusters should lead to an increase in our understanding of the problem if not to its resolution. Studies of dynamics in globular clusters also push spectroscopy to its limits because of the need for many radial velocities of relatively faint stars in systems with small (compared to clusters of galaxies) velocity dispersions. Gunn and Griffin (1979) obtained photoelectric velocity measurements accurate to about 1 km s^{-1} for 111 stars in the cluster M3. They then fit models to the observed light and velocity distributions and found no evidence for a population of heavy stellar remnants. This type of study requires many and usually multiple velocity measurements to eliminate binaries which contaminate the sample. Gunn and Griffin find fewer spectroscopic binaries in M3 than expected based on Population I field stars. Harris and McClure (1983) provide additional discussion on the multiplicity of field K-giants. Stauffer, et al. (1983) have discussed the rotation properties of K-stars in the Pleiades. This sort of spectroscopic study is often limited by slit effects and can benefit from the image scrambling as well as the multiplex advantage offered by fiber spectroscopy. The proceedings of several conferences over the past few years provide a good overview of

the problems associated with globulars. These include IAU Colloquium #68 edited by Philip and Hayes (1981), a NATO Advanced Study Institute edited by Hanes and Madore (1978), and IAU Symposium #85 on Star Clusters in general edited by Hesser (1979).

In addition to stars in galactic globular clusters, groups of globulars around other galaxies are likely targets for multiobject studies. Measurement of the velocity dispersions in external globular systems should provide a luminosity independent estimate of the mass, including the halo, of the parent galaxy. If the local chemistry problems are ever resolved, then spectroscopy of the integrated light of these extragalactic globulars should produce data on the evolutionary processes associated with the formation of different galaxy systems. Brodie and Hanes (1981) compare the integrated spectra of 24 galactic globulars with four spectra of 19th magnitude globulars near M87 to investigate the metallicity characteristics of the M87 system. They find the M87 clusters to be metal-rich compared to local clusters, but the statistics remain very small.

Dwarf spheroidal galaxies are another group of objects which have problems similar to globular clusters, but about which less is known because of their distance. Both dynamical and chemical studies of these objects require many spectra of stars in a localized region of the sky. Based mostly on photometric studies, Mould (1983) discusses the star formation history of nearby dwarfs. Aaronson (1983), Cook, et al. (1984), and Cohen (1983) have reported radial velocity measurements of a few objects in nearby dwarf spheroidal galaxies. They obtain somewhat contradictory values of the velocity dispersion and therefore mass-to-

light ratio in these galaxies. The resolution of this problem will require high dispersion spectra of many faint objects and may have a significant impact on the missing mass problem.

Spectroscopic Surveys

Many problems in astronomy can be addressed by collecting large numbers of spectra. Clusters of galaxies and stars have been discussed in detail in the previous sections. Some programs require many objects to be surveyed to identify interesting candidates for further study. In recent years, the Einstein x-ray satellite has observed many sources that have yet to be identified optically. Stocke, et al. (1983) have made optical identifications of a sample of sources from the Einstein Medium Sensitivity Survey. Between one and ten optical spectra were recorded for each source identification. When sufficient statistics are accumulated, this type of x-ray selected sample will allow studies of the spatial distribution of quasars, the evolution of clusters of galaxies, the x-ray properties of stars, and other topics. Griffiths, et al. (1983) studied the optical counterparts of x-ray sources in an Einstein Deep Survey field. As the limiting x-ray flux becomes fainter, the optical identification becomes less certain and more spectra of fainter objects are required. Identification of gamma ray sources is another similar task. Little is known of the identity of galactic plane gamma ray sources which lie in extremely crowded fields. The IRAS satellite is also providing new lists of infrared sources needing optical identification and study. Young, et al. (1984) have studied Abell 2151 at 60 and 100 microns where many sources have less than

obvious optical identifications. Redshifts of these sources will be useful for removing field contamination. All of these problems will benefit greatly from multiple object spectroscopic capability.

Spectroscopic followup is also needed with optical surveys which locate and study quasars and other objects via ultraviolet excess or variability studies. The Steward CCD Transit Instrument (CTI) being built by McGraw, et al. (1982) will discover thousands of interesting objects down to 24th magnitude (V). Redshifts and other spectroscopic data will be needed for this sample defined by photometric methods. This should require enough spectroscopic followup to keep even MX busy for a while. Schmidt and Green (1983) summarize the current quasar surveys. They predict of order 100 quasars per square degree down to a limiting magnitude of B=22. The exact number depends, of course, on the luminosity function and evolution model which is adopted. Clearly the study of quasars will soon be a multiple object spectroscopic field as well. Objective prism surveys such as those done by Osmer and Smith (1980) can benefit most from multiobject spectroscopy since much higher resolution spectra of interesting objects can be obtained over a field comparable to that of the objective prism. Much telescope time, on the KPNO 4m aperture plate system and others, has recently been devoted to the study of clusters of galaxies around low redshift quasars by Hintzen (1984), Koo (1983), and Dressler and Gunn (1983). Hintzen has shown that wide-angle radio-tail QSOs are often located in dense cluster environments. This type of project simply would not be done without the ability to obtain simultaneous spectra of many objects.

Optical spectroscopy can be used alone in a survey mode for studies of the distributions of "normal" optical galaxies. This type of study of supercluster structure by Kirshner, et al. (1981) was mentioned previously. Multiple object spectroscopy allows enough increase in effective telescope time to extend significantly the sample in redshift space and over larger areas of sky. The large number of galaxy spectra obtained in such surveys, as well as in dynamical studies of clusters, will also provide a large spectral database for studies of the properties of individual galaxies. Of particular interest is the strength of nuclear activity observed in a large sample of nearby and distant galaxies, as well as the star formation history which can be derived from the observed integrated stellar population in these galaxies.

CHAPTER 3

MEDUSA RESULTS FOR CLUSTERS OF GALAXIES

The previous chapter described a few of the many astronomical problems which can benefit from multiple object spectroscopy. This chapter presents some of the results obtained with the Medusa fiber spectrograph on the Steward 2.3m telescope. The Medusa aperture plate system is described in chapter 4. Results from the Medusa with intensified photographic plates have been published by Hill, et al. (1980b), and by Hintzen, et al. (1982). Spectroscopic data acquired in 1982 with an intensified CCD detector are presently in the reduction process. Preliminary results are presented here. The complete set of about 200 velocities will be published by Hill, et al. (1984). The data reduction process and the characteristics of the intensified CCD detector are outlined in chapter 7.

Dynamics

Large numbers of accurate radial velocity measurements are essential if we are to understand the dynamics of clusters of galaxies. Our major goals in early Medusa observations were to measure velocity dispersions, and to investigate the relationship between the dynamics of the optical galaxies and the x-ray emitting gas. Measurements of the optical profile of the line-of-sight velocity dispersion can be compared to dynamical models and to results from x-ray observations

Velocity Dispersions

A major contribution of the Medusa spectrograph has been the measurement of many cluster velocity dispersions. The velocity dispersion is reported as the rms deviation from the mean cluster velocity. A special relativistic correction is applied so that velocity has the same physical meaning at all redshifts. A correction factor is also applied to compensate for the enhancement of the velocity dispersion by measurement errors which add in quadrature. Roughly 50 galaxies are needed to reduce sampling errors in the dispersion down to the level of the individual measurement errors (50 km s^{-1}). Danese, DeZotti, and diTullio (1980) discuss the statistics of obtaining accurate measurements of the line-of-sight velocity dispersion. Figure 1, reproduced from Hintzen, et al. (1982), shows a plot of x-ray luminosity versus velocity dispersion for rich clusters of galaxies. The error bars are shown for 4points measured with Medusa. In only a few nights, Medusa has made a significant impact on this type of study. The measurement of the relatively low velocity dispersion of Abell 400 provides significant leverage on the apparent correlation. Hintzen and Scott (1979) and Quintana and Melnick (1982) provide more details on the empirical correlation of x-ray luminosity and velocity dispersion. Future work needs to include x-ray selected clusters to remove optical selection biases, as well as dispersion measurements which are limited to the cluster core in order to sample the same region as the x-ray gas.

As discussed in chapter 2, many velocities are required to obtain sampling which allows inversion of the velocity dispersion profile. Medusa has not yet collected enough redshifts to investigate

seriously the form of cluster potentials, but preliminary data look interesting. Our measurement of a dispersion of 345 (+79,-51) km s^{-1} in the core of Abell 400 is somewhat lower than the measurement of 500 km s^{-1} for a sample of spirals in the outer parts of the cluster by Bothun (1981). Many more redshifts are required to distinguish between a true radial gradient in the velocity dispersion and possible contamination from a supercluster background.

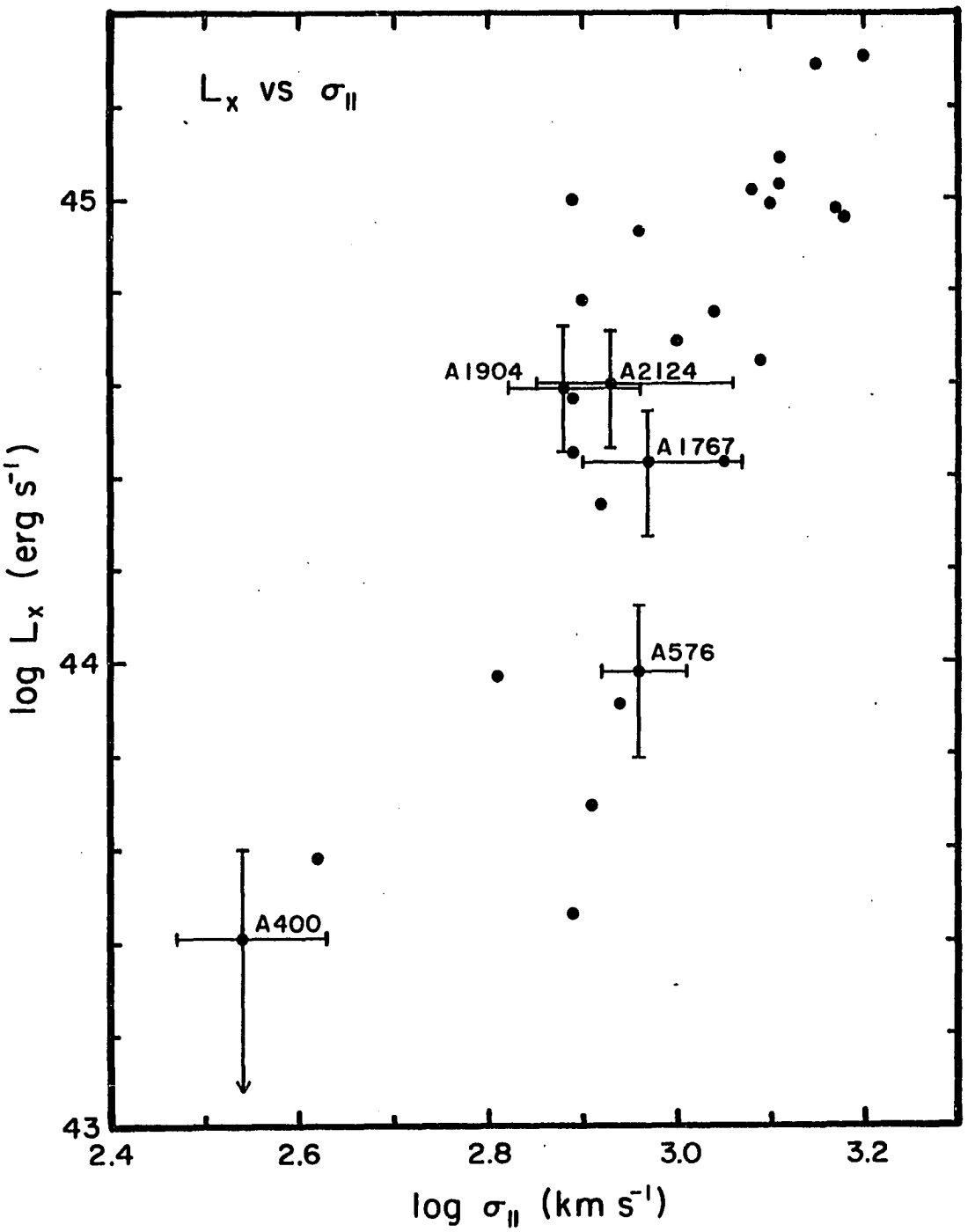

Figure 1. X-ray Luminosity vs. Velocity Dispersion

This plot of x-ray luminosity vs. radial velocity dispersion for clusters of galaxies is reproduced from Hintzen, et al. (1982). Points with error bars have velocity dispersions from the Medusa spectrograph. Other data are from Quintana and Melnick (1982), and McKee, et al. (1980).

Structure

The observation of structure in clusters on many scales was discussed in chapter 2. Because of the small numbers of galaxies involved in sub-clumps, many measurements are needed to untangle statistically real clumps from projection effects. No definitive results on the dispersions of small clumps have been obtained to date. On a larger scale, recent measurements of intensified CCD data show that the cluster Abell 993 is actually two clusters seen in projection. Preliminary measurements of 19 redshifts show nine galaxies in a cluster at 12,100 km s^{-1}, and seven galaxies in a cluster at 16,100 km s^{-1}. Three galaxies fell outside the three sigma limits for membership in either cluster. Both clusters have a velocity dispersion of roughly 300 km s^{-1}. The dispersion is nearly 2000 km s^{-1} if the two clusters are combined. Eyeball inspection of a photograph of A993 indicates that the nearby cluster is probably displaced slightly to the northwest of the distant cluster. Neither of these clusters is a strong x-ray source, but this is the sort of effect which must be removed when studying the true binary x-ray clusters. A993 also provides a nearby example of the problems of optically selecting rich clusters of galaxies for study when only surface density information is available. An intensified CCD spectrum from A993 is shown in the data reduction section of chapter 7.

Microwave Decrement

Figure 2 shows the cluster of galaxies Abell 576 reproduced from the Palomar Sky Survey. This cluster was of particular interest because of the large microwave decrement which Birkinshaw, Gull, and Northover

(1978), and others, had reported. This decrement was originally attributed to the Sunyaev-Zel'dovich effect, the diminution of the cosmic microwave background by Compton scattering on the x-ray emitting gas in the cluster. Microwave decrements, x-ray luminosities, and velocity dispersions are potential distance indicators (see Birkinshaw, 1979). The A576 region shows considerable complexity in both x-ray and radio observations. The x-ray flux for this cluster derived from HEAO A-2 data is smaller than the 4U value. Pravdo, et al. (1979) suggested that the disagreement is due to enhanced x-ray background in the A576 region. White and Silk (1980) reported Einstein observations which support Pravdo, et al. In any case, the fact that the A576 data lie somewhat below the empirical relation between x-ray luminosity and velocity dispersion shown in Figure 1 is not surprising in light of the observational uncertainties.

Using their x-ray observations, White and Silk demonstrated that the A576 source is remarkably cool, far from isothermal, and cannot be adequately approximated by a polytropic equation of state. On the basis of their detailed x-ray data and available optical and radio observations, White and Silk concluded that there is insufficient hot gas in A576 to produce the observed microwave decrement by Compton scattering. In their calculations, White and Silk assumed a radial velocity dispersion of 1135 km s^{-1} derived from measurements of 20 galaxies by Melnick and Sargent (1977).

Figure 3 shows a set of galaxy spectra from a 3 hour exposure on A576 taken in December 1980. The dispersion was 250 Å mm^{-1} from a 300 l mm^{-1} grating with a resolution of 12 Å. Velocities were measured from

this N_2 baked IIIaJ photographic plate and several others to an accuracy of 90 km s^{-1} by Hintzen, et al. (1982). The wavelength scale is labelled on the spectra along with galaxy ID numbers. The position of the redshifted calcium H and K lines is also indicated. The heliocentric redshift of A576 is 0.0381 $\pm$0.0005. The global radial velocity dispersion derived from measurements of 47 galaxies in A576 was found to be 914 (+113, -83) km s^{-1}. Since the cluster gas density varies with the square of the velocity dispersion, our observations imply that the gas density is only 2/3 the value adopted by White and Silk. This strengthened their conclusions from x-ray data, that there was too little hot gas to account for the observed microwave decrement. More recent microwave observations at 6 cm by Lasenby and Davies (1982) have failed to show any significant microwave decrement in A576. Rothenflug, et al. (1983) report Solid State Spectrometer observations showing in the center of the cluster a lower x-ray temperature which is consistent with the observed galaxy velocities. They suggest that the lower x-ray temperature may be due to a cooling flow in the x-ray gas or to the emission of individual cluster galaxies. Neither x-ray nor optical data are able to distinguish between these two modes. Birkinshaw and Gull (1984) describe the state of recent microwave decrement observations in several clusters.

The results above assume that both the gas and the galaxies are in equilibrium, and that their distributions reflect the same symmetric potential. Our sample of velocities in A576 provides no evidence for large-scale cluster rotation. Therefore, the line-of-sight velocity dispersion is a good measure of the gravitational potential of the

system. The radial velocity dispersion shows only a slow decrease with increasing radius from the cluster center. This seems to confirm the conclusion, which White and Silk draw from x-ray observations, that the binding mass of the cluster is distributed over a region significantly larger than the "galaxy core". Additional studies are underway to provide more data on the velocity structure of the galaxies in A576.

The Medusa spectrograph has collected about 800 spectra of galaxies as of February, 1983. The major portion of these (200 redshifts) will be published by Hill, et al. (1984). Figure 4 shows plots of raw spectra of five galaxies in the cluster Abell 2151 obtained with the intensified CCD detector at the 2.3m telescope. This single 20-minute exposure includes galaxies with visual magnitudes from 15.0 to 17.5. Additional exposures were taken to measure the redshifts of the fainter galaxies. The spectral resolution is 12 Å FWHM. The CCD allows more sophisticated data reduction including subtraction of the sky background obtained with fibers looking at empty areas of the field. Except for flexure, the fixed format of the CCD allows direct velocity calibration of each fiber by taking full-field comparison lamp exposures. This added complexity also requires more time spent at the computer to obtain a radial velocity. Therefore, most of this data remains unreduced. The next chapter describes the actual operation of the Medusa spectrograph which produced the data described here.

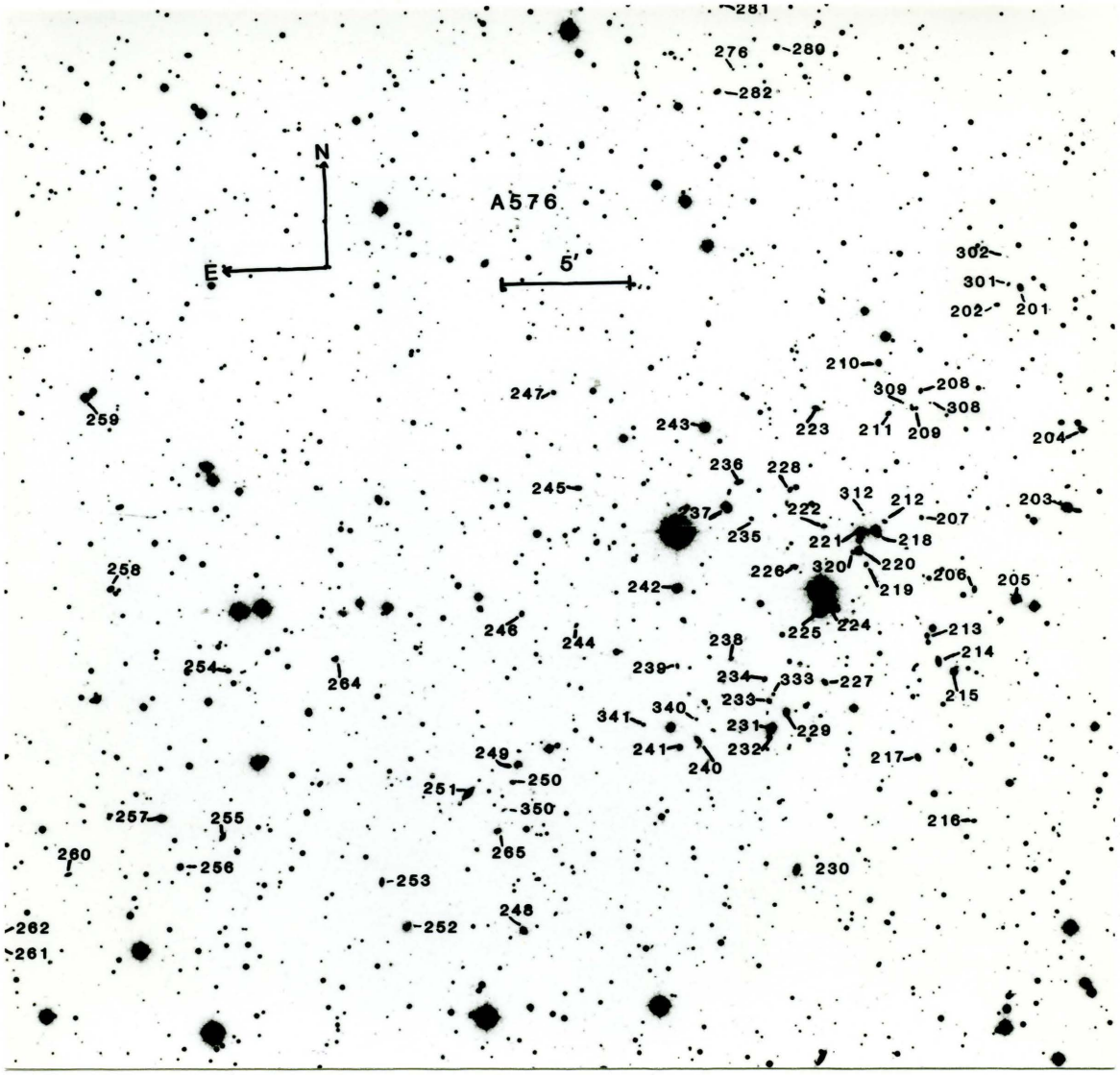

Figure 2. Photograph of A576

This figure shows a section of the cluster of galaxies Abell 576 reproduced from the Palomar Sky Survey. Numbered galaxies have been observed with Medusa.

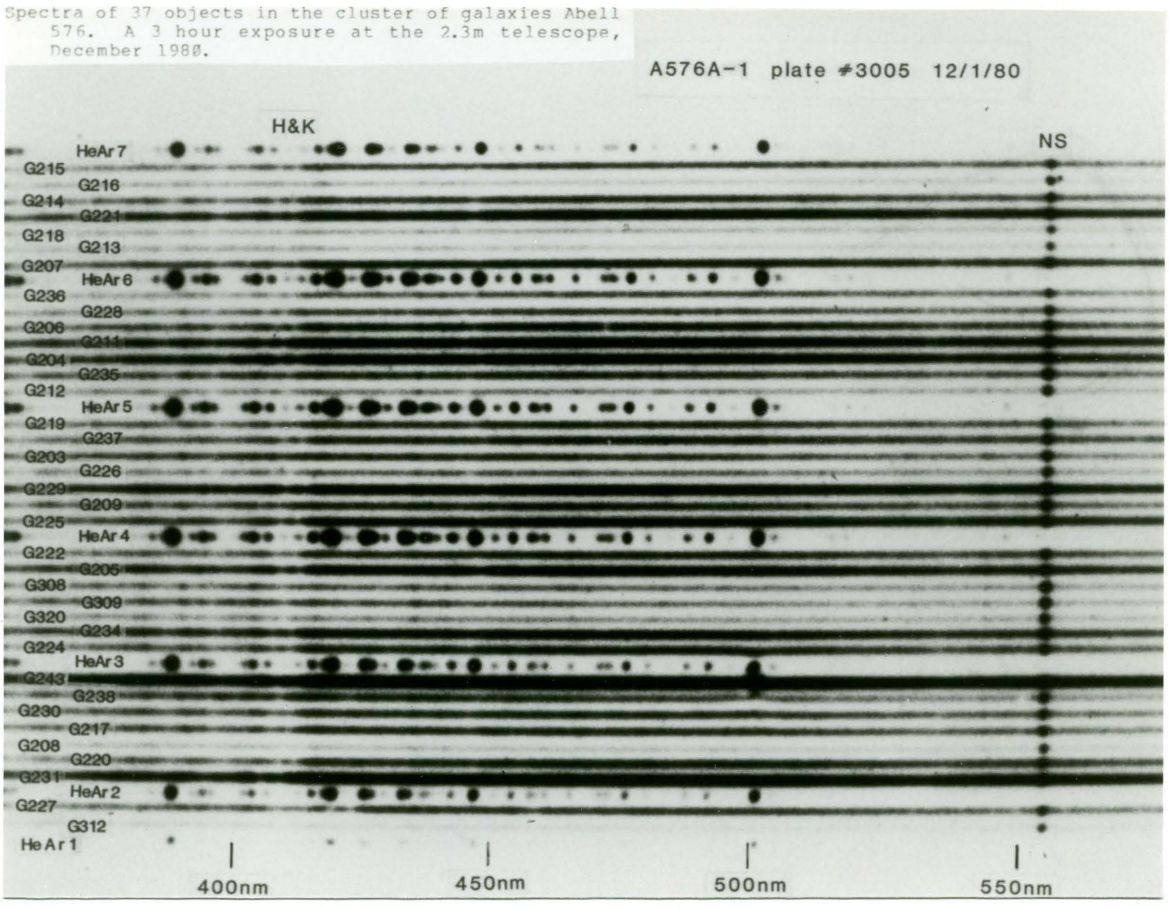

Figure 3. Photograph of 37 Spectra from A576

This figure shows intensified photographic spectra of 37 objects in the cluster of galaxies Abell 576. A three hour exposure at the 2.3m telescope, December 1980. The spectra are identified by galaxy number and blue is to the left.

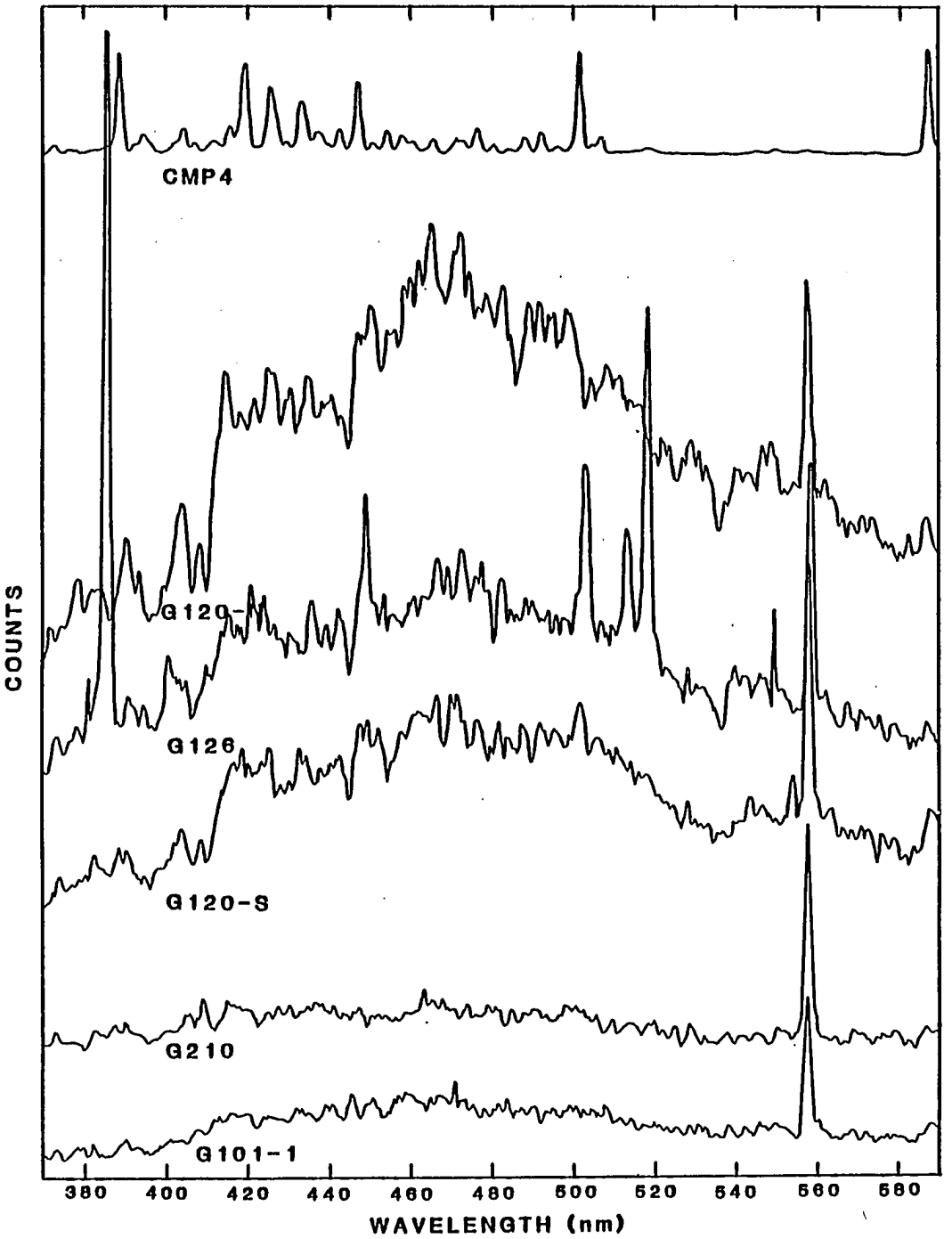

Figure 4. Plots of CCD Spectra from Abell 2151.

This figure shows raw Medusa spectra of galaxies in the cluster Abell 2151 (Hercules) were taken on 14 June 82 at the Steward 2.3m telescope (exp A2151-1.G6). These spectra are 5 of 37 which were extracted from a single 20-minute intensified CCD exposure. All galaxy spectra are plotted on the same scale with a vertical offset added.

CHAPTER 4

HISTORY OF FIBER SPECTROSCOPY AND THE MEDUSA SPECTROGRAPH

This chapter provides a general introduction and a brief history of multiple fiber spectroscopy, as well as a description of the Medusa spectrograph. Portions of chapters 4, and 5 were combined in a paper presented by Hill, Angel, and Scott (1983) at the Los Alamos Conference on Optics. The beginning of chapter 4 was extracted from a paper by Hill, Angel, and Richardson (1983) presented at the SPIE conference on "Instrumentation in Astronomy V," in London.

Overview -- Why Fibers?

Fiber coupling is now being used or tested at more than a dozen telescopes around the world and will clearly play an important role in the design of the next generation of large telescopes. Fiber optic coupling between a telescope and a spectrograph has several potential advantages over conventional slit spectroscopy. These advantages have been discussed previously by Angel, et al. (1977), Hubbard, Angel, and Gresham (1979), and Hill, et al. (1980a,b). Briefly these advantages include:

1) the possibility of simultaneous high or low resolution spectroscopy of many objects in the telescope field-of-view. Methods and results of multiobject spectroscopy have been discussed by Hill, et al. (1980b), Hill, et al. (1982), Hintzen, et al. (1982), Tubbs, Goss, and Cohen (1982), Hill, Angel, and Scott (1983), Gray (1983a,b), and

Ellis, et al. (1984).

2) stable, well-scrambled images for precision velocity measurements without slit effects. A system like this has been described by Heacox (1980).

3) remote or "psuedo-coudè" coupling to a floor-mounted spectrograph in order to avoid instrument flexure problems. The same spectrograph can be used at more than one telescope if suitable fiber links are available. This type of spectrograph is described by Barden (1983).

The basic components of a fiber coupled spectrograph system include: 1) a fiber head to mount the fiber in the focal plane. The fiber head will also contain any necessary guide optics or calibration lamps normally associated with the spectrograph. 2) the actual fiber link of one or more fibers to transfer the light from the telescope focal plane to the spectrograph(s). The length of the fiber cable may vary from 10 cm to 10 meters or more. 3) the spectrograph-detector combination which disperses and records the light coming from the fiber. This may be a conventional spectrograph modified to accept a fiber entrance aperture at its slit position. The spectrograph may be modified to accommodate the particular imaging properties of the fiber. Possible modifications include working at an input f/ratio around f/4 and removing the central obscuration present in many spectrograph cameras.

The two figures of merit for a spectrometer system are the throughput and the quality of spectra. A multiple fiber feed can increase the effective, if not the actual, throughput by arranging for

many objects of interest to fall within the entrance aperture. The actual optical throughput of the spectrograph has not been changed, ie. the area - solid angle and the resolution - luminosity products are constant, but the system is being used much more efficiently. In the case of a single fiber feed, as well as multiobject feeds, the image transfer characteristics of the fiber may improve the scientific quality of the spectra obtained.

Fiber Properties

Certain characteristics of fiber optics or optical waveguides make them very attractive for use in astronomical optical systems. Because of the limited astronomical market, optical fiber technology was and is developed entirely for the communications industry. Astronomers accordingly must choose which parts of existing technology they can adapt for their own uses.

Flexibility

Fibers are primarily useful for multiobject spectroscopy because of their flexibility. This allows multiple images from widely separated parts of the telescope field-of-view to be reformatted in a compact form at the spectrograph entrance aperture. Fiber bundles can be used to transfer an image to a remote focus, as in an offset guider, or between imaging devices, as in coupling image tube stages. This chapter will deal exclusively with single, step-index fibers which are proximity focus devices and require auxiliary optics if the fiber is not located in the focal plane. The single fibers are used to bring together the images of many objects at the spectrograph entrance aperture. Fibers

are also used to deliver comparison light from a remote source.

Size

Fused silica and glass, multimode, step-index fibers are available in diameters from 50 microns to 1500 microns; so matching the telescope platescale is rarely a problem. Step-index fibers have an abrupt change in refractive index between the core of the fiber and the cladding layer. This index change causes total internal reflection at the interface between these two layers. To make the nomenclature clearer in later parts of this paper, Figure 5 shows the structure and refractive index profile of a typical fused silica fiber. Miller and Chynoweth (1979), Marcuse (1981), Midwinter (1979), and other similar books provide details on the physics, material properties, manufacture, and measurement of fibers. Both plastic-clad silica fibers (PCS) and glass-clad fibers (AS) are used in astronomical spectroscopy.

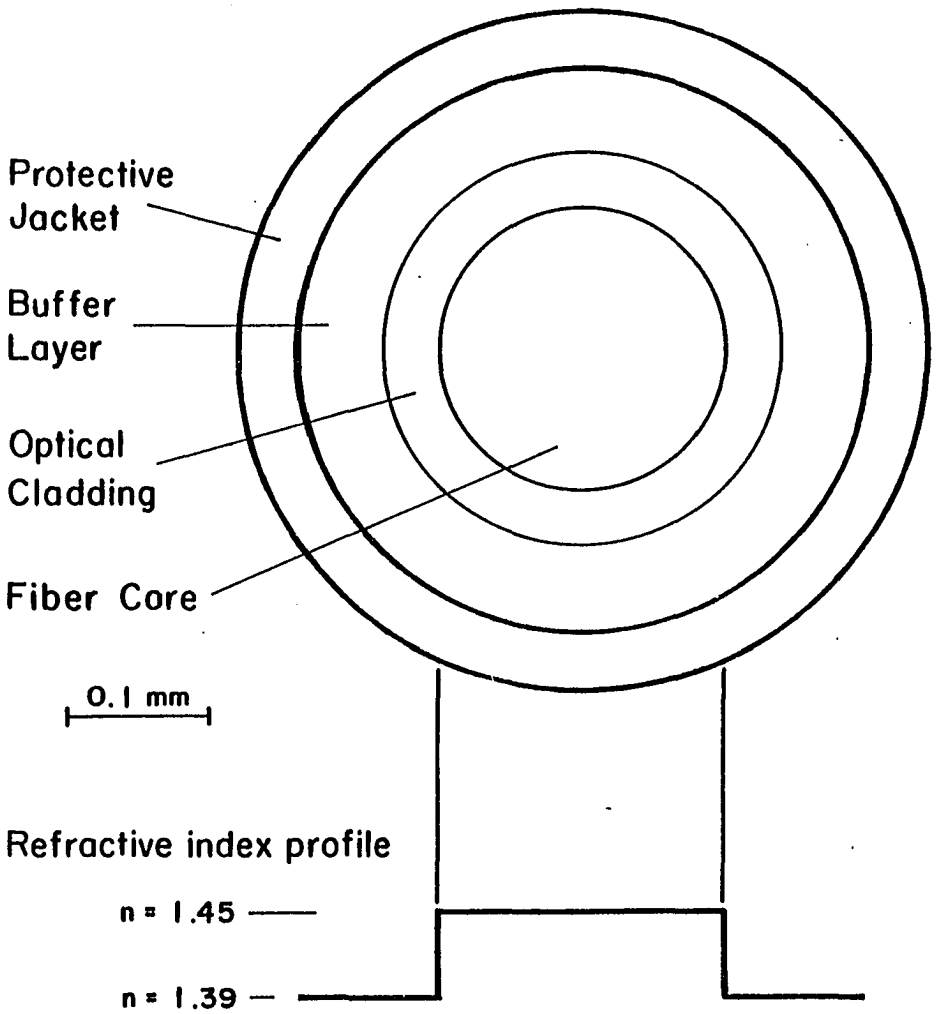

Figure 5. Optical Fiber Structure
This figure shows the physical structure and the refractive index profile of a representative plastic-clad silica (PCS) fiber.

Transmission

The excellent transparency of the fibers allows lengths of fibers of several meters to be used without significant loss of light in the fibers. A long fiber or set of fibers can be used to feed a floor-mounted spectrograph to avoid many instrument flexure and vibration problems. The optical transmission of lengths of fused silica fiber less than 20 meters is roughly the same as that of a thin plate of fused silica inserted in the beam. The transparency of most fused silica core fibers is limited by Rayleigh scattering at the ultraviolet wavelengths and by impurities such as H_2O, OH^-, and transition metal ions in the fiber. The losses are dominated by surface reflections from the fiber ends between the wavelengths of 380 nm and 1500 nm. See Powell (1983), Barden (1983), Barden, Staver, and Ramsey (1984), and Angel, et al. (1977) for measurements of the transmission of a selection of fibers. Figure 6 shows actual transmission measurements made by Powell of all-silica fibers. State of the art, silica, multimode fibers have attenuation less than 20 dB km^{-1} over significant portions of the visible and near-infrared wavelength range. The best fibers have attenuation less than 1 dB km^{-1} in the 1500 nm band. Rayleigh scattering in pure silica would produce 0.15 dB km^{-1} attenuation. Compare these to high quality optical glasses which have a typical attenuation of 1000 dB km^{-1}. Silica fibers have large losses redward of 2 microns due to water absorption. Attenuation in the fiber is measured by comparing the power transmitted through a long length as compared to a short length.

$$A = -10 \log[P_L/P_S]/[L_L-L_S] \qquad (4.1)$$

where A is the attenuation of the fiber at the measurement wavelength in units of dB km^{-1},

P_L, P_S are the measured power transmitted through long and short lengths of fiber,

and $L_L - L_S$ is the difference in length of the two fibers.

A typical attenuation found in a silica-core fiber such as QSF-AS is 20 dB km^{-1} at 600 nm. Using equation (4.1) and a 10m (0.01 km) length of fiber, I find the transmission to be 95%, not including end reflection losses.

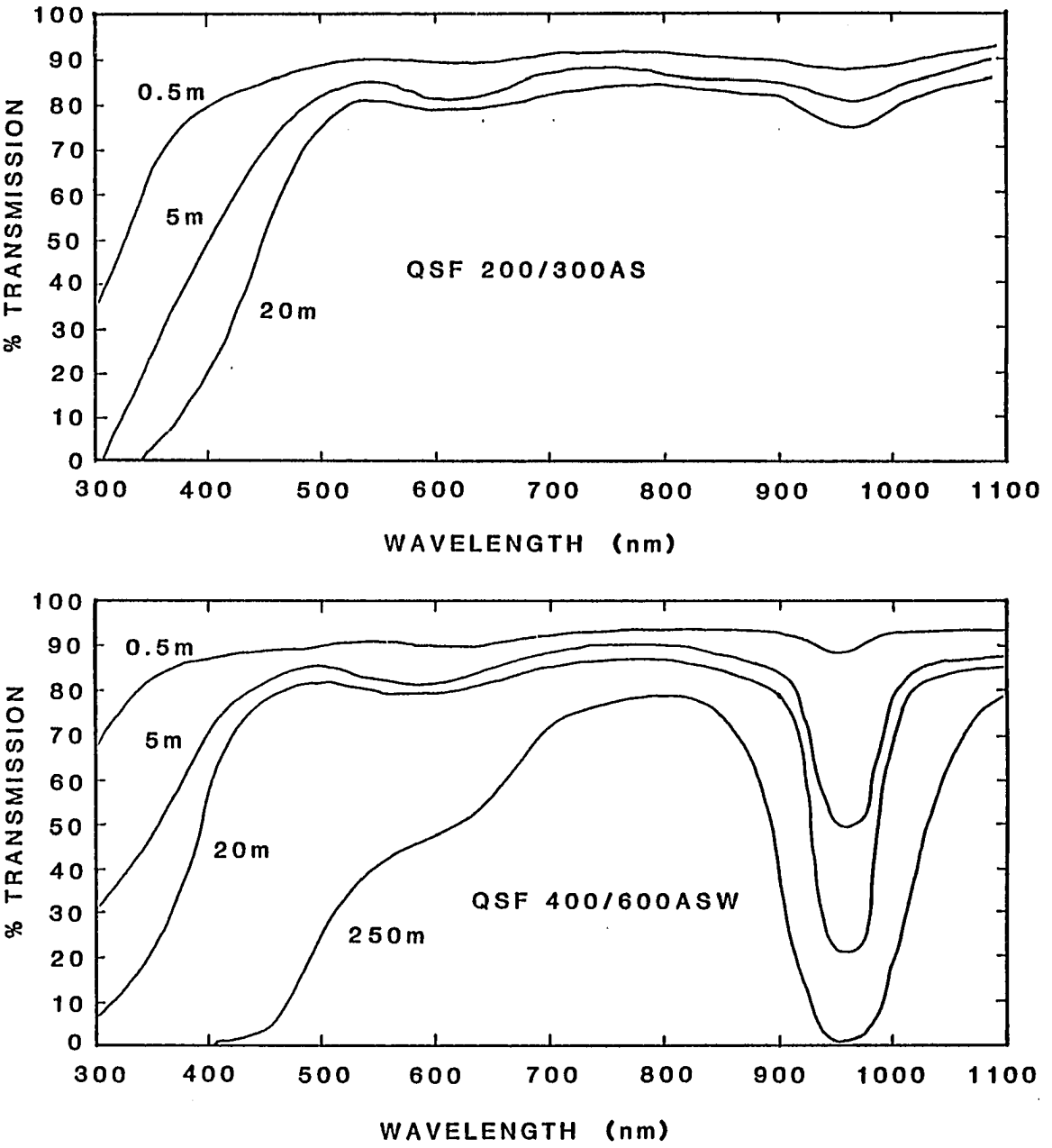

Figure 6. Fiber Transmission Curves

This figure, which is reproduced with permission from Powell (1983), shows the measured absolute transmission available through different lengths of silica fiber including end reflections. The "wet silica" fibers (QSF-ASW, 300 ppm OH) have improved ultraviolet transmission because the fibers have fewer scattering centers, but also show a strong absorption band in the near-infrared. The "dry" fibers (QSF-AS, 30 ppm OH) have improved red transmission at the expense of a longer ultraviolet cutoff.

Image Scrambling

Fibers are also useful in spectroscopy because of their image scrambling capability. In lengths of fiber long enough to produce a significant number of internal reflections, the position of the ray on the fiber face is not preserved, therefore any image detail on the entrance end of the fiber is uniformly blurred across the whole exit end of the fiber. This image scrambling eliminates slit effects such as line profile changes or radial velocity errors which are caused by incorrect centering of the object in the entrance aperture of the spectrograph due to guiding errors. Image scrambling eases the problem of identical spectrograph illumination between star, calibration lamps, and sky. This scrambling also causes the output image to be the same size as the fiber core in the best or worst seeing conditions.

Constraints on Spectrometer Design

The size and transmission properties of available optical fibers set only rough limits on the optical configuration used in feeding light to the fibers. Transmission in silica-core fibers limits the length of fiber that can be used for near-ultraviolet spectroscopy. This limit is only of concern for a floor-mounted spectrograph at a large telescope where the fiber length may exceed 10 meters. The choice between spectrographs mounted on the floor or on the telescope will be discussed in chapter 7. Focal ratio degradation in fibers makes an f/4 beam from the telescope optimum for fiber transmission. A detailed discussion of optical matching between telescope, fiber, and spectrograph is given in chapter 8. Fiber diameters in the range 60 to 400 microns are well

matched to spectroscopic apertures in use on large telescopes. Therefore, no significant problem exists in matching fiber diameter to image size at most Cassegrain or prime foci. Long lengths of fiber must be protected from physical damage with heavy jacketing if the spectrograph is not directly adjacent to the telescope focal plane. If the spectrograph is nearby or if strain relief is given to the fiber sheath, the fibers can enter the focal plane and slit area with only a light plastic jacket. The plastic jacket is generally thin enough that crowding due to fiber diameter is not a problem. Spacing of the fibers at the slit of the spectrograph is limited by the image spacing on the detector, or by optical elements such as microlenses on the end of the fibers. Spacing in the focal plane is usually limited by the size of the device that holds the fiber in place, rather than by the fiber jacket diameter. Diameter of the fiber jacket may be important if it is desired to assemble a group of fibers into a close-packed array as might be used to reformat an image. Fibers are not very efficient at this type of image slicing because of the problem of circular close packing of the round fibers. When the heavy fiber sheath is provided with strain relief, the weight of the fiber is less than a gram. It has no impact on the size or strength of the focal plane positioner because other forces require higher strength. While much time and effort goes into choosing a fiber type and mounting the fibers in the spectrograph, the specific fiber chosen has little impact on the positioners or their geometry. The optical properties of the fiber do, of course, affect the optical design and efficiency. The small size, lightweight, and relatively low cost of a set of fibers allows several sets of fibers to

be mounted on the same set of positioning arms. The corresponding slit assembly can then be chosen to suit the observing conditions at hand. A fiber probe might have fibers of 1,2, and 4 arcsecond apertures for different spectroscopic problems. The next section will describe the implementation of fiber coupled spectrographs on many telescopes in the past few years.

Fiber optics also have other applications in instrumentation for astronomy. In the Medusa and the MX Spectrometer several fibers are used to transmit light from a quartz lamp to the diffuser screen used for flat fields on the CCD. The fibers also transmit light from arc lamps used for wavelength calibration. This allows the lamps to be located well away from the crowded focal plane and light from a single lamp to be spread over a wide field. Fiber data links can also be used for data transmission over long cables without problems such as inductive noise pickup or ground loops.

A Brief History of Fiber Optic Spectroscopy

In 1977, Angel, Adams, Boroson, and Moore (1977) made transmission measurements on a 250 micron diameter, 10m length of Valtec plastic-coated silica fiber. They suggested the use of fibers to link an array of telescope dishes to a single instrument (FLOAT). Encouraged by the results of the transmission tests, Hubbard, Angel and Gresham (1979) mounted a single fiber on the Steward Observatory 36-inch telescope. They used this fiber link to record the spectrum of a single galaxy with a floor-mounted spectrograph. At that point, I (JMH) came along looking for a graduate research project and John Scott came along

looking for the "missing mass" in clusters of galaxies. Roger Angel had then collected the key ingredients for a successful instrumental collaboration: a scientific problem, clever new ideas, cheap graduate student labor, and cash. In December 1979, Hill, Angel, Scott, Lindley, and Hintzen (1980a,b) used 20 fibers mounted in an aluminum aperture plate to make the first simultaneous multiple object spectroscopic exposure on the cluster Abell 754. This aperture plate prototype was named the Medusa spectrograph, and has been taking scientific data continuously since then.

Since the original tests by Angel and a host of Steward graduate students, numerous instruments around the world have been built with fiber coupled spectroscopy in mind. A few examples include the Serkowski Radial Velocity Meter (RVM) at the University of Arizona Lunar and Planetary Lab which uses the image scrambling capability of a fiber to eliminate slit effects and flexure effects from a very high resolution spectrograph. Heacox (1980) and McMillan, et al. (1984) provide additional details on the RVM. Barden, Ramsey, and Truax (1981) at Penn State University did a preliminary study of the focal ratio degradation properties of fibers. The non-preservation of the focal ratio of the propagating beam is the main reason which prevents fibers from being implemented at all optical astronomical spectrographs. A suitable choice of spectrograph optics can minimize the degradation problem. Since 1981, Penn State has performed all of their spectroscopy at the 1.5m telescope with a dual fiber feed to a table-mounted spectrograph in a controlled environment room. Barden (1983) gives a summary of this system and some recent transmission measurements. Many

other groups in California, Hawaii, Chile, Europe, and Australia are actively considering single and multiple fiber feeds for spectrographs. Schiffer, Appenzeller and Ostreicher (1982) and Schiffer (1983) have used a single fiber to link a spectrograph to several telescopes between 40 and 75 cm in diameter where spectroscopy would otherwise not be feasible. They have also done the northernmost fiber optic spectroscopy above the Artic circle. This allows 24-hour spectroscopic coverage of short-period variable stars.

The Anglo-Australian Observatory has built and used a Medusa-like system for multiobject work at the AAT 4-meter and for two-dimensional spectroscopy of single objects in an image slicing mode. The Fibre Optic Coupled Aperture Plate (FOCAP) system is described by Gray (1983a,b). Ellis, et al. (1984) report on results obtained with the AAT multiple fiber system. A group of AAT users is now designing a mobile fiber spectrograph with individual fibers held magnetically to a steel plate in the focal plane (Ellis and Parry, 1983; Bingham, 1983a). Lund, and Enard (1983) describe the tests of the "Optopus", a 52-fiber aperture plate device used on the ESO 3.6m telescope. A small ring magnet holds each of the 52 fibers in holes drilled in a steel starplate. A Caltech - JPL collaboration conducted the first mobile fiber test at the prime focus of the Hale 200-inch at Palomar. Their stepper motor driven positioners are described by Tubbs, Goss, and Cohen (1982). Grainger (1981), and Robson and Grainger (1983) report on the use of fibers to combine an array of seven 37 cm telescopes.

The Medusa Spectrograph

This section describes the functional hardware known as the Medusa spectrograph. The Medusa spectrograph has been the working prototype for the MX Spectrometer and for a series of multiple fiber systems now in use around the world. A much more detailed description may be found in Hill, et al. (1982).

Instrument Description

The fundamental part of the Medusa is the fiber "nucleus". This box holds an aperture plate, with holes at the locations of galaxies in a cluster, in the 2.3m telescope focal plane. A schematic drawing of the nucleus is shown in Figure 7. 37 optical fibers run 20 cm from the aperture plate to another plate which forms the slit of the spectrograph. Interspersed among the galaxy fibers are seven fibers which carry light from a helium-argon comparison lamp for wavelength reference. Each nucleus with its aperture plate is used for the observation of one set of objects. After the observation of several hours is finished, the first nucleus is removed and a second one with a different aperture plate is put in its place. The nucleus resides in a spacer flange between the focal plane of the telescope and the normal Cassegrain spectrograph.

The fibers used are QSF300A from Quartz et Silice (now Fibres Optiques Industries). They are plastic-clad, fused silica, step-index fibers with 300 micron core diameter. The ends of the fibers are prepared by clamping a number of fibers in a slot in an aluminum plate. The whole assembly is then polished. The preferred polishing material

is Moyco Ultralap or a similar abrasive-coated mylar sheet made by other companies. A wet sheet of Ultralap is placed on a piece of plate glass and the fiber assembly is rubbed back and forth over this plate. The process is repeated with four grades of abrasive sheet from 23 micron silicon carbide to 0.3 micron aluminum oxide. This method of polishing fiber ends has proven far superior to all previous methods including scribing/breaking and polishing with sandpaper and cerium oxide. For maximum flatness it may be necessary to cement the fiber in a metal ferrule to prevent it from flexing during polishing. After all of the fibers have been prepared, the aperture plate box is assembled and the fibers are glued in place along with two coherent image conduits which are used for guiding and alignment.

Aperture plates are prepared by measuring the positions of the galaxies to be observed and a few reference stars for guiding on the glass copies of the Palomar Sky Survey with a two-axis Grant measuring engine at Kitt Peak National Observatory. The measured coordinates are converted to x-y positions in the 2.3m telescope focal plane. Holes are drilled at the x-y coordinates with a numerically controlled (N/C) milling machine. Fibers plugged into these holes are positioned in the focal plane with an accuracy of one arcsecond (100 microns). The construction and assembly of Medusa was described well by M. Pagrazio (1983), matte painting supervisor for the movie "Return of the Jedi", who said "Drilling thousands of holes can be pretty monotonous - but the effect can be spectacular."

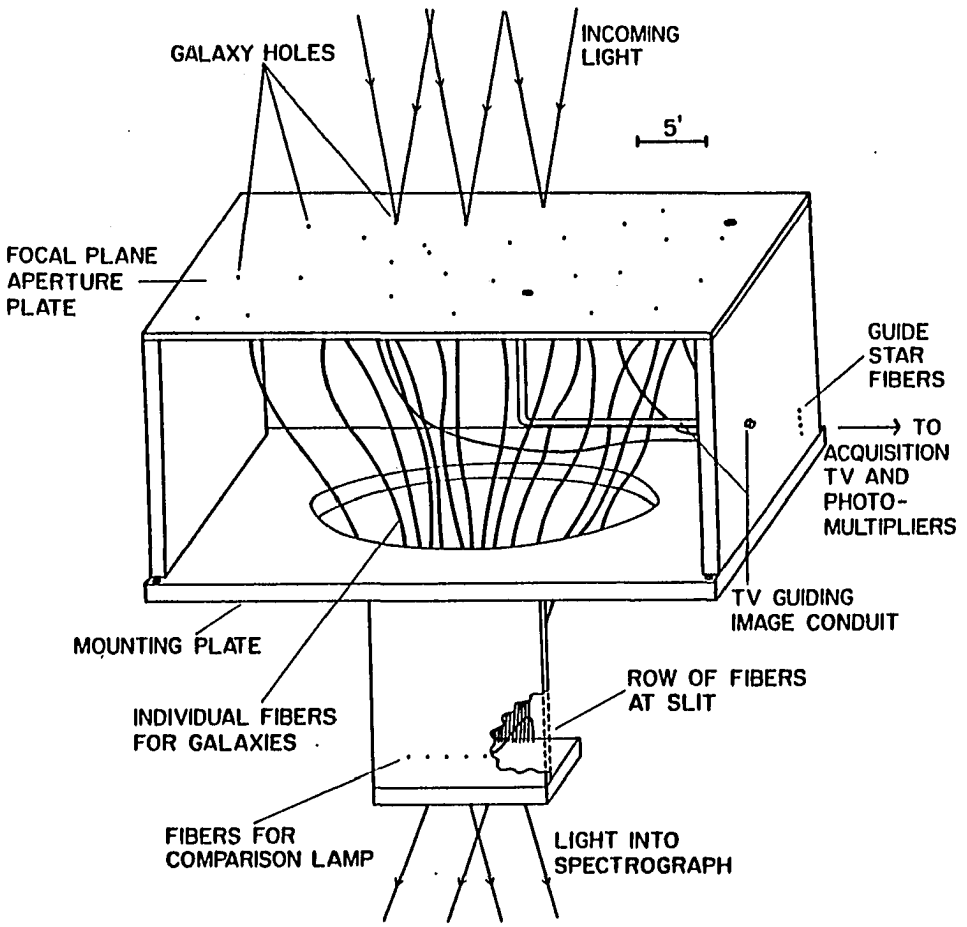

Figure 7. Schematic of Aperture Plate Nucleus of Medusa Spectrograph

Observing Procedure

Since December 1981, we have been using a 320 x 512 "thick" RCA CCD as the data collection device instead of the photographic plates used in the early Medusa work. The CCD is lens-coupled with a magnification of 1.5 behind the image intensifier at the output of the spectrograph camera. The data recorded for each cluster of galaxies includes nine 20-minute exposures on the target objects, three exposures of a helium-argon lamp for wavelength and velocity calibration, two exposures of a filtered quartz lamp and several CCD dark frames for detector calibration. Numerous short exposures are used rather than one long exposure to allow removal of cosmic ray events which deposit charge in the CCD at random places in the spectra. The helium-argon and quartz exposures are reflected from a plastic diffuser screen which slides into the telescope light path above the aperture plate. The quartz lamp provides a uniformly illuminated flat field to calibrate any nonuniformity in the CCD response. After obtaining the required number of exposures, the telescope is moved to the next object, a new aperture plate nucleus is inserted and aligned, and another sequence of exposures is begun. Setup and alignment requires 15 minutes per field. The previous nucleus is checked to make sure we know which fiber went to which galaxy. Then, the aperture plate is removed, and another plate for the cluster to be observed the next night is installed and "stuffed" with fibers. Table 1 lists the assembly sequence for installing MEDUSA on the 2.3m telescope. Table 2 lists a typical sequence of galaxy and calibration exposures that were taken with the CCD.

Table 1. MEDUSA Spectrograph Assembly Sequence

Pre-Run Preparation
- prepare and assemble fiber nuclei
- perform galaxy - fiber identifications
- prepare auxiliary MAFOS equipment
- check-in with mountain staff re. LN_2, etc.

Load Truck and Drive to Kitt Peak

Put CCD dewar on Vacuum Pump (formerly baked plates)

Remove previous instrument from telescope and add weight

Spectrograph Setup
- get B&C on floor
- remove reticon junk from B&C
- remove top dust cover from B&C
- check mirror and filter positions
- remove slit assembly and store
- remove TV optics and store
- remove wobble block or upper shutter
- cover holes with cardboard
- disable comparison mirror motor
- tighten bolts on Medusa flange
- mount Medusa flange on B&C
- bolt flange to spectrograph - 5 bolts,3/8" x 2",nuts
- install and tighten TV transfer lens,if not in place
- install guide photomultiplier box, thumbscrews
- check offset guider and dust cover clearance

Instrument Mounting
- add weight to top of telescope
- mount CCD micro rack, 5 1/4-20x1.5" bolts & nuts
- mount spectrograph - detector north w/rotator at 180
- check TV controls
- mount TV, 4 10-32 x 3/4 bolts,(connectors up)
- mount power supplies(CCD drivers,comparison lamp,etc.)

Detector Mounting
- Install blue button protector in image tube mounting flange, captive screws
- remove Schmidt camera cover
- remove photographic camera from image tube and store
- be sure to replace photographic camera after use
- remove image tube cathode cover
- blow dust off image tube with dry air
- mount image tube - 4 bolts, 1/2" x 2"
- connect air hose to image tube
- connect cooling lines with adapters($-20^{o}C$)
- connect HV cable to image tube, use dry air

Table 1, continued

mount transfer lens holder flange,4 bolts 1/4-20 x 3/4"
mount transfer lens, blow off dust,3 bolts only 10-32
check transfer lens settings, focus and f/stop

close valve and remove vacuum pump
blow dust off CCD window with dry air
mount CCD camera,
    3 bolts, 3/8" x 2.5" for adjustment,nuts,washers
    use thick(3/8") G10 plastic spacer
    sheathed signal cable down,(dispersion vertical)
connect dry air line to CCD
fill CCD dewar with liquid nitrogen

Cabling and Setup
install nucleus
cable up TV w/monitor in control room and outside
align and focus guide TV transfer lens (2 flashlights)
connect comparison and flat field lamps
cable CCD
install cereal box light baffles
install rotation alignment board near index ruler
focus Erfle eyepiece - 31 mm from flange
install grating - usually 300g/mm
adjust grating tilt - 3-4 degrees
adjust collimator - near 019

Balance Telescope ! !

Checkout and Alignment
turn on and test CCD,Z-80,.4, etc.
turn off lights!
check HV supply (polarity,etc)
    Spellman #3 uses 10.28 on dial for 25.4kV
turn on image tube while watching with CCD
allow image tube to stabilize 30-60 minutes
setup power supplies and counters in control room
for guide photomultipliers
align and rotate CCD
focus collimator and transfer lens
check comparison and flat field intensity

Feed the Observer

Begin the Observing Sequence
fill CCD dewar with liquid nitrogen
remove all dangling cables,tools, and TV monitors

Table 2. Exposure Sequence for Medusa with Intensified CCD

focus sequence for transfer lens and collimator

insert diffuser screen
    bias frames
    dark CCD frames
    quartz flat fields
    neon lamp
    helium-argon lamp
remove diffuser screen
    twilight sky if any left

acquire offset star
focus telescope

insert diffuser screen
    bias frame
    helium-argon lamp (top comparison exposure)
    quartz lamp (top flat field exposure)1-64 filter
remove diffuser screen

acquire field! turn up acquisition TV
turn on guide photomultipliers and tune rotation

    galaxy exposure /1 with side comparison
    galaxy exposure /2
    galaxy exposure /3
    galaxy exposure /4

insert diffuser screen
    helium-argon top comparison
remove diffuser screen

    galaxy exposure /5
    . . . . . .
    last galaxy exposure

insert diffuser screen
    bias frame
    dark frame if time permits
    helium-argon top comparison
    quartz flat field

replace nucleus and repeat sequence until dawn
at end insert diffuser screen
    bias frames
    dark frames
    helium-argon lamps
    neon lamps
    quartz lamps

Lessons Learned from the Medusa

Even while producing redshifts of faint galaxies faster than was previously possible with a two-meter class telescope, the Medusa has been a useful testbed of the general techniques of multiple aperture spectroscopy. The aperture plate technique has certain drawbacks which prevent it from becoming a general purpose instrument that can be used by a wide selection of astronomers on a routine basis. The requirement of drilling an aperture plate for each cluster of objects observed reduces the flexibility of the system. The galaxy coordinates must be measured two months in advance, often before telescope time is allocated, in order to get the holes drilled in time for observing. Even with a selection of aperture plates available, the two hours required to assemble a nucleus and insert the fibers into the aperture plate severely limit the ability of the observer to respond to changes in the observing conditions.

Many long hours are required to polish 288 fiber ends and assemble them into three nuclei required for a night of observing. This requires a highly trained and patient graduate student. The problem with highly trained graduate students is that they have a half-life of roughly two years and must be continually replenished. The Medusa currently requires one day of polishing and assembly time for each two hours spent observing at the telescope. The large number of fibers required for three aperture plate boxes also limits the sophisticated microlens tricks that can be done to match the fiber properties to the telescope and the spectrograph, since each fiber is inserted and removed from an aperture plate several times during an observing run. The

Medusa aperture plate also eliminates any possibility of adjusting the coordinates of individual objects at the telescope.

It is interesting to compare the complementary multiaperture system developed by Kitt Peak National Observatory at roughly the same time the fiber coupling experiments were being conducted at Steward Observatory. The system described by Butcher (1982) uses an aperture plate and a grism in front of a CCD camera. While maintaining the maximum throughput of an ordinary grism spectrograph, the bare aperture plate eliminates the sky background which normally limits spectroscopy with such systems. By drilling holes for 20 objects plus corresponding sky holes in the aperture plate, sufficient 4-meter telescope time is made available for recording spectra of very faint stars or galaxies in clusters. The aperture plates bring some of the same problems the Medusa has because of the lead time on plate preparation. Detector size limits the useable field-of-view to a few arcminutes. The number of objects which can be observed is about 20, but the aperture plate system still retains significant multiple object capability while eliminating the need for each user to bring his own trained graduate student to plug fibers into small holes and smear them with 5-minute epoxy. Dressler and Gunn (1983) describe a similar instrument used on the 200-inch telescope. They use a photographically reproduced aperture mask in front of the PFUEI spectrometer. This mask contains a small slit at each object position to get better quality sky spectra.

Given the lack of flexibility of both types of aperture plate systems, the next obvious step in the development sequence was to build a spectrograph with mobile fibers whose positions in the focal plane

could be controlled remotely. This led to the conception of the MX Spectrometer. The function and the design of the MX with fibers moving in the focal plane will be discussed in chapters 5 through 8. A proposal to the National Science Foundation to build a multiple fiber spectrometer was submitted in May 1981. This proposal was funded for a 2.5 year term beginning in the summer of 1982. The MX Spectrometer described here is the result of that work.

CHAPTER 5

THE MX SPECTROMETER: FOCAL PLANE POSITIONERS

When designing a multiple fiber spectrometer system to solve the observational problems outlined in chapter 2, there are many parameters which must be considered. The feasibility and desirability of fibers for spectroscopy have already been demonstrated by single fiber systems and by Medusa. This chapter discusses some of the many parameters which influence the design chosen for the MX Spectrometer. The purpose of the MX is to build an efficient, well-matched, spectroscopic system with the capability to record spectra of 32 objects in the telescope focal plane. This results in an order of magnitude increase in the amount of data obtained per hour of observing time. Since the target objects will never be in the same positions twice, the fibers must be accurately and repeatably positioned in the focal plane. The existence of 64 axes of motion forces the positioners which hold the spectroscopic fibers to be operated under computer control. Hill, et al. (1982) describe an early design of the MX. As construction is only just beginning, the details given here may not be the last word on the finished device. Funding considerations are such that we are building the positioners and the fiber head in early 1984, so it can be used with an unmodified Cassegrain spectrograph. Later in 1984, we will make modifications to our spectrograph to achieve optimum matching between the fibers and the best available two-dimensional detector.

Origins

The name of the MX Spectrometer has several possible origins. Early versions of the Medusa spectrograph were known as Multiple Aperture Fiber Optic Spectrograph (MAFOS) I, II, III, etc.. Thus "MX" is an obvious contraction of MAFOS X, the tenth operating version. "MX" may also stand for MultipleX spectrometer because of the multiple object capability for simultaneous spectroscopy. The real origin of the name "MX" derives from the fact that the distinguishing feature of this spectrometer is the mobility of the remotely controlled fibers. Therefore, "hostile observatories" will no longer be able to inspect our aperture plates and learn which galaxies we are observing. The fiber array can also be redeployed at a moments notice to respond to observing conditions requiring a different set of program objects. The MX will not live in a concrete silo and no attempt has been made to use radiation hardened subsystems other than optical fibers. Skyglow after a nuclear attack will certainly preclude the observation of faint galaxies.

Drivers and Constraints on the MX Design

The principal goal in astronomical spectroscopy is to get the most science or the largest quantity of scientifically useful spectral data out of each hour of observing time at the telescope. The achievement of this goal is moderated by available scientific and technical resources (ie. money, telescope time, and grad students). Based on the discussion in previous chapters, I am assuming that a fiber-coupled spectrometer is the system which is to be used to increase

spectral throughput. To achieve the maximum efficiency goal we must answer the following questions about the techniques which will be used:

What type of telescope should be used?

How should the fibers be positioned in the focal plane of the telescope and the entrance aperture of the spectrometer?

How many fibers will be used?

How will the positioning devices be controlled?

What type and size of fibers should be used to efficiently link the telescope and spectrometer?

What spectrometer-detector combination should be used?

How will the use of multiple fibers affect the spectroscopic observing techniques compared to conventional spectroscopy?

This chapter and the next summarize my thinking on the answers to these questions. The remaining portion of this chapter deals with the technology of positioning fibers in the focal plane. The design parameters will be discussed in a general sense for multiple fiber systems. The specific impact of these factors on the MX design which is described in this chapter will also be discussed. I am indebted to my co-workers and colleagues for their many contributions to this design over the last four years.

Focal Plane Fiber Positioners

The major technical problem to be solved before building MX is undoubtedly the mechanical placement of the fibers in the focal plane. Between 30 and 50 fibers must be actuated so that they can be precisely positioned in any pattern over the entire focal plane of the telescope.

The field size is nearly a degree (40 cm at the 2.3m) and each fiber needs to be positioned to better than 0.1 arcsecond (10 microns at the 2.3m). The positioner location must be accurate and stable to one part in 10^4. At the same time each individual positioning mechanism must remain small enough to allow space for free movement of the remaining positioners. There are several ways to achieve the placement of the fibers. A predrilled aperture plate in the focal plane is the simplest, but an aperture plate is inconvenient from both the optical and operational points of view because of its inflexibility.

Possible fiber positioner geometries divide into three classes. The first type parcels out separate areas of the field-of-view to each positioner. Each fiber would be allotted, for example, a 6 x 6 arcminute section of the focal plane to which it alone had access. This has the advantages that each positioner has a limited range of travel, and that collisions between neighboring positioners can be prevented mechanically. The major disadvantage to the "family plot" scheme is that the positioners are not free to move around the focal plane to acquire randomly placed target objects. One fiber positioner may have no galaxies in its allocated area while the neighboring positioner may have half a dozen galaxies in its area. A related scheme with additional freedom allows each fiber arbitrary motion in the focal plane provided it does not approach within "n" arcminutes of its nearest neighbors. This "gold mine" scheme allows each fiber to "stake a claim" on a section of the focal plane where other positioners may not intrude. The distance of closest approach is set by mechanical limits which prevent physical contact of neighboring positioners.

The alternative positioner geometry gives each positioner a wide range of travel, so that several positioners can access any position in the focal plane. Because of the increased freedom of motion, these positioners are also free to collide if the controlling computer makes an error and instructs them to do so. The advantage to this "communal farm" geometry is that the positioners are free to move around to match almost any random pattern of galaxies in the focal plane. Several fibers may work side by side to observe a tight group of galaxies. The price of this freedom is the need to check carefully before moving any probe to prevent the many possible fiber collisions. The closest approach distance is set by the size of the fiber probe tip.

The third possible fiber positioning option is similar to the aperture plate technique. A robot "graduate student" could be built to pick up the fibers and move them to their proper positions in the focal plane. Once positioned, the fibers would be held in place by clamps, magnets, suction, glue, or some other fastening device. This "remote planting" method offers the greatest freedom in choosing the fiber pattern if a compact and reliable hold-down mechanism can be found to secure the fibers. It appears that the complexity of a single robot arm operating in three dimensions is comparable to that of many simpler positioners attached individually to each fiber. I suspect that as much work in hardware and software would be required for this single complicated positioner as would be used in replicating 32 simpler devices for the other approaches. Obviously, these are not the only possibilities and there are certainly hybrid schemes which might contain features from several geometries. Tubbs, Goss, and Cohen (1982) give a

discussion of these and other possible positioner geometries which may or may not allow collisions.

MX Positioner Overview

The MX Spectrometer will have 32 fiber positioner probes operating in the telescope field-of-view. Each positioner arm will have one or more optical fibers attached to it. We have chosen the "fishermen-around-the-pond" approach for positioning the fibers. Each fiber is at the end of a rod which pivots outside the telescope field (θ motion). This rod is also able to move radially in and out of the field (r motion) to allow the fiber to be positioned anywhere within a trapezoidal shaped section of the circular field-of-view (45 arcminutes). Figure 8 from Hill, et al. (1982) shows the "Arp" schematic view of the positioners on a random field in the telescope focal plane. The "fishermen" approach allows most of the positioner parts, both mechanical and electronic, to remain fixed outside the telescope field-of-view. Only the thin fiber support rods actually extend into the focal plane area. Neighboring fiber positioners have considerable overlap in their individual areas of influence. Coverage of a randomly distributed cluster of objects is limited by the minimum approach distance of two neighboring positioners rather than by the number of objects in any given sector of the field. The overlap of positioner coverage obviously allows collisions between neighboring fibers and probes. I have taken the greedy approach by opting to maximize the coverage of objects in the field at the expense of allowing collisions without hard limits on individual positioner travel. The

space above and below the fishermen is not used. This allows space for guide optics or perhaps a second level of positioners. A schematic side view of the focal plane of the MX design is shown in Figure 9. By inverting the positioners and mounting them on a flange at the base of the offset guider box, instrument flexure at the focal plane can be reduced. Motion of the spectrograph relative to the rest of the telescope is unimportant.

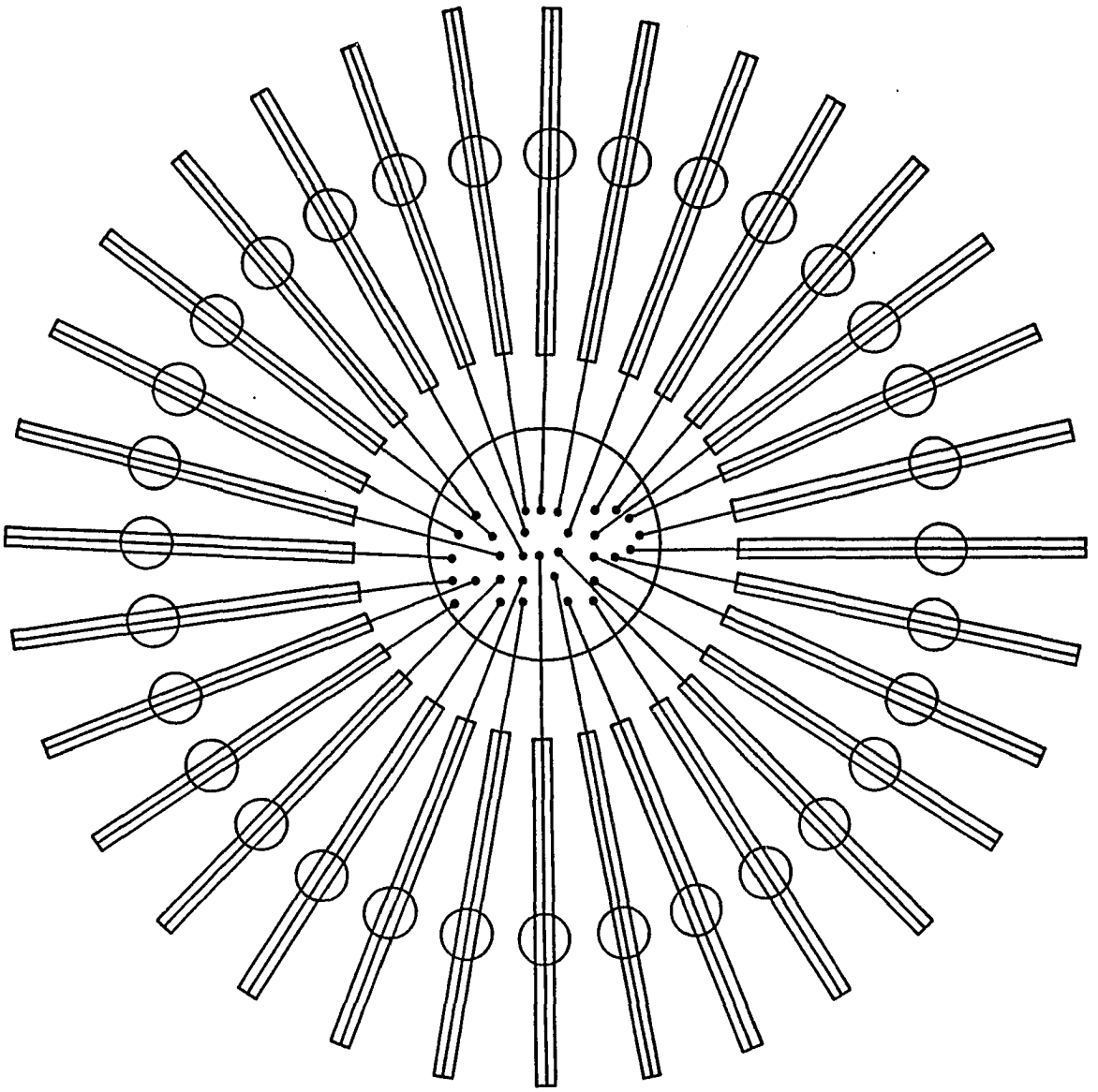

Figure 8: Arp Schematic View of Focal Plane Positioners

This figure shows the Arp schematic view from above of the MX positioners set on a random field in the telescope focal plane. Solid dots mark the position of potential quasar candidates within the field. The small circles mark the pivot points for the radial actuators.

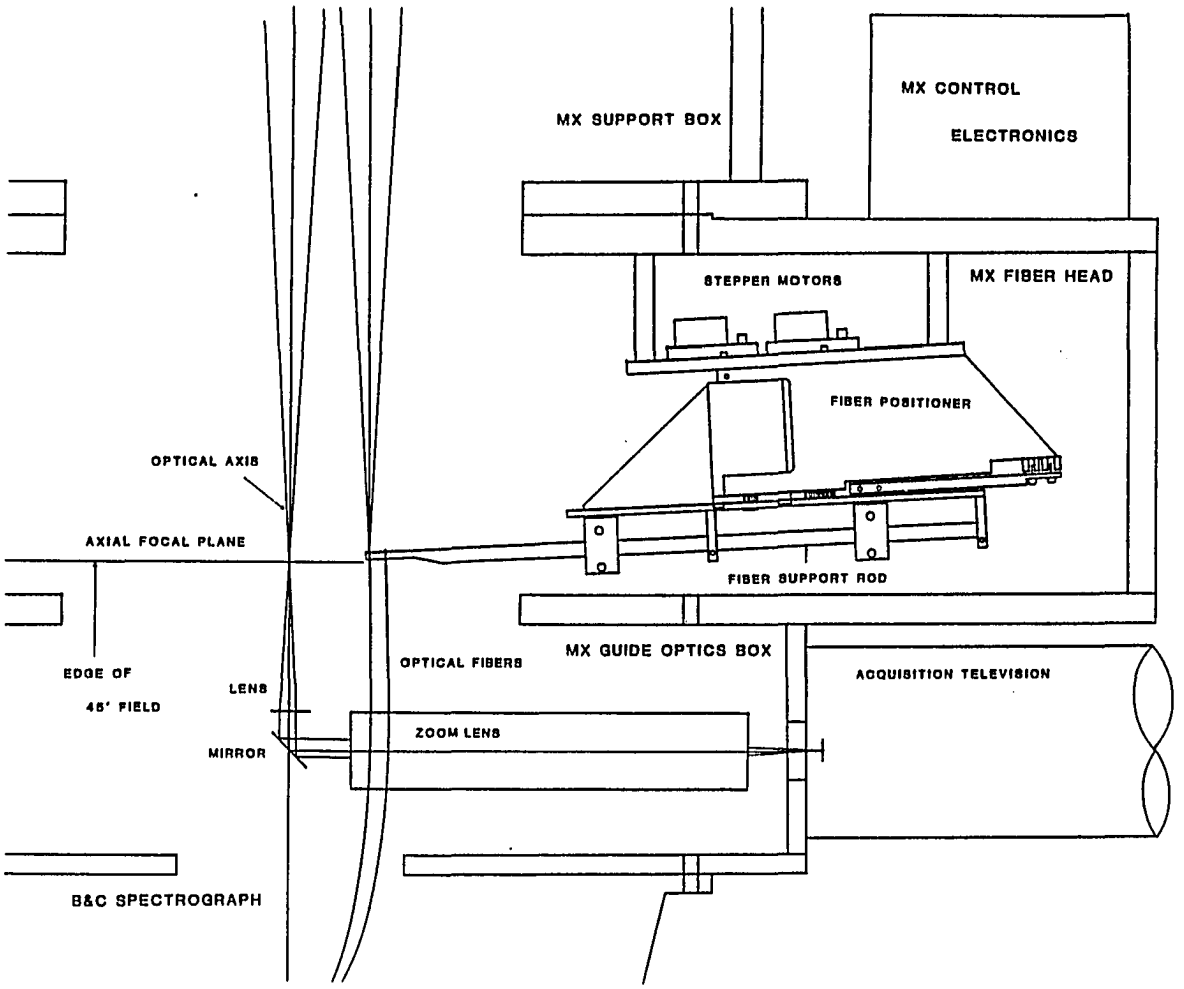

Figure 9: Side View of the MX Focal Plane Positioner Concept

This figure illustrates the operation of the fiber probes in the focal plane as seen from the side. One of the 32 probes is shown. The actual hardware is somewhat more complicated than the drawing indicates.

Positioner Details

In this section, I have tried to give enough details on positioner construction to allow useful design input to future instruments. Assembly details are not included. The motion of the positioners will be controlled by individual stepper motors geared down to drive a rack and pinion in the radial direction (r) and a gear sector in the theta direction (θ). The radial rack travels in a pair of linear ball bearings mounted on the theta positioner which itself rotates on a set of ball bearings. We have chosen to build the positioners with stepper motors because of the factor of three price difference compared to DC motors under servo control which we had previously considered. The original plan was to use Newport Research 850 series servo controlled DC motor positioners with built-in encoders. These lead screw based actuators offered 10 cm travel with 0.1 micron resolution at a price of $1000 each. The MX needs roughly 15 cm travel with only 5 - 10 micron resolution. The major cost difference between these two approaches is the optical shaft encoder required on each axis with the DC motor. The stepper motors allow counting the steps to determine the current position of the motors. In both cases, the position of the fiber must be determined relative to an optically determined base position. Both positioners require linear bearings to constrain the motion of the radial shaft. A Z-80 microprocessor system described in the next chapter will be used to control the stepper motors using CY512 motor controllers.

Prototype Positioners

Mark I. We have built and tested a single fiber positioner shown in Figure 10. This Mark I positioner has 170^{o} of rotation and 22 cm of radial travel, both of which are larger than the final design will require. The radial arm of the prototype positioner is a 6 mm diameter, stainless steel, 6 tooth cm^{-1} rack, driven by a 10 tooth pinion connected to a 48 step $revolution^{-1}$ motor geared down by 30:1 (Airpax K82430). The rotation section is similar, but uses half of a 10 cm diameter gear in place of the rack. Each step of the motor corresponds to 14 microns of radial motion. One arcsecond in the focal plane of the Steward 2.3m telescope is 100 microns. The rms repeatability of the positioner at any given step is 3 microns. The rms deviation from linear motion over 11 cm of travel was measured to be 17 microns. The peak deviation over the same travel was 50 microns. I thus expect to be able to position a set of fibers to within 0.5 arcsecond of each target object by dead reckoning from coordinates measured from photographic plates. Field alignment and guiding will probably be the dominant errors in fiber alignment with the target objects. Tests of the theta motion showed much larger positioning errors, apparently due to bending of the radial arm. I have calculated that the worst case deflection of the fiber arm would be 200 microns due to the change in gravity load at a zenith angle of 45^{o}.

Mark II. In Spring 1983, we built a second generation positioner with a stiffer radial arm. A larger (9 mm) rod is used to support the fiber in the focal plane, and a fine-toothed rack is clamped to this rod for the radial gearing. The Mark II positioner is shown in

Figure 11. The Mark II positioner was sufficiently stiff against self-deflection to make measurement difficult. A dial indicator, mounted on a 3/8" diameter rod on a magnetic base, deflected as much as the positioner in tests made by rotating the assembly 90^{o} with respect to gravity. Attempts to measure the stiffness by applying an external force to the radial rod were thwarted by back-driven rotation of the smaller stepper motors (K82236) through the gear train. At this point the positioner was deemed "stiff enough". By using a motor which has a low enough holding torque (2.2×10^{-3} Nm) to be back-driven through the gear train, a built-in safety clutch has been added to the system. If the positioner encounters a hard object while it is moving, ie. other positioners, loose dust covers, or the observer's head, the motor will simply stall without damaging the probe tip or gear train. The use of a small motor does not degrade the performance of the positioner. The acceleration response of a stepping motor is limited by the inertial load seen by the motor. The inertia seen by the motor is the load inertia divided by the square of the gear ratio. For small masses like a fiber support rod driven through a reduction gear train, the system is dominated by the inertia of the motor rotor. The acceleration response in a given drive configuration is basically that of the bare motor. Torque reflected to the motor is given by the load torque divided by the gear ratio. Again the small motor operating at a slow speed has no problem. The motor must have enough torque to overcome friction in the gear train and its own inertia at a given acceleration rate. While the fiber support rod was stiff enough for the MX positioner, it is important to note that the self-deflection of such a rod increases as

the cube of the unsupported length. The support rod stiffness may well dictate the positioner design in fiber spectrometers with physically larger fields.

Stepper motors and spur gears certainly do not represent the only drive technology available for fiber positioners. The DC servo motor and lead screw combination has already been described. Other possibilities include worm gears, chain or belt drives, friction drives, and Inchworm piezoelectric drives. We chose the spur gears and rack and pinion drives because of their low cost, ready availability, and lack of slippage. Non-reproducible errors in the gear train will always occur on the scale of one gear tooth or less. Combined with the known rotation of the stepper shaft, this eliminates the need for expensive position encoders. Possible encoders for fiber positioners include electrical or optical encoders on the positioner body as well as shaft encoders on various parts of the drive train.

The motion of the Mark II radial arm was measured with a Hewlett Packard laser interferometer by screwing a corner cube reflector to the end of the fiber support rod. All positioning measurements were made under control of a CY512 motor controller chip interfaced to an ASCII keyboard. A given position was always approached from the same direction to avoid lost motion in the gear train. A toroidal organic spring (rubber band) was used to preload the gear train against backlash. This will be replaced by a constant force spring in the final MX positioners. With 5.5 micron stepsize, the rms repeatability of a given step was found to be 4.3 microns. The overall positioning accuracy of the device is limited not by the 5 micron resolution but by

the linearity of the gear train. Duplicate interferometer readings were taken at 80 points spread over 11 cm of radial travel. A series of orthogonal polynomials was fit to the measured data points. The quadratic term was smaller than the linear term of the polynomial by a factor of 10^8 (ie. zero), implying that the rack gear is a remarkably linear device. The peak-to-peak deviation from a linear fit was 70 microns (14 steps) with an rms deviation of 21 microns. Studying the residuals reveals that the majority of the error is periodic with a period of roughly 2500 steps. One rotation of the pinion driving the rack requires 2400 steps. Therefore, the error is probably due to an eccentric pinion or to imperfections in the final stage of the stepper gearbox. With a peak-to-peak error of less than one arcsecond, the stepper motor and gear train should impose no significant restrictions on the pointing accuracy of the individual fibers. MX exposures requiring subarcsecond alignment will require active peak-up on the target field due to limitations in the measurement of celestial coordinates from plates and measurement of the 2.3m platescale.

The stepsize of each positioner is constrained by the desired resolution, positioner speed, and gear accuracy. The best positioning possible is ± 0.5 step with a perfect gear train or encoder feedback. The small stepper motors are capable of speeds up to 300 steps s^{-1}. Thus, with 5 micron steps, it requires 100 seconds for the radial positioners to extend to the full range of travel. Results of the Mark II test have led me to reduce the gear ratio on the production positioner to give 10 micron steps and 50 second travel time. The theta gear train was also adjusted to give a similar stepsize at the center of

the field. Limits on the end of positioner travel are set by optical slotted switches interupted by small flags on the moving parts of the probe. Logic connected to these optical switches inhibits the stepper drive output when a limit crossing is detected. This logic also allows the positioner to back away from the limit by turning the motor in the reverse direction. In the event of computer failure, followed by limit failure, a runaway positioner will simply run out of teeth on the drive gear and stop. This mechanical safety requires operator intervention to recover, but it prevents physical damage to the drive train.

Mark III. An engineering drawing of the Mark III final design positioner is shown in Figure 12. Each of the 32 positioner pairs will have 15 cm of radial travel and 25^{o} of rotation travel. A photo of the final design prototype positioner was to be shown in the next figure. Production delays in the machine shop have prevented completion of this probe. This design is much more compact than the earlier probes, and is stiffer against deflection. An extra gear stage was added to the azimuth drive to allow the same stepper motors to be used on both axes. The acquisition of stepper motors of the correct size and gear ratio turned out to be a problem if delivery time was to be less than six months. I am most grateful to the Steward Observatory Instrument Shop for their outstanding contributions to the design and construction of the MX positioners. A future paper will describe the testing of the Mark III prototype and our experiences with mass production on the N/C mill.

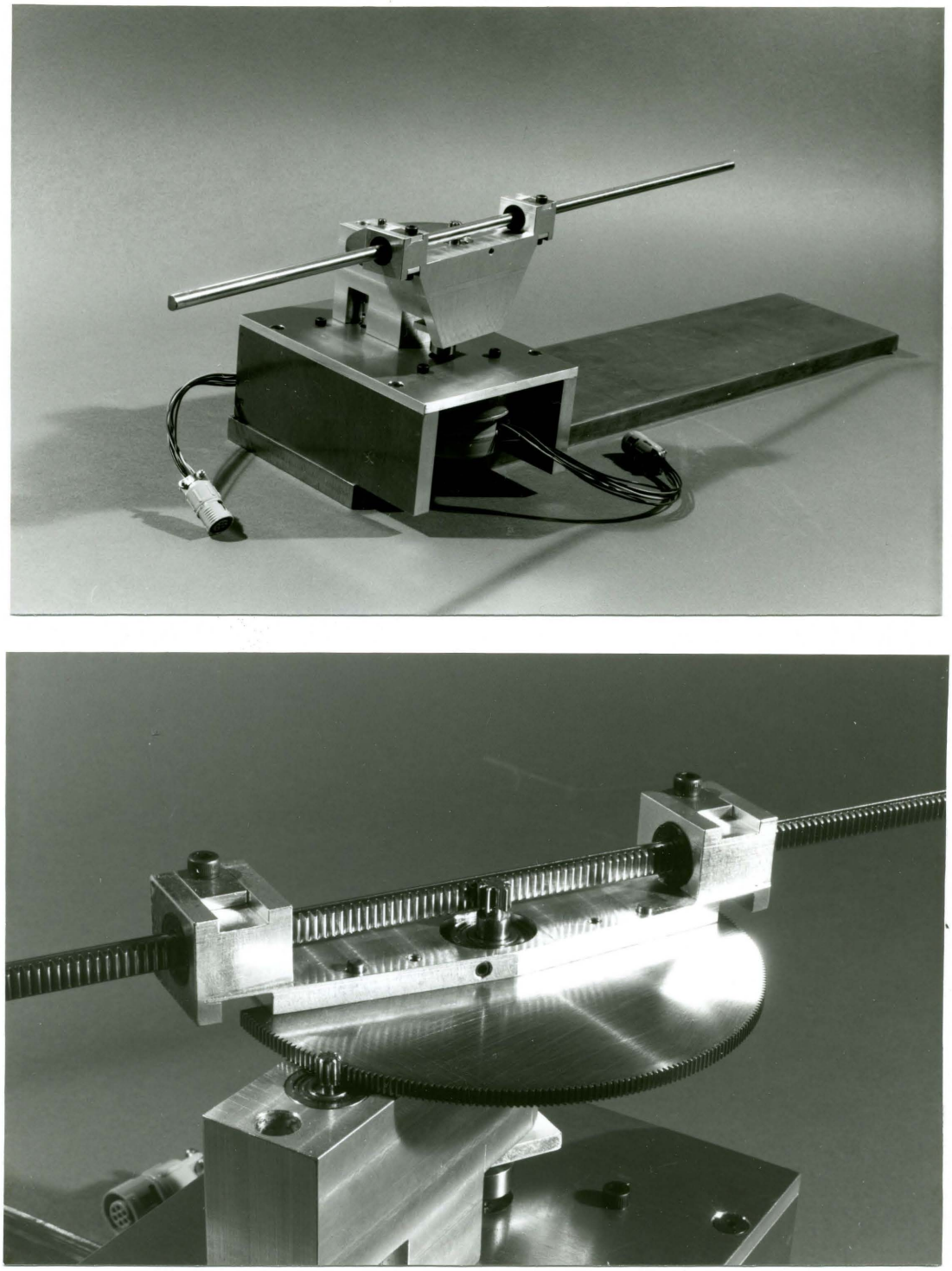

Figure 10. Mark I Prototype Fiber Positioner

This figure shows two views of our first design of a fiber probe driven by stepper motors. The fiber support rod serves a dual function as the rack for the radial drive.

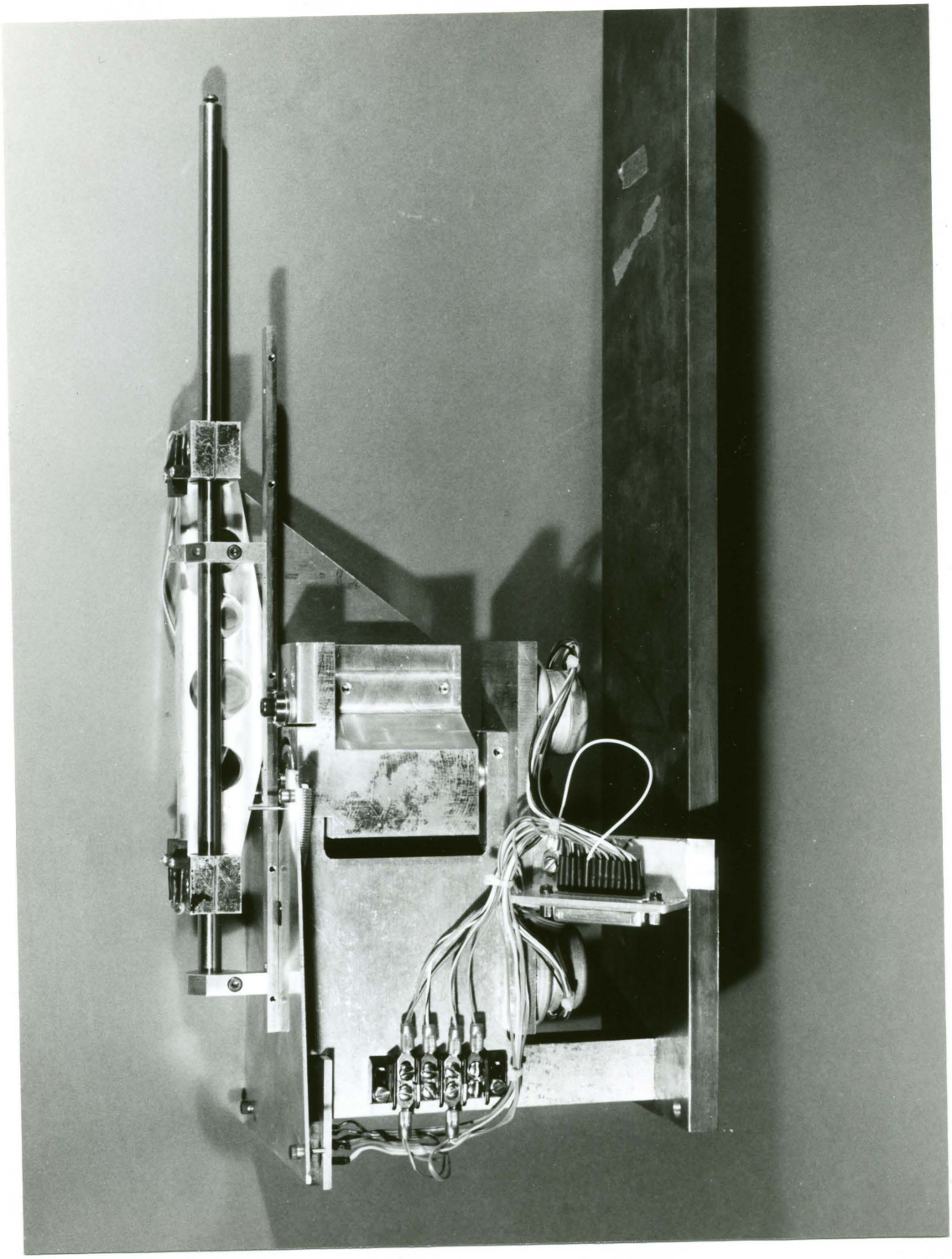

Figure 11. Mark II Prototype Fiber Positioner

This figure shows the improved fiber positioner with a larger support rod to increase positioner stiffness.

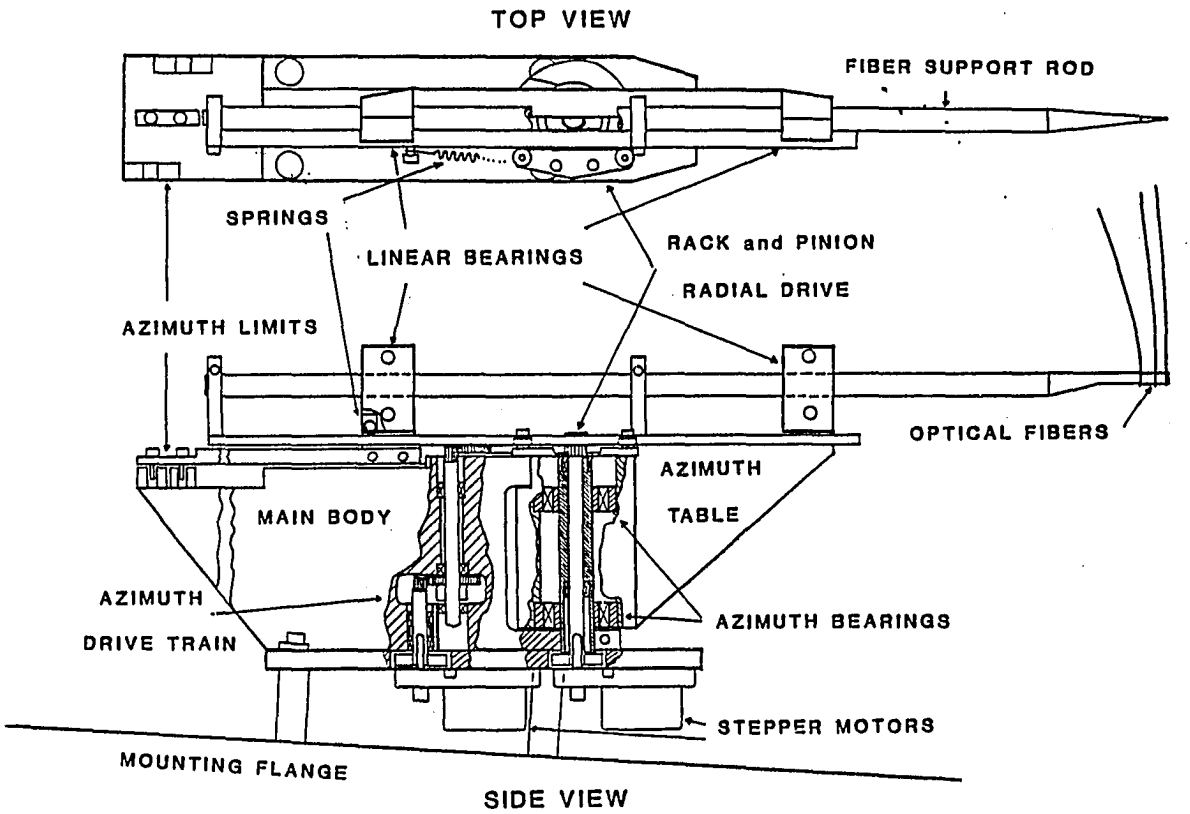

Figure 12. Engineering Drawing of Mark III Fiber Positioner

This figure shows the engineering drawing which evolved from the testing of the first two prototype positioners.

Coordinate System

Having chosen the fishermen-around-the-pond positioner layout, the question of a coordinate system must be addressed. The control microprocessor must convert a list of celestial coordinates (RA,DEC) to a list of motor step sequences that will allow each positioner to move to the correct position. The computer must also check the coordinates to avoid collisions before they occur. The collision avoidance problem will be discussed in the next chapter. Figure 13 shows the top view of several positioner arms in the focal plane. Only the moving parts are shown, as non-moving parts have no danger of collisions. This figure shows how several objects in the same sector of the field can be observed. Collisions are most likely to occur at the probe tips or at the inner radial bearing where the positioner occupies the largest angle as seen from the field center. The pivot radius of the positioners is chosen by a compromise between increased angular travel, which drives the pivot to a circle of larger circumference, and increased mechanical tolerance on the angular motion and deflection of the probe, which drives the pivot close to the edge of the field. The pivot position chosen is at the smallest diameter which will prevent the 5 cm tapered tip of the probe from entering the linear bearing at full retraction. Any single fiber positioner can reach from the outer edge of the field to just beyond the center. The 25 degree sector of rotation around the positioner pivot allows access to 20% of the focal plane if other positioners permit. This is sufficient overlap with the other 31 positioners to cover most nonuniform distributions of target objects. Figure 14 shows the range of travel of a single positioner and the

coordinate systems used to describe positions in the focal plane.

Two major coordinate systems are used with MX. A Cartesian (x,y) grid centered on the optical axis of the telescope is used to define the absolute positions of the target objects and the positioners. A local polar (r,θ) coordinate system which corresponds to their natural motions is centered on each of the fiber positioners. Each probe uses the field center as its angular zero point. This polar mapping is used when assigning target objects to each probe. Because the azimuthal and radial positions of the probes are coupled in the gear trains, a correction factor must be applied before the actual motor motions are calculated. The conversion equations between these two coordinate systems are given in Equation (5.1).

$$r_m(N) = [(X(N)-X_m)^2 + (Y(N)-Y_m)^2]^{0.5} \qquad (5.1)$$

$$\theta_m(N) = \arctan[(Y(N)-Y_m)/(X(N)-X_m)] - \arctan[Y_m/X_m]$$

where r is the distance from the positioner pivot, θ is the azimuthal distance measured from the field center, N is the target object number, and X and Y are Cartesian coordinates with the origin at the field center. The usual computational precautions must be taken to avoid the discontinuities in the tangent function.

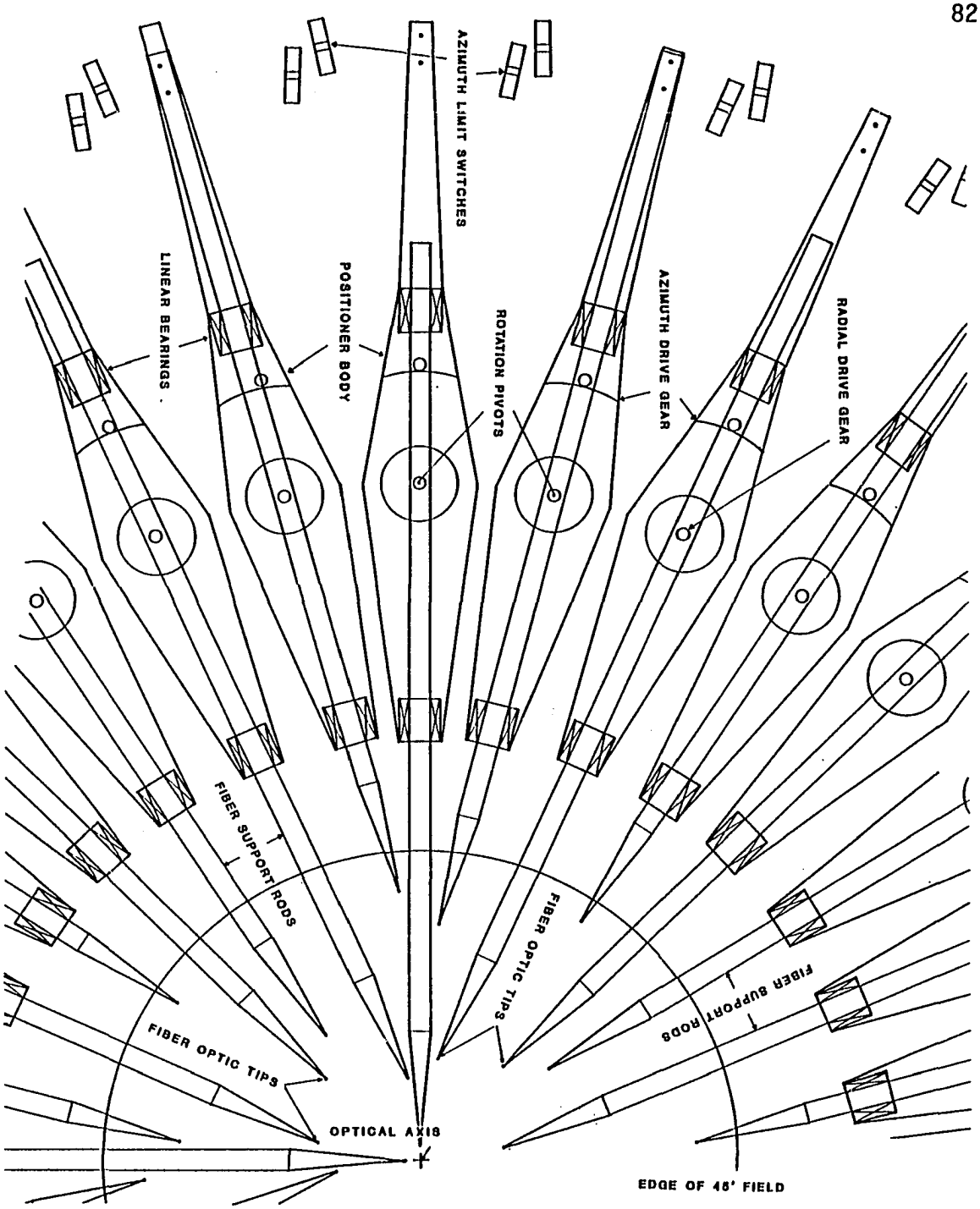

Figure 13. Top View of the MX Focal Plane

This figure provides a schematic view of a section of the MX focal plane as seen from above. The rotating portions of the fiber positioners are shown. Optical limit switches depicted as small rectangles set the maximum rotation of each fiber probe. The pivot positions, drive gears, and linear bearings which hold the fiber support rod are also shown.

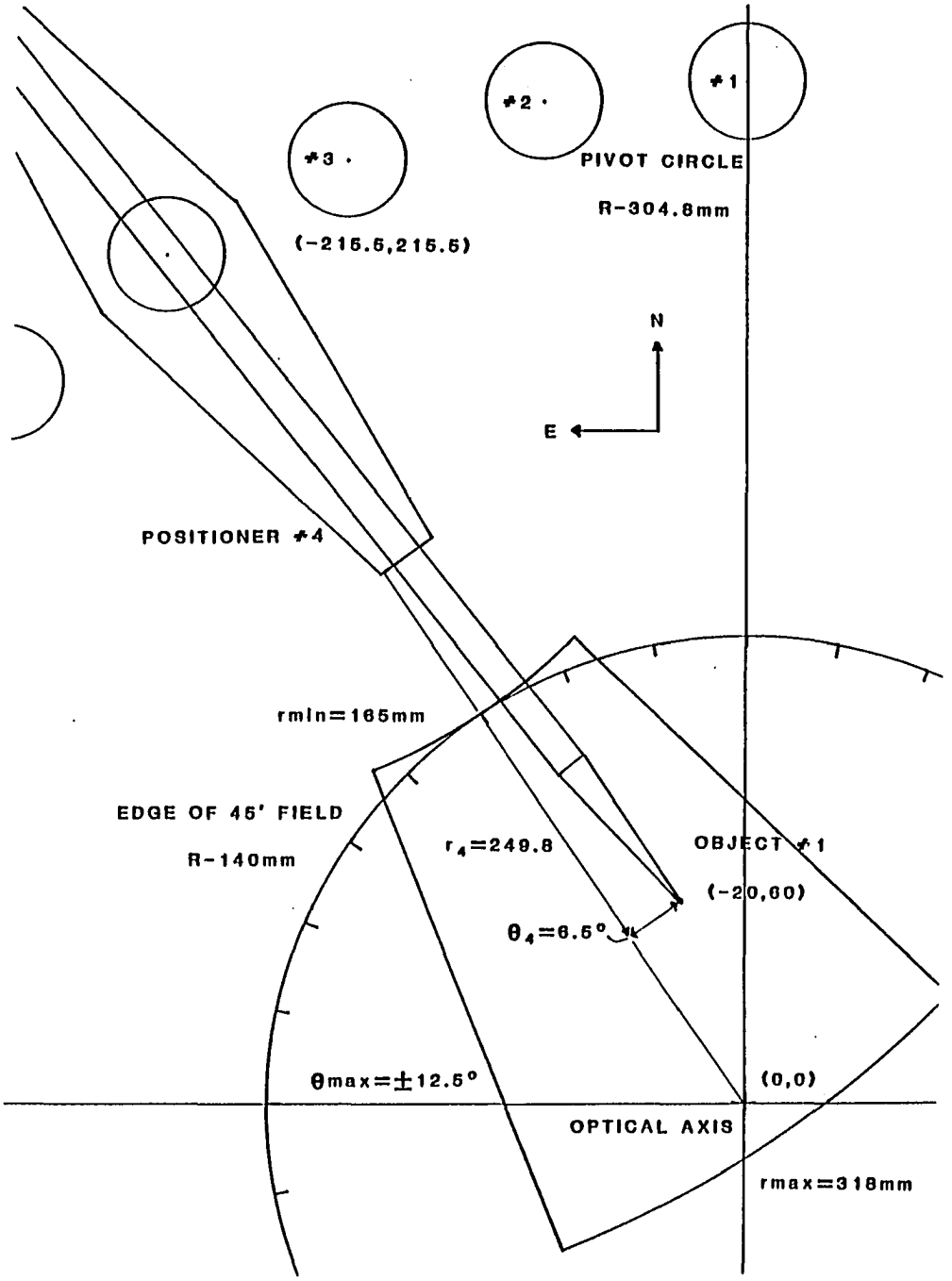

Figure 14: Range of Travel and Coordinate System

This figure shows the maximum range of travel in the focal plane of a single MX positioner. This range is set by the limit switches on the probe and assumes no obstruction by other probes. The azimuth travel is 25^{o} and the radial travel is 152 mm. This figure also shows the coordinate systems used in configuring the fiber probes. A global Cartesian system (x,y) and local polar (r_m, θ_m) coordinate systems are used.

Number of Objects to Observe

The number of simultaneous spectra that can be obtained is limited by the number of fibers and positioning probes that can be squeezed into the focal plane, and by the number of available target objects. Some minimum number of at least six fiber probes should be used to overcome system losses other than those in a normal spectrograph and to generally make the trouble of multiple object spectroscopy worthwhile. The maximum number of fibers that can be used is limited by the space occupied by each fiber and its support arm in the focal plane, at the spectrograph entrance aperture, and on the detector. The useful number of fibers is also limited near a thousand per square degree by the number of interesting objects on the sky and by our ability to deal with the resulting data rate. Based on Medusa experience, I have chosen 32 fiber probes as a convenient multiple of 2 that can fit in the focal plane at reasonable cost. For faint object work, some additional fibers to record sky spectra can be added to each probe without the need for additional positioning arms.

Field Size

The size of the telescope field of view covered by fibers should be as large as possible. A large field allows the study of many objects simultaneously. For clusters of galaxies or stars, a one degree field should be adequate. At $z = 0.1$, a typical rich cluster of galaxies will cover a 0.5 degree field. For nearby clusters and for supercluster studies, a larger field is needed. For rare or unclustered objects such as quasars, a very large field is needed. In general, the field should

be large enough so that several spectroscopic exposures are needed to cover all the objects of interest with the available number of fibers. Multiple exposures allow the problems of crowding of positioner arms to be alleviated by observing tightly clustered objects in several sequential exposures. Taking several exposures of a given target field also eliminates potential dynamic range problems that might arise from observing bright and faint objects simultaneously. A large field places stricter tolerances on the mechanical performance of the devices which position the fibers because of the increase in range of travel. The MX will cover a 45 arcminute diameter field at the Ritchey-Chrétien focus of the 2.3m telescope. This size was limited by the possible range of positioner travel, the optical aberrations and vignetting of the telescope, and by physical size constraints of the instrument mounting surface.

Third-order aberration calculations were carried out for the R-C focus of the Steward Observatory 2.3m telescope. The results of these calculations are summarized in Table 3. All calculations were done from the nominal optical configuration assuming a standard Ritchey-Chrétien design, since the actual mirror figures were unavailable. The optical calculations show that the focal plane has a radius of curvature of 1.67m. This was confirmed by the measured value of 1.4 m from a focus plate kindly provided by Dr. E. Roemer. Field curvature causes the position of the best focus image at the edge of the field to be 6 mm higher (concave toward incoming light) than at the axial focus position. To maintain sharp images and avoid loss of intensity due to focus errors, the heights of fibers must be adjusted according to radial

distance from the optical axis. Fortunately, the curvature is not so severe that z-axis actuators are needed. Actuating the positioner arms in the z-direction would add unnecessary expense and complication. The 32 positioner arms have been divided into two groups so that the tilt of every other arm compensates for the curvature by lying tangent to either the inner or outer portion of the focal surface. The focus curve for best images with allowable error tolerances and the assigned positioner tilts are shown in Figure 15. The slopes of the positioner tangents were determined by a least squares fit to the focus curve in the region of interest. Figure 16 shows the axial view of the range of travel of several positioners in the inner focal plane group. These regions outline the normal working range of the probes for minimum blockage of other positioners and best image quality. The inscribed circles show the locations where the operating plane of the positioners intersects the best image surface. Figure 17 shows the corresponding information for the outer focal plane positioners. All 32 probes will be mechanically the same, but will be mounted at different angles to reach the correct portion of the field.

The image size at the edge of a 45 arcminute diameter field was calculated, neglecting seeing, to be 0.6 arcseconds rms in the best image surface. The image size at the same radius in the axial focal plane was found to be 2.4 arcseconds. Higher order aberrations will make some modifications to these figures, but the images are of more than sufficient quality to accommodate spectroscopy over a wide field. Optical distortion of the platescale across the field is predicted to be of order 0.1 arcsecond and is henceforth neglected.

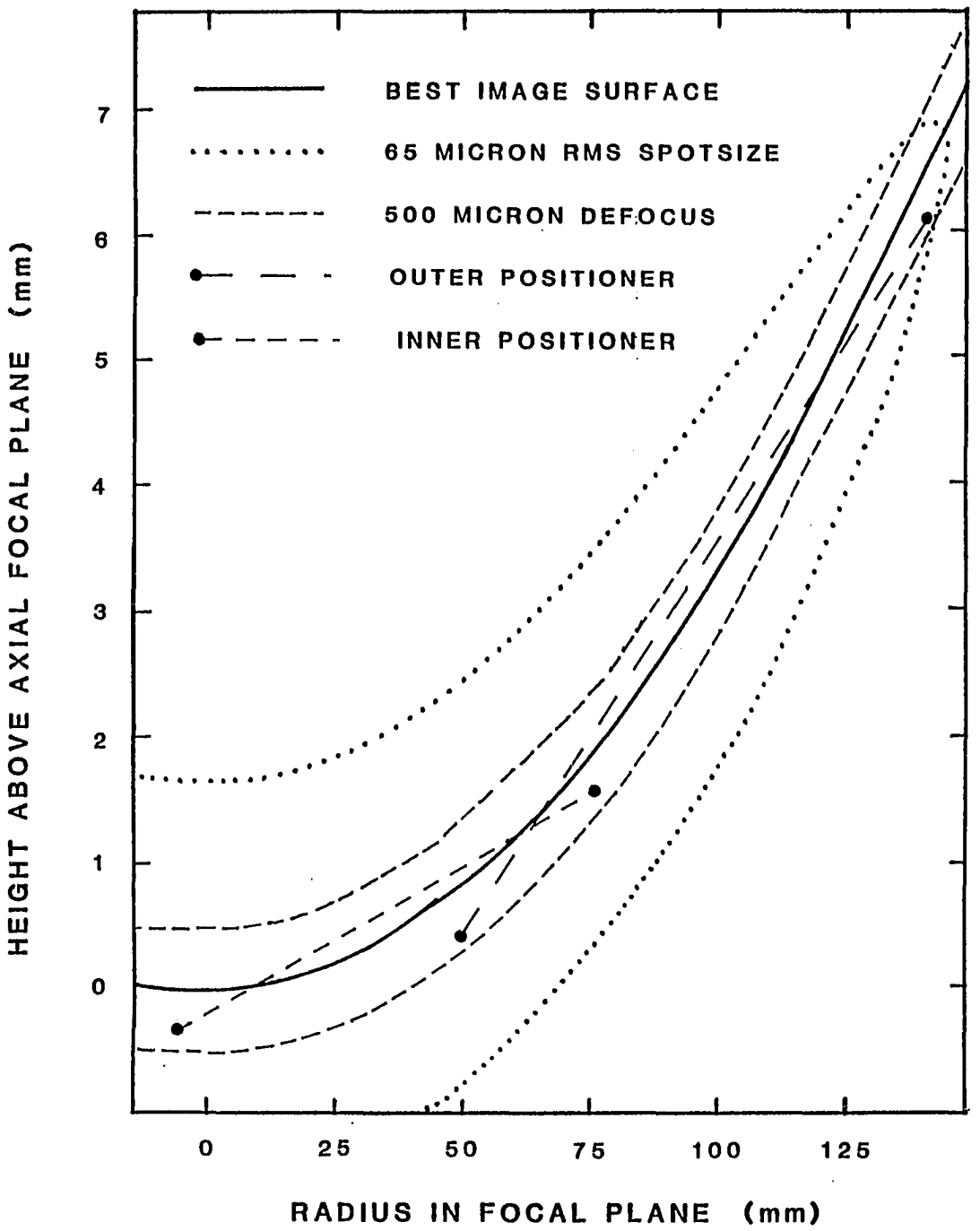

Figure 15. Field Focus Curve

This figure shows the field focus curve for MX positioner arms in the 2.3m focal plane. Height of the best-focus image plane above the axial focal plane is plotted against radial distance from the optical axis. Error tolerances on the image size, and the path of the two groups of positioners are also plotted.

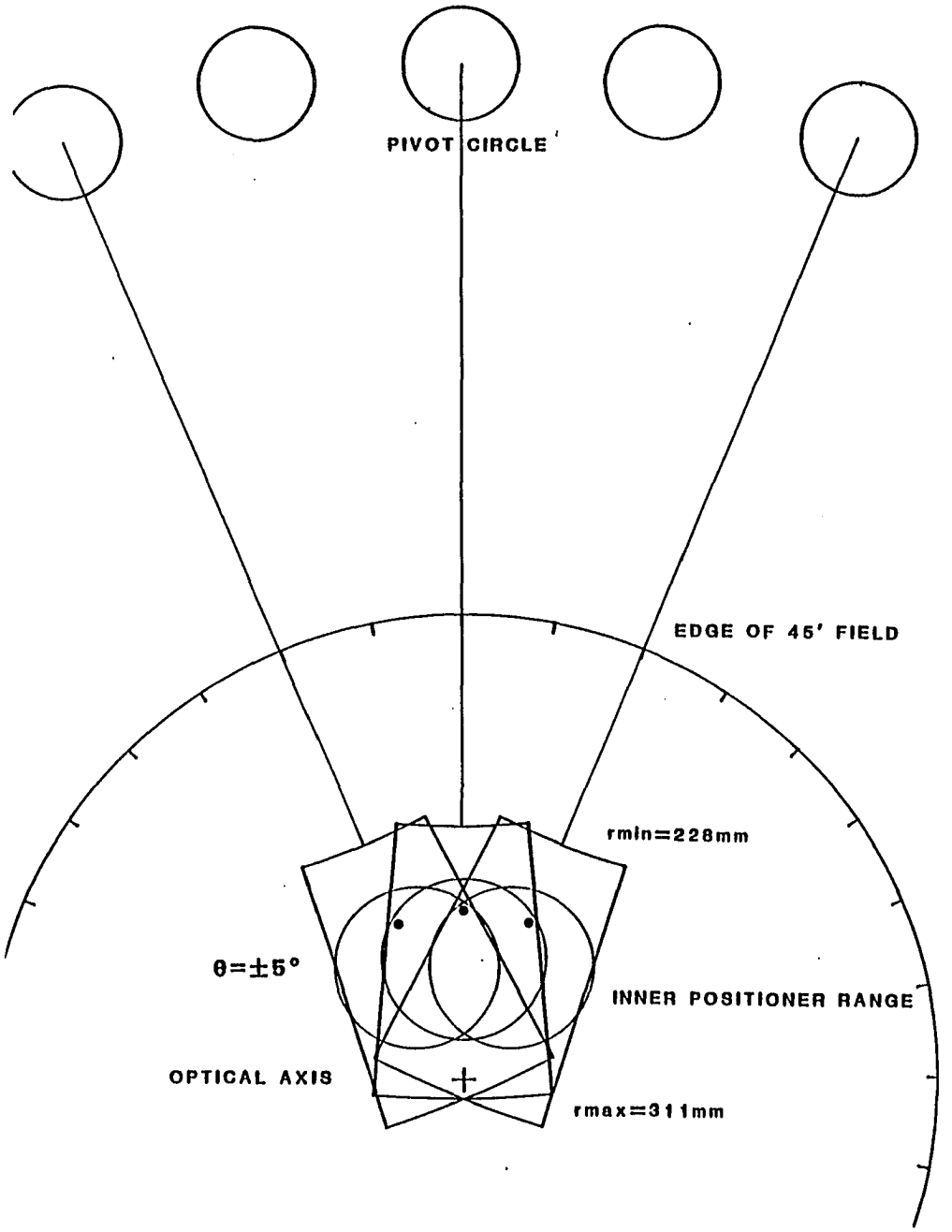

Figure 16. Inner Focal Plane Positioner Coverage

This figure shows the range of operation of three of the inner 16 focal plane positioners. The trapezoidal shape outlines the normal range of travel. The cross indicates the center of the focal plane. The dots mark the optimum observing position for each probe. The small circle marks the locus of intersection of the positioner plane with the best-focus image plane.

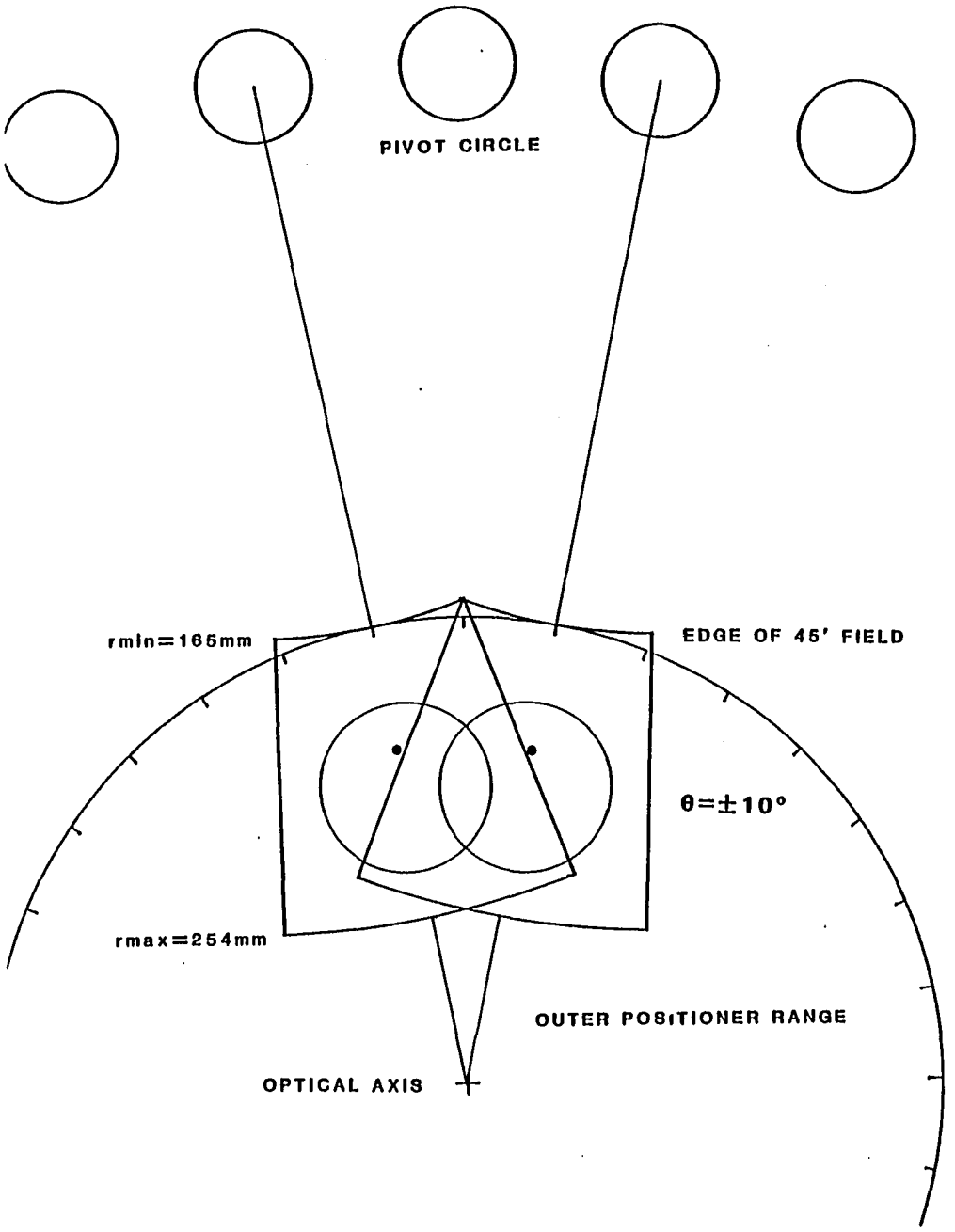

Figure 17. Outer Focal Plane Positioner Coverage

This figure shows the range of operation of two of the outer 16 focal plane positioners. The trapezoidal shape outlines the normal range of travel. The cross indicates the center of the focal plane. The dots mark the optimum observing position for each probe. The small circle marks the locus of intersection of the positioner plane with the best-focus image plane.

Table 3. Optical Parameters and Aberrations

This table lists the optical parameters and the calculated third-order aberrations of the Steward Observatory 2.3m (90") telescope. A standard R-C design was assumed. Physical dimensions were taken from engineering drawings.

Optical Element Specifications	
focal length of primary	607 cm
diameter of primary	229 cm
focal length of secondary	-230 cm
diameter of secondary	65 cm
effective focal length - R-C	2062 cm
focal ratio of R-C focus	f/9
separation of primary and secondary	448 cm
back focus distance	97 cm
sky baffle diameter	54 cm
height of baffle above focal plane	325 cm
plate scale	9.8 arcsec mm^{-1}
Results of third-order calculation	
medial focus radius of curvature	1.67 m
measured radius of field curvature (concave)	1.4 m
rms spot size at radius of 22.5 arcmin	
in best image surface	59 microns
in axial image plane	240 microns
distortion at 22.5 arcmin radius	12 microns
sky baffled field diameter	19 arcminutes
unvignetted field diameter	34 arcminutes
vignetting of 45 arcminute field	<20% at edge

Closest Approach of Fibers

In addition to allowing observations over a wide field-of-view, the MX must also be able to observe objects which are closely spaced on the sky. This is important for observations of galaxies or stars in dense cluster cores and for spatially-resolved spectroscopy of nearby galaxies. Medusa has been used to observe multiple nuclei and the halo of the cD galaxy NGC 6166 at the center of A2199. Fibers in the aperture plate were spaced as close as 10 arcseconds with 3 arcsecond apertures. In positioner geometries which assign each probe a specific section of the focal plane, the study of closely spaced objects is limited by the number of probes that can access a particular spot. In positioner geometries which allow multiple probes to enter a specific section of the focal plane, the limit is set by the distance of closest approach of the fibers and by the angular extent of neighboring probes. The distance of closest approach is set by the diameter of the probe tip. If 2 mm spherical microlenses are used, the tips of the MX probes will be 2.4 mm wide allowing a minimum approach distance of 25 arcseconds on the 2.3m telescope focal plane. Objects closer than this separation must be observed in a second exposure with the probes rearranged. Taking multiple exposures is usually necessary when observing rich clusters where close spacing is most likely.

A crude estimate can be made to indicate how frequently the MX will miss galaxies in a cluster because they are too close to other galaxies. Struble and Rood (1981) provide the following equation:

$$G(s_{max}) = 1-\exp(-n_o \pi s_{max}^2) \qquad (5.2)$$

where G is the probability that the nearest neighboring galaxy lies

within angular distance s_{max} (mm on PSS). The galaxies are assumed to be distributed randomly with average surface density n_0 (per square mm). Assuming the clusters studied by Struble and Rood are typical, I considered them as the candidate observing targets. A typical cluster at redshift 0.1 would have 200 objects within a 24 arcminute field. Table 4 shows the percentage of galaxies with neighbors closer than s_{max} (arcsec) tabulated as a function of s_{max}. Thus for a random galaxy density of 0.44 galaxies arcmin^{-2}, I find that 29% of the galaxies will have a neighbor closer than 30 arcseconds. Considering that six exposures would be required to measure all the redshifts in this cluster, a 30% obstruction loss in any given exposure is not of great concern. The non-uniform distribution of galaxies in a cluster could increase the obstruction of neighbors by a factor of order two. Only in observing very tight clusters of objects, say 50 objects in a 5 arcminute diameter field, will the MX be likely to become packing-limited rather than probe-limited. This would argue for increasing the number of fiber probes. Unfortunately, the number of probes is limited by available detector area and by mechanical constraints in the focal plane. For studies of tightly packed objects, a transfer lens or the f/45 secondary can be used to magnify the field-of-view so the fibers and their closest approach distance appear smaller on the sky. This is called the "dense pack" mode of operation.

Table 4. Neighbor Probability

This table lists the probability (G) of finding a neighboring galaxy within a given radius (s). This is related to the fraction of galaxies in a rich cluster which would be blocked by the MX positioner arms in a single exposure.

Radius = s_{max} (arcseconds)	Probability = G (percentage)
05	01.0
10	03.8
15	08.3
20	14.3
25	21.4
30	29.3
35	37.7
40	46.1
45	54.2
50	61.9
55	68.9
60	75.1
65	80.4
70	84.9
75	88.6
80	91.5

generating equation (5.2):

$$G(s_{max}) = 1-\exp(-n_o \pi s_{max}^2)$$

parameters for the typical cluster:

redshift	z = 0.1
size = Abell diameter	24 arcmin = 20mm on PSS
number of objects	200

Alignment, Guiding, and Acquisition

One of the major problems in the design of MX is how to correctly align 32 optical fibers on the images of 32 galaxies in a short period of time and keep them there for a long spectroscopic exposure. This section describes some of my solutions to this problem.

Guiding

Guiding for multiple object spectroscopy is similar to guiding for direct imaging in the sense that nearly all of the focal plane is being used and "spillover" light from a reflective entrance aperture is generally not available. Reflective slits cannot be easily used because of crowding of other positioners which leave no space for the optics. One possible, but not very practical, technique for spillover guiding would be to mount flexible coherent imaging conduits directly above each radial arm. This flexible bundle with microlens optics could reimage the slit at a remote camera. The most accurate form of guiding for multiobject work requires that one or more of the probes be equipped with an imaging fiber bundle. Several of the probes would then be dedicated to looking at guide stars while their neighbors looked at galaxies. Since all of the probes operate in the same coordinate system, this technique should be limited by the accuracy of the coordinates and the seeing. If an offset guider probe is available, it can be used for guiding, freeing the fiber probes for spectroscopy. To be effective for field acquisition, the guider probe must have a precisely known offset relative to the fiber focal plane.

Since the 2.3m telescope did not have an accurate offset guider available, and it was desirable to use all available probes for spectroscopy, a third alternative was chosen for MX. Unlike the photographic plates or aperture plate system, the fiber probes do not completely block the focal plane. Much of the incident light is not collected by the fibers and continues past the probes. It is possible to collect this light with a lens and reimage the original focal plane for guiding. The original MX configuration will reimage the center of the focal plane onto the acquisition television. This requires a star in the center of each field observed. In practice, finding a 15th magnitude star near the center of a 45 arcminute field is not a problem. An offset guider with reimaging optics could also operate below the focal plane. This would allow a wider range of guide star selection.

Probe Alignment

To align the fiber probe coordinates with the acquisition and guiding optics, each fiber probe will be equipped with a downward looking fiber illuminated by an LED. When moved to the center of the field, this fiber will appear like a star image, allowing the proper offsets to be added to the coordinate system of that probe after the illuminated fiber has been centered on an index mark. Because of the limited speed of the individual positioners, this alignment procedure will take over an hour to complete. Therefore, once the offsets are known for all positioners, the zeropoints of the optical limit switches on the probes will provide index points for the local coordinate system. After power-up, all positioners can be retracted to the back limits to

reinitialize the coordinate system. It may be desirable to maintain coordinate offsets in nonvolatile memory to check on zeropoint stability from one day to the next. Corrections will also be made to the coordinate system based on the temperature of the probes and which of several fibers on each probe is being used.

Acquisition Optics

Two optical systems will be used for field acquisition. First, a wide-field eyepiece and folding mirror in the instrument support box will be used to set the telescope offset and initial focus on a bright star. This Erfle eyepiece will also be used if the observer wishes to verify the field against a finding chart. Final acquisition will be carried out by centering the guide star in the one arcminute field of the guide optics. The guide optics consist of two achromatic lenses used to relay the central portion of the spectroscopic focal plane onto the acquisition television at a magnification of 2.5x. A two-element achromat (100 mm f.l.) is used as the first lens to recollimate the light from the slit. The simple lens contributes some field curvature, but provides the largest physical clearance for the fibers and probes. A folding mirror directs the beam off to the side of the MX housing where a camera lens (250 mm f.l.) is used to reimage the focal plane onto the intensified acquisition television camera. The camera lens provides easy focusing capability and makes the optical train more compact at a given focal length. A zoom lens may be used to vary the scale of the guide optics. A diagram showing the folded optical path is given in Figure 18.

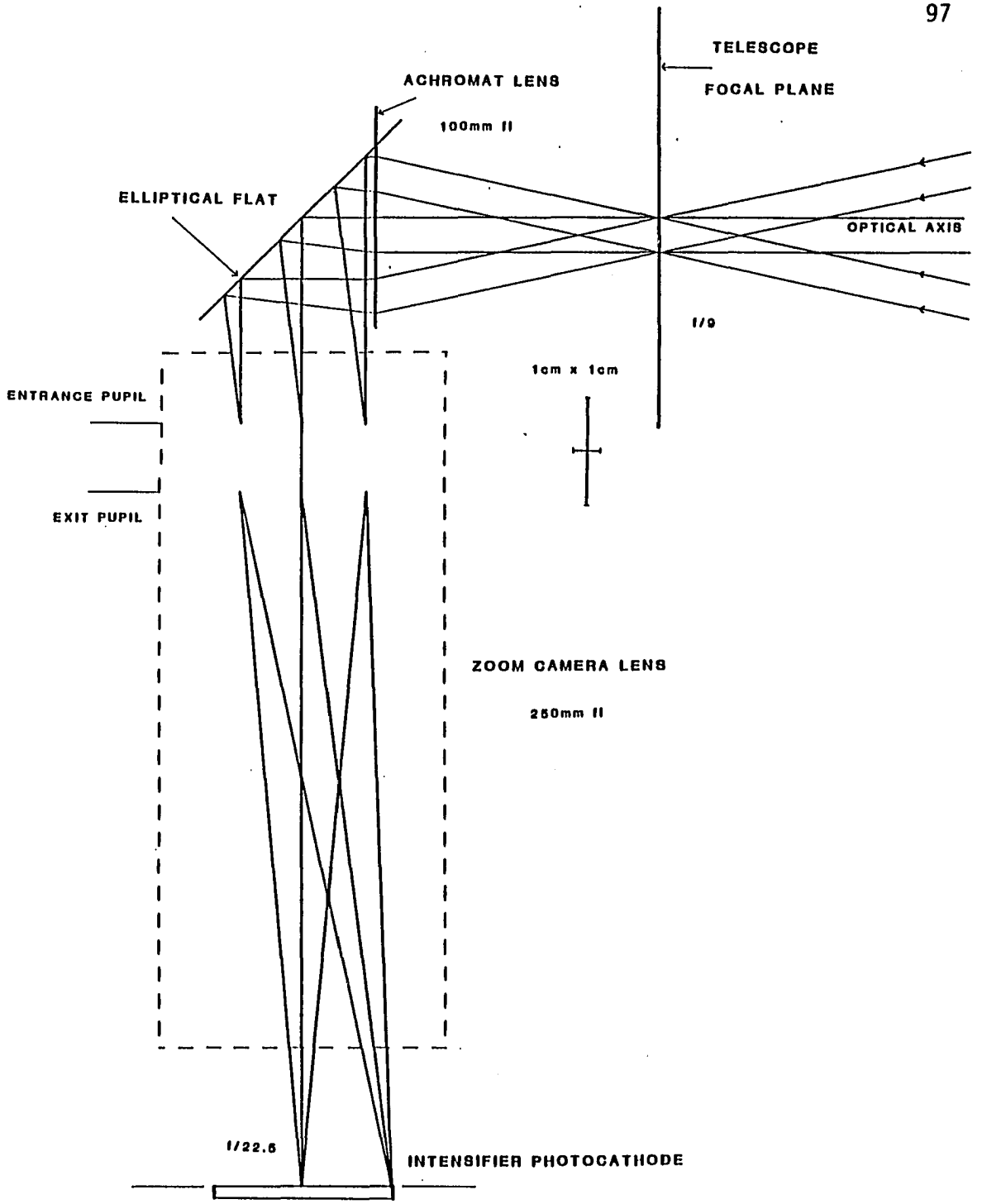

Figure 18. Guide Optics Diagram

This figure shows the optical layout of the MX guide optics. Light passing through the primary focal plane is collimated and magnified at an auxiliary focal plane viewed by the intensified acquisition television. The transverse scale of the light beams has been magnified by a factor of four for clarity.

Focus

Focus in the fiber focal plane will be set with a knife-edge test. Several of the probes will have small knife-edges mounted beside the fibers in the focal plane. Defocusing the guide optics will allow observation of the pupil during the knife-edge test while the probe scans the image. Once the guide optics have been set to the proper focal position, the telescope can be refocused by observing a star on the television. A major advantage of reimaging guide optics is the ability to use knife-edge focusing rather than rastering single fibers across the image or viewing the image with a coherent fiber bundle.

Field Alignment

When acquiring a new field, the appropriate guide star will be centered in the guide optics. If some probes are also looking at guide stars, the presence of guide stars will be verified at the star fiber outputs. The alignment of the probes as a group can be verified by using a folding mirror to send the integrated light at the spectrograph slit to a photomultiplier or TV. If the spectroscopic sources are too faint, stars in the same field can be briefly observed to verify guide star centering. With more sophistication, the positions of the individual fibers on the target objects could be verified. The fiber slit might be imaged on a detector as in the peak-up mode. After initial setup of the instrument, field rotation will be assumed correct. An index point on the 2.3m telescope instrument rotator controls the overall positioner rotation. Multiple index points would allow rotation of the entire instrument to observe a given object through several

fibers over the course of a series of long integrations. Observations through more than one fiber should help eliminate any peculiarities associated with the transmission of a given fiber and allow improved spectrophotometry and sky subtraction.

Peak-Up of Positions

For some fields, the locations of the target objects may not be well enough known to position the fiber probes accurately. In this case it is desirable to "peak-up" the individual positioners for maximum signal on each object. Peak-up is accomplished by observing the output of each fiber while moving either the telescope or the fiber probes in a raster pattern around the position of the target object. A time sequence of measurements of the fiber output will reveal the position of maximum signal. After this process is complete, the fiber probe is set to the position of the observed maximum.

One way to look at the fiber output without dispersion is to replace the spectrograph grating with a plane mirror. Each spectrum at the detector is then reduced to a single dot and the slit assembly is imaged as a row of dots corresponding to the individual fibers. Now, by clocking the CCD detector (TDI) or by tilting the grating mirror, the image of the slit can be moved across the detector simultaneously with the rastering of the fibers on the sky. The maxima of the resulting traces can then be used to optimize the fiber positions. At low spectroscopic dispersions (100), this process might require 10% of the available observing time to achieve the necessary signal-to-noise and would only be used when needed. At higher dispersions, the relative

time used would be proportionally less, and peak-up might be used in a routine fashion.

The challenge of implementing the peak-up mode of MX is to make the hardware and software efficient enough that the peak-up time is determined by the number of photons available from the target objects. The major tasks are:

1) replacing the grating with a mirror
2) locking the telescope pointing
3) rastering the probes
4) scanning the image on the detector
5) recording the scanned image
6) analyzing the image for the positions of maximum signal
7) feeding the proper coordinates back to the probes

This requires that the MX, telescope, detector, observer, and their controlling computers all work in synchronism, and may well represent the most challenging software problem associated with MX. While peak-up is being considered in all aspects of the MX spectrometer design, time constraints will certainly prevent its implementation until other parts of the system are fully operational in the "seat-of-the-pants" positioning mode which relies on stable positioners and accurately measured coordinates.

Positioning Errors

In conventional single object spectroscopy, acquisition and guiding are accomplished by observing the light of the target object reflected from the edges of the spectrograph entrance aperture. When

observing 32 objects, a reflective slit for each object is not a practical solution to guiding or alignment. Instead, the fibers must all be positioned by dead reckoning and aligned with the star field as a group. Many sources of error exist here which are not normally a problem in optical spectroscopy, but which sometimes occur when working in the infrared or at other wavelengths where the source is not visible, and offsetting of the telescope is required.

Misalignment of the fibers on the target objects can cause a loss of light which is just as serious as low quantum efficiency, focal ratio degradation, or other problems which degrade system throughput. The most fundamental positioning errors for multiobject work result from inaccurate coordinates measured from a photographic plate. Galaxy positions can be measured on the Palomar Sky Survey plates to an accuracy of 0.5 arcsecond. Plates from the prime focus of the 4-meter telescope or other high quality photographs yield better coordinates, but are not always available. Since the coordinate measurements in epoch 1950 are made relative to reference stars, which hopefully have small proper motions, it is necessary to perform a complete transformation to the epoch of observation. Precession over 30 years causes relative coordinate shifts of up to 10 arcseconds over a 45 arcminute field. The first-order term in this error is simply a field rotation. The reason Medusa did not have to worry about this problem is that the rotation of the aperture plate was set in an empirical fashion to maximize the signal. Assuming the telescope is working properly, the MX positioners should have absolute pointing within an arcsecond, and somewhat better relative positioning (0.25 arcsec). Another possible

error is differential refraction across the field-of-view. The amount of refraction, R, and the differential refraction, ΔR are given by (Allen, 1976):

$$R = 58.3"\tan(z_a) - 0.67"\tan^3(z_a) \qquad (5.3)$$

$$\Delta R = 58"[\tan(z_a) - \tan(z_a+\Delta z_a)]$$

where z_a is the zenith angle.

This gives monochromatic differential refraction of one arcsecond in a 45 arcminute field at a zenith angle of 45^o. This correction can easily be included in the MX coordinate transformations and should not change in a significant fashion during exposures less than three hours. Watson (1984) discusses the problems of refraction when implementing fibers on a Schmidt telescope with a six degree field-of-view. Chromatic image spread by atmospheric refraction is of course a problem, but is no different for fibers than for conventional spectroscopy with a circular entrance aperture.

The telescope and instrument can introduce additional positioning errors. The telescope plate scale changes slightly with temperature. The change in plate scale is caused by a shifted focal position when the lengths of the telescope tube and mirror cell change ($3x10^{-6}$ $^oC^{-1}$) and by the change in focal length of the fused silica telescope optics ($5x10^{-7}$ $^oC^{-1}$). The positioner calibration also changes due to a finite coefficient of thermal expansion ($2.5x10^{-5}$ $^oC^{-1}$ for aluminum). The change in length of the positioner rods is the only significant factor to consider in correcting the focal plane coordinates for temperature. Both the mounting flange and the individual positioners for MX need to be made stiff enough that deflections due to

the changing gravitational field are insignificant. As discussed in the previous section, the fiber probes must also account for focus changes across the field. The permissible errors in focus are larger than in transverse position because of the slow divergence of the f/9 beam. Fortunately, all of the above errors can be calibrated or calculated away to at least first order. The next chapter describes the design of the hardware and software aspects of the positioner control system.

CHAPTER 6

THE MX SPECTROMETER: POSITIONER CONTROL

This chapter will describe the electronics and computers which control the motions of the MX fiber positioners. In order to reconfigure the MX probes between spectroscopic exposures, it is necessary to move all 64 stepper motors simultaneously. This is clearly a task for a computer. We have chosen to use a pair of microprocessors to separate the hardware interface function from the user interface function. The MX fiber head will have an onboard Z-80 microprocessor which will control the steppers and communicate with the outside world via one or more serial ports. The Z-80 mounted on the spectrograph head will be designated the "instrument micro". In the control room, a second Z-80 system will be responsible for communications with the instrument micro, the observer, the CCD controller, and the telescope controller. This computer is called the "support micro".

Support Microprocessor

The principal purpose of the support micro is to provide administrative support for the rest of the system. It provides communication and calculation capability for other parts of the MX network, and is therefore code named "Starbase 32". The support computer will include a terminal, video graphics display, floppy disk drives, and four serial I/O ports. The support microprocessor is a single-board Z-80 system built by DY-4 Systems, Inc. (DSTD-764).

The Z-80 board includes CPU, 64K memory, disk controller, and 4 channel serial I/O. We have added a STD-bus video graphics card also built by DY-4 (DSTD-777A). This card is built around the NEC-7220 graphics processor chip and supports color graphics with 640 x 480 pixels. The support computer also has a pair of 8" single-side, double-density floppy disk drives by Shugart (SA801R). A terminal (Intecolor 2400) and a color video monitor are also part of the support computer package. Figure 19 shows a schematic layout of the support computer software. The support software will be written mostly in compiled CBASIC.

Communication

The support micro must communicate with the instrument micro in order to transfer commands, target coordinates, and positioner status. A serial link between the two computers allows the operator to interact with the motion of the positioners without allowing hardware damage if an inaccurate command is given. The instrument micro will reject illegal motion commands. Command transfer between the two computers is designed so that either machine could be replaced by an ordinary terminal or by another computer with suitable serial I/O. Talking to the instrument control micro with a "dumb" terminal would, of course, require large amounts of typing and a detailed knowledge of the system operation. The support computer acts as an intelligent buffer between the astronomer and the details of MX control. In addition to providing information and processing power, which facilitates control of the instrument, the support computer takes care of preparation of coordinates for future observations. The support micro supplies

information to the astronomer via the terminal and a video display. Display of both probe positions and object positions on the video display is useful when observing many objects simultaneously, otherwise astronomers with fewer than 16 fingers might become confused. In what might be called "phase two" software development, the support micro will also communicate with the CCD controller and the telescope computer via serial links to gain information needed to adjust the assigned probe coordinates for maximum signal, and to record relevant exposure information on tape or disk headers. The support micro will also take care of calibration and diagnostic routines for the instrument, as well as downloading software to the instrument micro.

Coordinate Processing and Storage

After communication, the second major task of the support computer is to allow the astronomer to prepare coordinates of target objects for each field to be observed. When the MX spectrometer is completed, the only items requiring advance preparation before observing will be measuring the positions of target objects, processing the celestial coordinates for use by the MX, and preparation of finding charts. The measuring process will likely be automated since thousands of accurate coordinates will be needed on each observing run. Automatic measurement will provide sufficient numbers of target coordinates to allow backup programs to be carried out under poor conditions and very faint clusters to be studied efficiently when excellent conditions prevail. The support computer will handle all the manipulations needed to convert a master list of celestial coordinates (RA,DEC) for target

objects in each cluster into a list of 32 (x,y) positions to be observed in each individual exposure. All relevant astronomical transformations, such as precession and gnomic projection, are performed on a given cluster list. Then, the support micro derives the list of 32 objects from the master list with some interactive observer input to indicate the objects of choice. At the time of observation, the list of 32 object positions is sent to the control computer. Final conversion of x,y coordinates into a certain number of steps for the motors is done by the instrument control micro.

Probe Target Assignment

To choose probe - galaxy assignments the astronomer will provide a list of 32 or more galaxy targets in each field. The list will include right ascension, declination, coordinate epoch, magnitude (if known) and a priority code (0-9). Objects which are most important for reaching observational goals are assigned a higher priority code in the list. This list may be typed into the support computer directly, and edited, or it may already be stored on floppy disk. The list must also include a suitable guide star which will be located at the center of the field. The first step is the transformation of all coordinates to apparent coordinates at the epoch of observation. This prevents field rotation due to effects such as differential precession. The second step is gnomic projection of the celestial coordinates onto the focal plane at the proper plate scale. All objects outside the 45 arcminute field of the telescope are eliminated from consideration.

The next step is the assignment of candidate objects to individual fiber positioners. The polar coordinates (r,θ) of all objects are calculated in the frame of a given positioner. Coordinate conventions in the focal plane are given in Figure 14. The target list is "scanned" for objects within "normal sensor range" (focal plane space) of that positioner. If no objects are found, a search is conducted with extended sensor range out to the mechanical limits of positioner travel. When multiple target objects are found, they are assigned up to two additional priority points based on their location relative to the optimum operational position of that probe. The range of operation and the optimum points of operation for the two classes of probes, inner and outer, are shown in Figures 16 and 17. Additional priority weight may be based on the magnitude of the target object. The target object with highest accumulated priority is assigned for observation, and the x,y coordinates are placed in the target file. After assignment, the target priority is set to zero in the selection list to prevent a second assignment of the same object. Each new target assignment is checked on the collision map to avoid possible contact with other probes. All objects within the minimum approach envelope of the positioner are also given zero priority. The assignment procedure continues until all 32 positioners have targets assigned. If no target is found, the probe will remain in the retracted position or will be assigned to collect sky photons. Probe assignment will be done first for the inner ring of 16 probes and then for the outer ring. Sequential assignments will alternate diametrically across the ring to maintain balanced positioner angles. After assignment of all the probes to a

target object and a preliminary anti-collision check, the target coordinates are stored for later transmission to the control micro.

This type of weighted assignment procedure should have no problem with a cluster of randomly positioned galaxies. It remains to be seen how well it will deal with highly clumped clusters or with the degenerate case of all 32 fibers arranged in a straight line for quasi-long slit observations. This target assignment technique was chosen because it most resembled the method I used when drawing probe assignments by hand on example fields. Other possible weighting schemes include "equal area in the focal plane" and "equal number of nearby objects" which might work better when there is a dense clump of objects on one side of the field. In no sense is the above procedure mathematically optimized to choose the "best" solution, nor is it guaranteed to assign every object if the number of objects is equal to the number of probes. An optimized solution to this problem is prohibitively complicated to solve on a small microprocessor in a short period of time, an may not be well defined because of the complex nature of the anti-collision constraints. The above algorithm treats potential collisions as a separate problem to be dealt with in a serial fashion with iteration.

Peak-Up Calculations

The third major task of the support micro is the collection and analysis of data in the peak-up mode. The rastering of the probes must be coordinated with the reading of the CCD. To interact with the CCD controller, the support micro will act as a smart terminal for the FORTH

data acquisition program on the .4 computer. The information on the detector and relevant raster data must be combined to provide an improved set of target positions for the control micro. The support micro will carry out all of the necessary calculations. Additional information on the peak-up mode was given in the previous chapter.

Instrument Microprocessor

Unlike the support micro, the instrument control micro has a relatively limited set of jobs which it executes without assistance from the observer. Figure 20 shows a schematic layout of the control software tasks. The two main software functions are communications and motor control. Most of the software will be written in Z-80 assembler. Executable code is downloaded from the support micro. Given its mission to explore strange new clusters and observe galaxies man has never observed before, the control computer is code named "Enterprise". Because it is somewhat more specialized in function, the control computer is made up of individual STD cards. The CPU is a 4MHz Z-80 by Mostek (CPU1A). The control micro also has a two channel serial I/O card (MDX-SIO2) and 64K of nonvolatile memory (UMEM-64-00B with Hitachi CMOS RAM). The control computer also contains a video card to provide enough memory to allow stand alone operation of the anti-collision algorithm. Each of the stepper motors is controlled by an intelligent controller chip (CY512). The CY512 chips for stepper control are mounted in pairs on cards connected directly to the STD bus.

Motor Control

The principal task of the control microprocessor is to move the fiber probes in an intelligent, safe, and reliable fashion to the assigned galaxy positions. The control computer receives a list of coordinates from the support computer and translates the x,y pairs into the correct number of steps for each motor. After verifying that no collisions will occur, each motor controller is loaded with a set of instructions containing the calculated coordinates. On command from the observer, the control micro instructs each CY512 to execute its program and move the fiber probe to the correct location. After all motion is complete, the control micro verifies that each motor is in the correct position by querying the CY512 controllers. Each controller is given a reset command to remove motor power during the spectroscopic integration. This removes several hundred watts of heat load from the spectrograph. Finally, a status message is sent to the support computer indicating that motion is complete. After the spectroscopic integration, the probes are returned to their retracted neutral positions to await the next assignment.

CY512 Stepper Controllers

The MX will use the CY512 intelligent positioning stepper controller chip made by Cybernetic Micro Systems to make counting motor pulses more reliable and to simplify the problems of interfacing 64 stepper motors to a microprocessor. The microprocessor in the positioner box will handle all communications with the individual motor controllers on a modified STD bus. The CY512 is a 40 pin LSI device

($60 each) that accepts parallel TTL input and produces the four outputs needed to control a four-phase stepper motor. Each CY512 controller can store up to 48 instructions for a series of motions in an internal program buffer. These instructions are executable on command. The CY512 maintains its own internal status and position registers. It calculates how far and which direction to move when it receives an absolute position command. The CY512 also takes care of ramping the motor step rate during acceleration and deceleration at a user-selectable rate. This allows all of the motors to be controlled simultaneously with minimum software overhead. Most importantly, the CY512 eliminates most of the real time software which would be needed if the microprocessor drove each stepper directly through a non-intelligent driver chip. The CY512 chips are mounted in pairs on 32 VME-style cards (Schroff - Europac) connected to the STD bus. These cards also contain the limit switch logic. The TTL output of the CY512 is fed to a quad Darlington driver chip (Sprague ULN 2068B) for amplification before being connected to the motor. The stepper motors are driven with a L/4R unipolar drive.

Collision Avoidance

The control computer will check each set of assigned coordinates carefully for possible collisions before moving any motors to the positions required for the next cluster of objects to be observed. After some thought and advice from others, several methods are under consideration for the anti-collision algorithm to be used with MX. The MX design of fishermen-around-the-pond positioners has several features

which simplify the problem of finding collisions between 32 positioners, each of which has two degrees of freedom of motion. First, all collisions will occur in the focal plane or can be projected onto that plane. Second, because of the radial symmetry of the problem, any collision which occurs while a probe is extending into the focal plane will be seen in the final configuration of the probes for that target field. This assumes that all probes are moved from their neutral retracted positions to their final target positions in a monotonic fashion. Angular rotation of the probes should occur before radial extension of the arms, and should be roughly simultaneous for all probes. This feature allows a single anti-collision map to be drawn before any motion occurs, rather than a continuous series of maps to be drawn as the probes move. Third, collisions always occur at the surface or perimeter of a positioner body. Two other constraints which would make the problem nearly trivial are unfortunately not true. These are that only collisions with nearest neighbors are allowed, and that collisions always involve probe tips. A combination of these constraints, which is true, says that collisions among nonneighbor probes always involve at least one probe tip. A failsafe electrical system will prevent damage during a collision by stopping all motors if it detects electrical continuity between any of the probes. Each probe will be electrically isolated from the other parts of the spectrometer housing.

The two major contenders for anti-collision algorithms are digital simulation of the focal plane in computer memory and the semianalytical approach of searching all possible combinations of N x 32

intersecting lines for collisions. Both methods are described here with the caveat that only preliminary software tests have been carried out. Each positioner can be represented in the focal plane by a polygon with a finite number of sides (N), typically 4 to 12. The exact location of each polygon can be stored as an array of coordinates of the vertices, which are uniquely determined by the target object location in the field once the mechanical shape and mounting point of the assigned positioner are known. If the perimeter of each polygon is mapped on a grid, it is easy to find collisions by asking if any pixel in the grid has more than one occupant. A simple algorithm can be used to "connect the dots" and draw in memory a continuous perimeter around all the vertices. If a collision is ever found, the control computer will simply refuse to move the probes to that configuration. The contents of the focal plane array can be used to drive a bit-mapped video display for visual feedback. Collisions can also be detected by checking the intersections of the polygon sides with all of the other positioners.

The major problem with the digital simulation technique is the large amount of memory required to make a high resolution map of the entire focal plane. 36 megapixels are needed to map a 60 cm square focal plane to a resolution of 100 microns. Such a fine grid is needed to prevent near misses from excluding the observation of close pairs of objects. Because a Z-80 does not usually come with 4.5 megabytes of memory, a slightly more clever approach is required. The entire focal plane is mapped at a coarse resolution of 1 mm, using only 45K bytes of memory. Whenever a possible collision is detected, that area of the focal plane is mapped in a small grid at higher resolution. This allows

a great savings in the amount of memory required at the expense of greatly increased computing time, since the entire focal plane must be remapped in the fine grid each time a possible collision is detected in the coarse grid. I estimate that the computation time increases as roughly the inverse of the product of memory size and the fourth power of the resolution, based on the number of pixels and the number of local maps needed to resolve near misses detected at coarse resolution. It may be most time efficient to check the entire area at the finest resolution in subparcels on the first pass and use the coarse grid only for the visual display. More computing time is required to draw lines in memory than originally expected because of the requirement of producing continuous lines. In this case, each pixel in a line must have neighbors with adjacent faces rather than corners, otherwise diagonal lines could intersect without having common pixels.

Rather than the direct bit-mapped representation of the positioners, a hierarchical representation such as the quadtree approach could be used to define the positioner polygons. A quadtree is a structured list of all pixels in an object which divides the picture or map into successive levels of quadrants until all of the quadrants of a given node are colored the same or the pixel level is reached. For MX, the quadtree method will save memory space only when the focal plane map is larger than one megabyte. The quadtrees for each probe would make the search procedure faster after the initial structured list had been generated. Hunter and Steiglitz (1979) describe operations on images using quadtrees. The octree techniques would be very useful if it were necessary to search for collisions in three dimensions where bit-maps

are less efficient.

The intersecting line methods offer enormous memory savings compared to bit-map methods. Only the polygon vertices need to be stored in memory. If each probe is represented by a 10-sided polygon, it is necessary to check for the mutual intersection of 320 line segments. This requires roughly 1500 individual checks to be made. The actual computational time may be even faster than drawing pixels in an array at high resolution. Roughly 6K bytes of memory are needed to store all relevant parameters. A coarse focal plane map will still be used for visual feedback to the operator.

Spectrograph Control

Pending construction of a smart control box for the cassegrain spectrograph, the control micro will relay commands to this box via its second serial port. The control micro will transfer commands to the spectrograph controller for comparison lamps, grating tilt, acquisition mirrors, etc.. If sufficient serial ports were available, this task would be handled directly by the support computer.

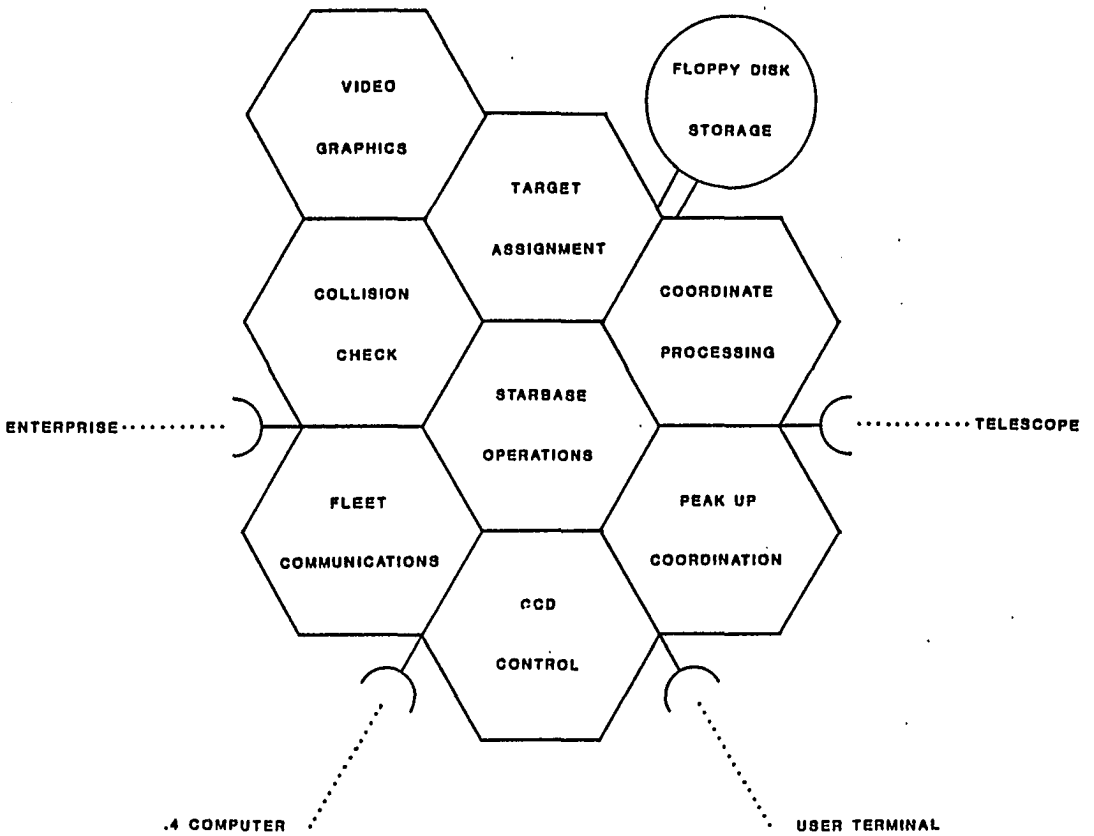

Figure 19. Support Computer Software Tasks

This figure illustrates the major tasks of the support computer software as well as the communication links to other parts of the galaxy. The hexagons represent the major program tasks and their relationship to other tasks and the four serial communication links.

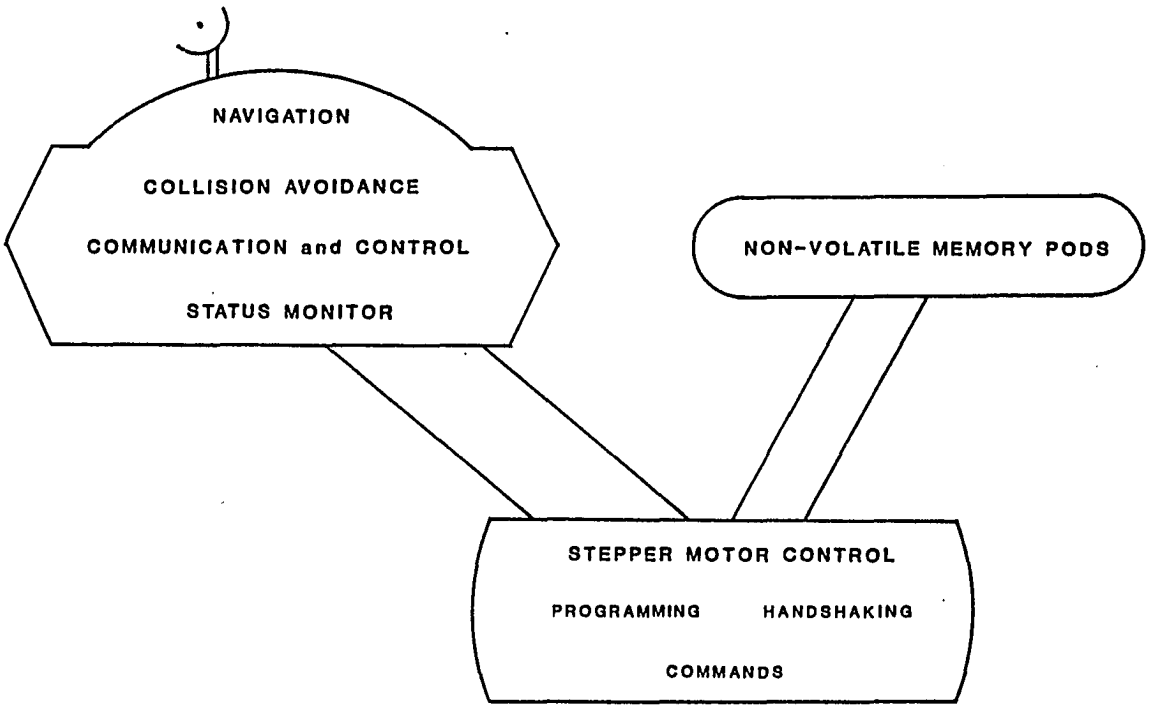

Figure 20. Control Computer Software Tasks

This figure illustrates the major software tasks of the control computer "Enterprise" on its mission to seek out new clusters and observe where no spectrograph has gone before.

CHAPTER 7

THE MX SPECTROMETER: OPTICAL PERFORMANCE

The previous two chapters described the operation of the multiple fiber head of the MX Spectrometer. While the mobile fiber probes are the major technical development associated with MX, having 32 fibers is not useful unless you are prepared to deal with the photons after they leave the fibers. This chapter discusses the expected optical performance of the MX Spectrometer system. In addition to spectrometer and detector performance, the data reduction system for multiple fiber spectra is described.

Expected MX Performance

With good optical matching, spectra should be collected by MX at 25 to 30 times the normal single object rate. Hill, et al. (1982) give signal-to-noise calculations for the anticipated performance of the MX. Based on Medusa experience, low dispersion spectra should give velocities of galaxies accurate to 40 km s^{-1} with a CCD as the detector. The performance of the complete spectroscopic system is still limited in non-fundamental ways by the telescope, spectrometer, and detector. The next section will discuss the optical efficiency of fiber optic spectrometer systems. The following section will describe the observed performance of Medusa with an intensified CCD detector. Later sections will discuss possible spectrometers and detectors that might be used with MX. More detailed signal-to-noise calculations will be given for

several spectroscopic examples using the observed Medusa performance as a baseline.

System Optical Efficiency

Tables 5 and 6 list optical efficiency calculations for the existing Medusa system and the planned MX system. These calculations are based on known spectrograph performance and measured fiber properties as well as expected improvements in detectors such as CCDs. Major areas open for improvement of the system efficiency are fiber focal ratio degradation, spectrograph camera efficiency, and detector quantum efficiency and noise. Operating efficiency and system stability are not included in these tables as they are difficult to predict and quantify. Real life observing may therefore proceed at a slightly slower pace than the tabulated efficiencies would indicate. Improvements in fibers have significantly reduced the focal ratio degradation problem. This can be seen in the 75% improvement of MX over Medusa feeding the same spectrograph. Fiber performance and limitations on system design are discussed in chapter 4, and in chapter 8. Once the fiber size and detector pixel size are known, a significantly more efficient camera can be built than presently exists in the Cassegrain spectrograph of the 2.3m telescope. The current camera has a 30% central obstruction which is a major light loss in fiber spectroscopy, since there is no Cassegrain hole in the fiber-scrambled pupil. The construction of a new camera will probably be a part of Phase 2 MX development pending the outcome of experiments with Littrow Schmidt fiber spectrographs and other optical systems described at the end of

this chapter. Finally, CCD developments seem to hold promise of obtaining 60% or greater quantum efficiency over most of the optical spectrum with readout noise of 10 electrons or less. Remember of course, that this carrot has been dangling for quite a few years now. Some optimistic combination of the above improvements should make the MX Spectrometer an extremely efficient spectroscopic instrument. The following section discusses the performance of the intensified CCD detector package used for actual observations with the Medusa spectrograph.

Table 5. MEDUSA Optical Efficiency

This table contains the estimated optical efficiencies of the various components which make up the Medusa spectrograph system.

Telescope		
2 aluminum reflections	$.85^2$	
Cassegrain obstruction	.89	
telescope efficiency		.64
Fiber Optics		
transmission (0.2m)	.98	
end reflections	.92	
focal ratio degradation loss (f/4.5 onto f/6.75)	.44	
single object efficiency		.40
multiplex gain (37 fibers)		37.00
group efficiency		14.80
efficiency without fiber feed		1.00
Cassegrain Spectrograph (B&C)		
collimator - aluminum	.85	
grating - low dispersion	.60	
camera - 2 aluminum surfaces		
- 6 air/glass		
- 30% obstruction	.40	
spectrograph optical efficiency		.20
Detector - Intensified CCD		
image tube - DQE	.12	
analog CCD - adds noise		
System Total Efficiency		
single object efficiency		.006
net efficiency		.22

Table 6. MX Optical Efficiency

This table contains the estimated optical efficiencies of the various components which will make up the MX Spectrometer system.

Telescope		
2 aluminum reflections	$.85^2$	
Cassegrain obstruction	.89	
telescope efficiency		.64
Fiber Optics - option 1 = bare QSF-ASW fibers		
transmission (1.0m)	.93	
end reflections	.92	
focal ratio degradation loss (f/6.0 onto f/6.75)	.85	
Fiber Optics - option 2 = lensed fibers		
lens transmission incl. reflection	.85	
fiber transmission	.85	
focal ratio degradation (f/3.9 onto f/4.0)	.95	
single object efficiency		.70
multiplex gain (32 fibers)		32.00
group efficiency		22.40
efficiency without fiber feed		1.00
Long Fiber Link (10m) trans. above 400nm		.80
Cassegrain Spectrograph (B&C)		
collimator - aluminum	.85	
grating - low dispersion	.60	
improved camera	.79	
spectrograph optical efficiency		.40
Detector - CCD		
barefoot CCD - hope for 800x800 3ph	.60	
System Total Efficiency		
single object efficiency		.10
net efficiency		3.44

Intensified CCD Performance

Original data with the Medusa Spectrograph were taken with baked IIIaJ photographic plates lens-coupled behind a Carnegie magnetic focus image tube. In December 1981, the photographic plate on the image tube spectrograph was replaced with an RCA 320 x 512 CCD chip. The CCD provides increased efficiency, larger dynamic range, linear response, fixed detector format, and "readily available" data processing. The 40 electron readout noise of the RCA chip prevents the use of the CCD barefoot without the image tube. This section discusses the reality of these improvements and the performance levels that can be achieved with future systems with and without fibers.

Transfer Lens. The RCA CCD worked very well on all our observing runs even though it was in an experimental camera. Some problems were encountered with the transfer optics between the image tube and the CCD. To match the scale of the spectrograph camera (2 arcsec mm^{-1}) to the CCD it was necessary to magnify the output of the image tube by a factor of 1.5 onto the CCD. This required a different transfer lens than had been used for photographic spectroscopic work at a transfer ratio of 1:1. A 85 mm focal length f/1.2 Elgeet Navitar lens was used on the first observing run and proved to be quite radioactive! Each 20 minute exposure contained hundreds of "cosmic" ray hits. This data should still be useable for measuring radial velocities with some extra effort required during data reduction. A non-radioactive Elgeet Navitar lens was used during the second observing run which was mercifully cloudy. This lens was found to have a loose element which gave rise to some rather strange flexure effects. Only the fact that my

hands did not smell like developer prevented me from returning to the intensified photographic plate after this run. Once these problems were corrected the transfer lens worked acceptably well, although the corners of the frame show some astigmatism and coma since the lens was designed to work at 1:1 magnification rather than 1.5:1. The transfer lens was nominally set to f/1.5 to suppress image halos and was therefore effectively operating at f/3. Optical efficiency and resolution of the lens-coupled system are discussed in the following sections.

Resolution. Ideally, the spectral resolution should be limited by the projected width of the entrance aperture and not by the detector or spectrograph optics. At least two detector pixels are needed per resolution element to avoid loss of resolution as set by the entrance aperture. With 3 arcsecond diameter fibers, the Medusa system operated marginally in the slit-limited domain. The light distribution of a 300 micron diameter, circular core fiber is 260 microns FWHM in a one-dimensional profile, neglecting diffraction. The Boller & Chivens Cassegrain spectrograph optics demagnify by a factor of 5.4 with negligible aberration to give 48 micron images at the camera focal plane. Cromwell (1984) reports a demagnification which is 20% higher (6.5) than the value derived from the alleged focal length of the camera or my measurement. This local mystery remains unresolved at the present time. General wisdom and measurements by Lesser (1983) show the image tube -- transfer lens combination to have a resolution of 35 microns. This resolution is dominated by the image spread within the image tube proper. The image tube resolution convolves with the slit size to give 59 micron images before magnification onto the CCD. Magnification by

1.5x gives 89 micron images at the CCD convolved with 30 micron pixels to produce an expected line width of 94 microns (3.1 pixels). This resolution is achieved in practice and has been measured to be 3.0 pixels on a typical set of spectra. The performance has also been verified by experiments with a long narrow slit instead of the fiber apertures. A 15% increase in resolution could be achieved by changing the camera focal length so the 1.5x magnification occurred before the image tube with a 1:1 transfer lens coupling to the CCD. If a different CCD such as the Texas Instruments 800 x 800 chip with 15 micron pixels were used, some demagnification (up to 0.5) would be needed after the image tube stage. If this chip were used barefoot, the existing camera provides a better match to the pixel size. A demagnification of 4 would be best for two arcsecond fibers and 15 micron pixels. Additional resolution could also be gained by using smaller fibers at the cost of collecting fewer photons from resolved galaxies or point sources in bad seeing. The size of the entrance aperture is determined by a series of tradeoffs between optical throughput, sky background, resolution, and available fiber sizes. Larger entrance apertures collect a larger fraction of the object photons at the expense of resolution and increased sky background. Statistics of various aperture sizes are shown later in Table 10. Larger apertures are used in spectrophotometry to collect as many of the incident photons as possible. Image size and, therefore, aperture size is determined by diffraction, seeing, atmospheric dispersion, and the physical size of the target objects. In general, the aperture size is chosen to maximize signal versus background noise when this is consistent with the desired resolution and

available apertures. Entrance apertures between 1.0 and 4.0 arcseconds are expected for the MX, with 2.5 to 3.0 arcseconds being the best compromise for faint, slightly extended galaxies in good seeing. Smaller apertures would be useful for stellar spectroscopy at higher resolution. Bingham (1979), and Woolf and Angel (1980) provide additional discussion of the selection of aperture size. Enard (1983) reviews the coupling of grating spectrographs to large telescopes. Medusa spectra have historically been taken with a 300 l mm^{-1} grating giving 250 Å mm^{-1} reciprocal dispersion at the image tube and 166 Å/mm at the CCD.

Detection Efficiency. The intensifier used in front of the CCD was the Carnegie C33063 2-stage magnetic tube (Blue RCA Photographic) with a permanent magnet. The photocathode of this tube has a peak quantum efficiency of 28% at 400 nm. Allen, et al. (1983) have shown that similar tubes amplify only 55% of the primary photoelectrons. I estimate that the blue light (360 - 440 nm) detective quantum efficiency is roughly 15%, dropping to zero above 650 nm. The image tube gain is $4x10^4$ photons emitted from the output phosphor for each input photoelectron. The Elgeet Navitar transfer lens operating at an effective f/ratio of f/3 transfers roughly 1.3% of these photons onto the CCD. Because of this light loss, the availability of a fast, high resolution lens or a high quality fiber optic boule is an important consideration in the design of intensifier and detector packages. The CCD is a vintage 1980, "thick", 320 x 512, RCA CCD. Its quantum efficiency at the peak wavelength (460 nm) of the phosphor is approximately 40%. I therefore expect that each photon event will

generate some 208 electrons (32 ADU) in the CCD. Given the projected image tube resolution of 50 microns at the CCD, each photon event is spread over four pixels. The 50 - 70 electrons generated in each pixel are compared to the 40 electron readout noise of this chip. Individual photons are not detected at the two sigma level, and readout must be done in an analog integration mode. Even with additional gain, single photon events would be difficult to detect in the presence of the noise events described in the next section. A series of 20-minute integrations were used to avoid large dark levels and to allow removal of cosmic ray events from the galaxy spectra. The low photon rates of faint galaxy spectroscopy do not present a dynamic range problem at this gain level. More serious rate limits occur in the collection of flat field and comparison frames.

Noise Sources. The fundamental noise limit in the spectroscopy of faint objects is set by the photon noise limit of the source. Additional noise is introduced by the sky background and by the detector. Tradeoff of source photons against sky background were discussed in an earlier section. This section discusses the detector noise introduced by the intensified CCD. Uniformity of response across the detector will be ignored as a noise source since it can be calibrated out at the 1% level as discussed in the following section. Image tube and CCD experts will please excuse the simplified treatment of complicated problems.

The image tube introduces five sources of noise. These include ion events, signal-induced background, window scintillations, dark emission, and phosphor afterglow. The ion events are caused by residual

gas atoms being ionized by high energy electrons and then generating a photoelectron event by striking the back side of the photocathode. The ion events produce a pointlike image. Window scintillations have been reported in other systems when cosmic rays enter the sapphire window of the image tube. The scintillation produces hundreds of electrons over a spot a few millimeters in diameter. Both of these events are almost indistinguishable from other noise sources in the CCD. Examination of intensified Medusa plates suggests that the ion event rate is of order one per minute over the portion of the image tube covered by the spectra. Signal-induced background in the image tube is of a very diffuse nature. It can be seen in some CCD frames near bright objects, but has little effect on radial velocity measurements. Thermal dark emission from the photocathode is a negligible noise source when the image tube is operated at -20°C. Afterglow of the image tube phosphor after bright emission lamp frames causes a helium signature to appear frequently in our spectra. The only cure for this effect is to take longer, fainter comparison frames and to allow a longer waiting period before resuming galaxy exposures. A similar effect due to trapped charge can be seen in some CCDs, although not in this RCA chip. Induced image tube background and phosphor afterglow appear to impose a tighter limit on total dynamic range than the CCD limit of 10^4. Quantitative dynamic range measurements have not been made.

Noise sources in Medusa spectra which are introduced by the CCD include: readout noise, defective pixels, dark current, inefficient charge transfer, and cosmic rays. The readout noise of 40 electrons rms is caused by the output amplifier on the chip, and is among the lowest

reported for RCA CCDs. The readout noise may potentially improve to the level of only a few electrons in future devices. Image tube gain is needed to boost the faint signal above the readout noise level. Dark current is a problem with this chip, but is reduced to the acceptable level of 0.2 electrons $pixel^{-1}$ sec^{-1} by operating at $-140^{o}C$. Three defective columns and about a dozen hot pixels are the major cosmetic defects in the present chip. These are easily removed by subtracting a dark frame. Luminescence of the horizontal shift register prevents the use of the last few rows on the chip. Cosmic rays hitting the CCD are the major variable cosmetic defect in Medusa frames. Approximately 80 cosmic ray hits are observed in a 20-minute exposure. These range from single pixel hits, to 10 pixel wide blobs, to streaks that cross the entire chip. The single bright pixels are easy to remove during data reduction. The diffuse background can only be removed on a statistical basis and will limit velocity accuracy at some level.

Calibration. The major calibration needed for redshift measurements is the dispersion curve of the detector. Multiobject observations complicate the issue by requiring many dispersion curves. Medusa was calibrated by illuminating the aperture plate and fibers from above with diffuse light from helium and argon lamps. Because a fixed format detector is being used, the resulting emission line spectra can be used directly to find a dispersion curve for each corresponding galaxy spectrum on the detector. The major problems are those encountered with most non-fiber radial velocity measurements. First, either there are not enough lines in the spectrum to produce an accurate

dispersion curve, or they are not distributed evenly. Typically 15 He and Ar lines are used between 370 and 590 nm to fit a third-order dispersion curve. Second, flexure in the patched together detector chain during the night makes the CCD a not quite fixed format detector. Individual frames must be separately aligned with calibration frames before coadding the galaxy spectra for extraction to one-dimensional format. This problem should become significantly smaller as the detector hardware improves. Geometrical distortions caused by the image tube and transfer lens are mapped transversely in the process of extracting the CCD spectra to one dimension. Longitudinal components of these distortions are compensated by the dispersion curve fits. The f/3 beam onto the CCD is slow enough that focus variations across the RCA chip are unimportant. Other factors which ultimately limit the velocity calibration, but are not currently important include: cosmic rays, CCD noise, phosphor afterglow, image tube stability, and CCD charge transfer efficiency. The use of diffuse light for calibration relies on the image scrambling properties of the fibers to make the output light distribution identical to stellar illumination. Careful measurements are needed to determine when this approximation breaks down and when more complicated calibration optics are needed. No quantitative results on absolute velocity calibration are available, as data reduction is still in progress.

The lack of a shutter before or after the image tube causes some image trailing during CCD readout. The detected image is clocked across the chip under the live image. This is only significant for short exposures of bright comparison lamps. The large ratio of exposure time

to readout time eliminates the problem for galaxy frames. No systematic effects in the velocity measurements have been seen. In practice, the addition of a shutter or a pair of shutters would have the greatest impact by reducing the amount of image tube afterglow.

Flat field spectra are needed to calibrate out spatial response variations in the image tube and CCD detector combination. Medusa has used filtered quartz lamp illumination through the fibers. Problems with this approach are discussed here. The strong color dependence of the quartz lamp is partially removed by blocking some, but not all, of the red light with a Corning 1-64 blue filter. CCD noise, with the exception of cosmic rays, is not a serious problem for flat field measurements. The accuracy of the calibration is limited to more than 0.2% by the few hundred thousand electron full-well capacity of the CCD via Poisson photon statistics. When flat spectra are used rather than a full flat field, this accuracy can only be achieved in the brightest parts of the frame. Areas on the edges of the spectra and between spectra remain uncalibrated, causing problems if significant flexure occurs. If a full frame flat field is done with a lamp after the grating, the color dependence of the flat field is lost. Full frame or uniform illumination data are useful if only CCD response variations are to be removed, and not image tube or fiber variations. As with all flat field data, there is a problem collecting many photons in a short period of time without damaging the image tube or exciting afterglow in the phosphor. Photon rate would be a problem if a photon counting detector were used.

Future Detectors of Interest

The use of improved spectroscopic detectors with MX in the future merits some discussion. Again, a complete discussion is outside the scope of this dissertation. Timothy (1983) has given an excellent review of state-of-the-art spectroscopic detectors. It is painfully obvious that MX will generate sufficient numbers of resolution elements to completely fill the format of all available detectors. The three major contenders for the MX detector are a bare CCD, an analog readout intensified CCD, and a photon counting image intensifier which may also include a CCD. The major characteristics needed in such a detector include: a large two-dimensional detector format to accommodate many spectra, high detective quantum efficiency, uniform response, low or zero readout noise, low background, high spatial resolution, and of course, finite cost.

Charge Coupled Devices

Perhaps the simplest spectroscopic detector that is competitive today is the CCD. The designation "barefoot" is often applied to distinguish it from CCD systems involving intensifiers, phosphors, upconverters, or other imaging gadgets to make photons more detectable. A silicon CCD potentially offers quantum efficiencies above 80% over the entire visible spectrum with somewhat lower response from the atmospheric cutoff out to one micron. CCDs also offer very stable geometry, light weight, and a readout noise of only a few electrons. Unfortunately, all of the desirable properties are not yet available in a single device. A disadvantage of a CCD is that it must operate in a

cryogenic environment to suppress dark current in long exposures. Readout noise of 10 to 100 electrons, imperfect charge transfer efficiency, low quantum efficiency, and manufacturing blemishes have prevented CCDs from replacing image intensifiers as the frontline spectroscopic detectors. I believe this will change in the future unless high quantum yield photocathodes become available. The development of near infrared arrays will also enhance the capabilities of MX by extending the wavelength coverage to two microns.

Intensified CCDs

An image intensifier with an analog (integrating) CCD readout is most likely to be used with MX because it already exists, and has been described in the previous section. The major performance limitations of such a device are the limited quantum efficiency of the photocathode, and the resolution of the image tube. A better quality tube with slightly higher gain would be desirable. Additional gain would make readout noise and other effects less significant relative to photon events. Given existing image tube front end performance, the dynamic range is limited fundamentally only by the number of CCD frames readout and coadded to form a single image and by the well depth of the CCD. High photon rates require frequent readout of the CCD to prevent saturation. Frequent readout results in larger quantities of data that must be stored and processed.

Photon Counting Systems

Photon counting systems increase the gain of the intensifier chain to the point where the readout device can record the locations of single photon events. This is the optimum detection scheme in low signal applications. Like analog readout, the quantum efficiency is limited by the first photocathode. By measuring the centroid of the recorded photon events, resolution can be increased beyond the readout pixel size to the limit of the photocathode itself. The major limitation of most photon counting systems is the data rate resulting from the recording of individual photons. This imposes many constraints on the readout device and its associated electronics. Television based photon counting detectors have been in use for many years, but suffer stability, resolution, and calibration problems. Despite their names, the two newest, "serious", photon counting candidates are "MAMA" and "2D-Fruitti". Both of these detectors are used here as examples of a whole class of devices under development. The MultiAnode Microchannel Array is being developed by Timothy and is described in his review. Many anodes are used to locate the centroids of photoelectron events from a microchannel plate intensifier. This technology may allow very large format detectors (4096^2).

Another potential detector for MX and other spectroscopic applications is the CCD readout photon counting device built by Shectman (1983b) called "2D-Fruitti". This detector is a very high gain image tube chain readout by a Fairchild CCD at video rates. Photon events above a certain threshold are centroided in real time and their positions recorded. A frame subtraction scheme is used to remove

defects and events which occur in more than one frame. The photon detection rate of this device is limited by confusion of events on the CCD, the speed at which the CCD can be readout, and by the time required to process and store the individual photon events. The major advantage of this type of photon counting detector is the high resolution provided by event centroiding. While the current device does not achieve the numbers discussed here, a new readout package should have roughly this capability. Allow a factor of two for overoptimistic assumptions.

Assume a 300 x 500 pixel CCD behind an image tube chain. The Fairchild imagers have covered readout registers so integration time is not lost while reading the chip. Suppose each amplified photon event covers nine pixels on the CCD. The image tube chain needs a resolution of 100 microns which is achievable with reasonable effort. In a given frame only 10% of the pixels can be occupied to prevent coincidence problems between photon events. This means that no more than 1700 photon events per frame can be counted. If some areas have more events than this mean density, they will become nonlinear. Nonlinear regions do not effect the data in other parts of the field. This is an advantage over the multiple anode readout photon counters which must avoid photon coincidence over the entire readout area. If a 18 MHz pixel rate can be achieved, the CCD can be readout at nearly four times normal video rates (120 frames sec^{-1}). This allows up to 200,000 photons sec^{-1} to be collected over the array. Data processing at this rate is challenging, but not impossible. The device performance is limited by the maximum clocking rate of the CCD chip. This is roughly six times the pixel rate of current one-dimensional Reticon readouts.

The trick, of course, is that centroids are now being computed in two coordinates simultaneously. There are a few ways to do the centroiding, but most involve a series of shift registers and fast logic gates.

What kind of performance will such a detector give? Suppose the MX spectrometer needs 64 spectra across the chip with 2000 effective pixels (from centroiding) along the dispersion. This implies a maximum mean counting rate of 1.5 events $pixel^{-1}$ sec^{-1}. Two hours are therefore required to accumulate 1% counting statistics. By only reading out segments of the CCD chip, higher frame rates and therefore higher counting rates per pixel can be obtained. Given the rates discussed above, this detector behind the MX on the 2.3m telescope would saturate on low dispersion spectra of objects brighter than 16th magnitude. While not perfect, this is an acceptable data rate for faint object spectroscopy, but may cause problems for arc and flat field calibration frames.

Signal-to-Noise Calculations

This section describes signal-to-noise calculations to estimate the operational performance of the MX on a variety of spectrometer - telescope combinations. The signal-to-noise estimates include source photons, sky photons, and detector noise. Transmission estimates were made for the entire spectroscopic system including a one airmass atmosphere. The photometric data used for five representative wavelengths are shown in Table 7. Absolute photometry was obtained from Johnson (1966). The atmospheric transmission data were found in Allen (1976). Typical Kitt Peak sky brightness data from Bessel (1979) was

used in the background calculations. Table 7 also lists quantum efficiencies for the image tube used with the Medusa spectrograph and a slightly idealized CCD which might be used with MX. Telescopes were assumed to have two aluminum reflections and a 10% central obstruction. This gives a effective collecting area of $0.5D^2$ cm^2, where D is the diameter of the primary mirror. The area of the spectrograph entrance aperture was used in the sky background calculation. For point sources, the transmission was varied with aperture size to simulate seeing effects under good conditions. A one arcsecond aperture was assumed to transmit 50% of the light from a point source and a four arcsecond aperture was assumed to transmit all of the light (1"=50%, 2"=75%, 3"=90%, 4"=100%). The spectrograph efficiencies used in this calculation are those listed in Tables 5 and 6.

For each combination of telescope, spectrograph, and detector, the number of detected photons arriving from the source, sky background, and noise sources were calculated for an individual pixel on the detector. I have assumed that all pixels perpendicular to the dispersion add in a noiseless fashion. The signal-to-noise ratio is given by:

$$S/N = \text{Source Photons} / (\text{Source} + \text{Sky} + \text{Noise}^2)^{0.5} \qquad (7.1)$$

The actual signal-to-noise in each pixel would be roughly 1.7x lower if there were 3 pixels perpendicular to the dispersion and the readout noise was dominant. This factor of 1.7 could be recovered by combining pixels along the dispersion to obtain the signal-to-noise ratio in a resolution element. Table 8 gives the expected number of detected photons and the signal-to-noise ratio for data taken with the Medusa and

the intensified CCD. My qualitative impression when comparing these results with actual data is that the calculation is too optimistic by about a magnitude. This might be expected because the calculation has not included image tube background, cosmic ray hits, or the effects of poor seeing which appear in the observations. Table 9 gives the expected MX performance with a bare or intensified CCD and a 1000 second exposure on the 2.3m telescope. The combined improvements in fiber transmission, spectrograph throughput, and CCD quantum efficiency provide a factor of 25 improvement over the Medusa system.

Table 10 gives MX signal-to-noise calculations as a function of entrance aperture or fiber size. The conclusion I draw for point sources is that increasing the entrance aperture beyond two arcseconds diameter offers little gain in S/N at the expense of decreased resolution. For nearby galaxies which are slightly extended or in bad seeing, the large aperture will collect more source photons. The signal-to-noise calculations in these tables could be in error by an order of magnitude because of the many assumptions made in characterizing the detector system. Relative comparisons between different parameters should be accurate to roughly 10% because the systematic efficiency errors are eliminated. Table 11 compares MX performance for a series of exposure lengths. In these calculations, quantum efficiency, exposure time, and telescope aperture (area) all have exactly the same effect on the number of collected photons.

Table 7. Photometric Calibration Data

This table lists the calibration data for absolute flux, sky brightness, and quantum efficiency which was used to carry out the signal-to-noise calculations.

Parameter	Units	Data				
Wavelength	Angstroms	3600 U	4400 B	5500 V	7000 R	9000 I
Absolute Flux (mag 0.0 star)	10^{-15} W cm^{-2} nm^{-1}	4.35	7.20	3.92	1.76	0.83
Photons Above Atmosphere (0.0)	# sec^{-1} Å^{-1} cm^{-2}	788	1595	1085	620	376
Atmospheric Transmission	%	51	71	82	91	95
Photons (0.0 at the ground)	# sec^{-1} Å^{-1} cm^{-2}	402	1132	890	564	357
Sky Brightness	magnitude arcsec^{-2}	22.2	22.5	22.2	21.9	18.8
Sky Photons	10^{-6} sec^{-1} Å^{-1} cm^{-2} arcsec^{-2}	1.04	1.60	1.43	1.08	11.4
Image Tube Quantum Efficiency	%	12	12	8	2	0.1
CCD Quantum Efficiency	%	60	70	80	80	40

Table 8. Medusa Signal-to-Noise vs. Source Magnitude

This table lists the detected photon statistics for the Medusa spectrograph with the intensified CCD. Statistics for each of five colors are given for a range of source magnitudes.

Telescope Diameter:	230 cm
Fiber Diameter:	3 arcsec
Fiber Transmission:	40%
Spectrograph Transmission:	20%
Pixel Size:	4 Å
Exposure Time:	10000 sec
Image Tube Quantum Effic.:	12% max.

Magnitude 16	U	B	V	R	I
# Source Photons	1463	4121	2159	342	11
# Sky Photons	75	115	68	13	7
Signal-to-Noise	37.30	63.32	45.74	18.16	2.58

Magnitude 17	U	B	V	R	I
# Source Photons	582	1641	859	136	4
# Sky Photons	75	115	68	13	7
Signal-to-Noise	22.72	39.16	28.21	11.15	1.29

Magnitude 18	U	B	V	R	I
# Source Photons	232	653	342	54	2
# Sky Photons	75	115	68	13	7
Signal-to-Noise	13.24	23.57	16.88	6.62	0.59

Magnitude 19	U	B	V	R	I
# Source Photons	92	260	136	22	1
# Sky Photons	75	115	68	13	7
Signal-to-Noise	7.14	13.43	9.52	3.68	0.25

Magnitude 20	U	B	V	R	I
# Source Photons	37	104	54	9	0
# Sky Photons	75	115	68	13	7
Signal-to-Noise	3.48	7.01	4.90	1.85	0.10

Magnitude 21	U	B	V	R	I
# Source Photons	15	41	22	3	0
# Sky Photons	75	115	68	13	7
Signal-to-Noise	1.55	3.30	2.27	0.85	0.04

Magnitude 22	U	B	V	R	I
# Source Photons	6	16	9	1	0
# Sky Photons	75	115	68	13	7
Signal-to-Noise	0.65	1.43	0.98	0.36	0.02

Table 9. MX Signal-to-Noise vs. Source Magnitude

This table lists the detected photon statistics for the MX spectrometer with the bare CCD and with an intensified CCD. Statistics for each of five colors are given for a range of source magnitudes.

Telescope Diameter:	230 cm
Fiber Diameter:	3 arcsec
Fiber Transmission:	70%
Spectrograph Transmission:	40%
Pixel Size:	4 Å
Exposure Time:	1000 sec
CCD Quantum Efficiency:	80% max.
Readout Noise:	10 electrons

Magnitude 16	U	B	V	R	I
# Source Photons	2559	8414	7555	4791	1517
# Sky Photons	131	235	240	181	955
Signal-to-Noise	48.45	89.96	85.03	67.27	29.91

Magnitude 17	U	B	V	R	I
# Source Photons	1019	3350	3008	1907	604
# Sky Photons	131	235	240	181	955
Signal-to-Noise	28.82	55.19	51.99	40.77	14.82

Magnitude 18	U	B	V	R	I
# Source Photons	406	1334	1197	759	240
# Sky Photons	131	235	240	181	955
Signal-to-Noise	16.08	32.65	30.54	23.54	6.68

Magnitude 19	U	B	V	R	I
# Source Photons	161	531	477	302	96
# Sky Photons	131	235	240	181	955
Signal-to-Noise	8.15	18.05	16.68	12.52	2.82

Magnitude 20	U	B	V	R	I
# Source Photons	64	211	190	120	38
# Sky Photons	131	235	240	181	955
Signal-to-Noise	3.74	9.05	8.25	6.01	1.15

Magnitude 21	U	B	V	R	I
# Source Photons	26	84	76	48	15
# Sky Photons	131	235	240	181	955
Signal-to-Noise	1.60	4.11	3.71	2.64	0.46

Magnitude 22	U	B	V	R	I
# Source Photons	10	33	30	19	6
# Sky Photons	131	235	240	181	955
Signal-to-Noise	0.66	1.75	0.64	0.45	0.07

Table 9, continued

Image Tube Quantum Efficiency 12% max.

Magnitude 16	U	B	V	R	I
# Source Photons	512	1442	755	120	4
# Sky Photons	26	40	24	5	2
Signal-to-Noise	22.07	37.46	27.06	10.74	1.53
Magnitude 18	**U**	**B**	**V**	**R**	**I**
# Source Photons	81	229	120	19	1
# Sky Photons	26	40	24	5	2
Signal-to-Noise	7.83	13.94	9.99	3.92	0.35
Magnitude 20	**U**	**B**	**V**	**R**	**I**
# Source Photons	13	36	19	3	0
# Sky Photons	26	40	24	5	2
Signal-to-Noise	2.06	4.14	2.90	1.10	0.06

Table 10. MX Signal-to-Noise vs. Aperture Size

This table lists the detected photon statistics for the MX spectrometer with the bare CCD. Statistics for each of five colors are given for a range of entrance aperture sizes.

Telescope Diameter:	230 cm
Fiber Transmission:	3 arcsec
Spectrograph Transmission:	40%
Pixel Size:	4 Å
Exposure Time:	1000 sec
CCD Quantum Efficiency:	80% max
Readout Noise:	10 electrons
Source Magnitude	+20

1 Arcsecond Aperture	U	B	V	R	I
# Source Photons	36	117	105	67	21
# Sky Photons	15	26	27	20	106
Signal-to-Noise	2.91	7.53	6.92	4.89	1.40

2 Arcsecond Aperture	U	B	V	R	I
# Source Photons	54	176	158	100	32
# Sky Photons	58	104	106	80	424
Signal-to-Noise	3.68	9.03	8.28	5.99	1.35

3 Arcsecond Aperture	U	B	V	R	I
# Source Photons	64	211	190	120	38
# Sky Photons	131	235	240	181	955
Signal-to-Noise	3.74	9.05	8.25	6.01	1.15

4 Arcsecond Aperture	U	B	V	R	I
# Source Photons	71	235	211	134	42
# Sky Photons	232	417	426	322	1698
Signal-to-Noise	3.56	8.57	7.77	5.67	0.99

6 Arcsecond Aperture	U	B	V	R	I
# Source Photons	71	235	211	134	42
# Sky Photons	523	938	958	724	3819
Signal-to-Noise	2.71	6.58	5.92	4.32	0.67

8 Arcsecond Aperture	U	B	V	R	I
# Source Photons	71	235	211	134	42
# Sky Photons	929	1668	1703	1287	6790
Signal-to-Noise	2.15	5.25	4.70	3.43	0.51

Table 11. MX Signal-to-Noise vs. Exposure Time

This table lists the detected photon statistics for the MX spectrometer with the bare CCD. Statistics for each of five colors are given for a range of exposure times.

Telescope Diameter:	230 cm
Fiber Diameter:	3 arcsec
Fiber Transmission:	70%
Spectrograph Transmission:	40%
Pixel Size:	4 Å
CCD Quantum Efficiency:	80% max.
Readout Noise:	10 electrons
Source Magnitude:	+20

100 Seconds	U	B	V	R	I
# Source Photons	6	21	19	12	4
# Sky Photons	13	23	24	18	95
Signal-to-Noise	0.59	1.76	1.59	1.05	1.27
300 Seconds					
# Source Photons	19	63	57	36	11
# Sky Photons	39	70	72	54	286
Signal-to-Noise	1.53	4.15	3.76	2.62	0.57
1000 Seconds					
# Source Photons	64	211	190	120	38
# Sky Photons	131	235	240	181	955
Signal-to-Noise	3.74	9.05	8.25	6.01	1.15
3000 Seconds					
# Source Photons	193	634	569	361	114
# Sky Photons	392	704	719	543	2865
Signal-to-Noise	7.37	16.72	15.28	11.40	2.06
10000 Seconds					
# Source Photons	643	2114	1898	1203	381
# Sky Photons	1307	2345	2396	1809	9549
Signal-to-Noise	14.20	31.30	28.63	21.57	3.80
30000 Seconds					
# Source Photons	1929	6341	5693	3610	1143
# Sky Photons	3920	7036	7187	5428	28646
Signal-to-Noise	25.01	54.62	49.97	37.77	6.61
100000 Seconds					
# Source Photons	6429	21136	18977	12034	3810
# Sky Photons	13067	23453	23955	18092	95486
Signal-to-Noise	45.93	99.98	91.48	69.22	12.08

Choice of Spectrometer

Unlike the multiaperture grism techniques which are limited entirely to low dispersion, the MX will be able to do high dispersion spectroscopy as well as low. High dispersion spectroscopy is possible because all of the objects are in a straight line at the slit. The image scrambling properties of the fibers improve velocity and line profile quality. The useful dispersion will be limited by the available spectrograph and by the number of source photons available. This will make a very powerful tool for stellar spectroscopy as well as for the study of clusters of galaxies. The criteria for choosing a spectrometer design include: spectral coverage, resolution, and optical efficiency. The spectrometer must also be designed to match the detector area and pixel size to the telescope optics. Our first spectrograph will be the existing Cassegrain spectrograph mounted on the telescope below the fiber head. Lengthening the fibers will allow the use of one or more spectrographs on the observing floor or in a warm room.

Low Dispersion Spectrograph

Because of my immediate personal interest in low dispersion galaxy spectra, a high-throughput, compact, CCD spectrograph may be built for low resolution work. A likely design for this spectrometer includes refractive camera lens optics with a grism dispersion element. Similar systems are being used with CCDs on several telescopes around the country. A conventional grating or prism could also be used as the disperser. The design is heavily influenced by how far out into the ultraviolet or infrared you wish to work. Reflective systems such as

spectroscopic Schmidt cameras would be most useful if they were fast enough to be used off-axis. The central obscuration in a typical spectrograph camera is a significant light loss in systems where the fiber scrambling fills in the secondary hole in the telescope pupil. Designing a camera fast enough to work at f/1.7 monochromatic, off-axis is a serious challenge. Schmidt cameras of the solid, folded, or Cassegrain varieties are potential candidates. Bingham (1983b) describes a folded, solid, Schmidt-type design for use in a CCD spectrometer. This camera works at f/0.6 monochromatic. An Ebert-Fastie spectrograph provides good quality images with a grating and a single paraboloid acting as camera and collimator, but it has no demagnification to match the slit to the detector pixels. Other exotic spectrograph designs may exist which take advantage of fiber flexibility to improve optical performance. A low dispersion spectrograph could also be a useful focal reducer for direct imaging if the dispersing element were removed.

A typical low dispersion spectrograph design is described here. A slit assembly would contain 50 optical fibers of 200 micron diameter corresponding to two arcseconds on the sky. The collimator would have a field large enough to cover a 3 cm long slit and would operate at f/8 to allow for some focal ratio degradation. The disperser could be a grism or a 300 l mm^{-1} grating in a mount which already exists. Two possible choices for the camera focal length depend on the detector to be used. If a bare CCD were used, an f/2 camera giving 2 arcseconds = 50 microns would be needed. If an intensified CCD were used, a scale of 2 arcseconds = 120 microns on the image tube would be more appropriate.

This would be followed by a transfer lens demagnifying 2:1 onto the CCD (30 micron pixels). Wavelength coverage would be in the range 380 nm to 650 nm plus whatever other coverage came for free. This spectrograph would be fairly inexpensive because many of the usual bells and whistles such as guide optics, comparison sources, and slit assemblies are already built into MX.

Littrow Schmidt Spectrograph

In the longer term, we plan to build a fiber spectrograph capable of medium to high (10^5) resolution work. A likely candidate is the Littrow Schmidt design proposed by Angel. This spectrograph would use a single set of Schmidt optics as both the camera and the collimator. A detector such as a CCD and a row of fibers are placed side-by-side in the focal plane. The grating placed in the parallel beam can then be used in Littrow mode where it is most efficient. This allows high dispersion spectroscopy with an extremely compact and efficient spectrometer. The problem, of course, is that the spectrograph optics provide no demagnification for matching the slit to the detector pixel size. Also, positioning the detector beside a conventional slit is very difficult. Fibers provide the flexibility to snake into the dewar beside the CCD chip without serious problems. Microlenses on the ends of the fibers allow the f/ratio of the incoming beam to be changed to match the detector pixel size. The major problems with this type of fiber spectrograph are: working with optics inside or very near the detector dewar; mounting the fibers very close to the detector focal plane; avoiding large central obstructions; and

obtaining microlenses to work at f/ratios faster than f/2. All of these problems appear soluble. A paper on the Littrow Schmidt spectrograph by some permutation of Lesser, Angel, Hill, and Woolf is in the contemplation phase.

Floor-Mounted Spectrograph

The light transmission properties of fiber optics allow consideration of running a long fiber bundle from the telescope to a floor-mounted spectrograph. This bundle, which links the fiber positioner head on the telescope to the spectrograph entrance aperture, would consist of 64 individual optical fibers in a protective jacket. The main advantage of a remote spectrograph is the lack of flexure problems caused by the varying gravitational field as the telescope moves around the sky. The increased stability has relatively less effect on redshifts of galaxies at low resolution with the existing Cassegrain spectrograph designed for such use. Mechanical stability becomes progressively more important as the spectral dispersion increases. A long fiber feed also provides easier spectrograph access for optical adjustments. Both the optics and the detector can operate in a temperature- and humidity-controlled environment. The remote fiber feed significantly reduces the load on the telescope because the fiber positioner box extends the telescope-mounted spectrograph 30 cm below its normal position as well as adding several hundred pounds of additional weight. By removing the requirement that the fiber head carry the additional weight of the spectrograph, some cost savings are realized, as well as additional space for guiding and acquisition

optics. The MX mounting box will be conservatively designed to support the Cassegrain spectrograph, if necessary. Use of the MX fiber head with a floor-mounted spectrograph provides a test bed for fiber links that will be used with larger telescopes in the future.

Another minor advantage of having the spectrograph on the telescope is the ease of termination of fiber bundles when no protective jacket or strain relief is required between spectrograph and telescope. Running fibers to a floor-mounted spectrograph may increase the cost of fibers, but could lead to cost savings in future spectrograph construction. Typical fiber costs are $1-2 per meter for unsheathed silica fiber. Even a 20 m link with 64 fibers would be a minor cost compared to the total spectrograph system.

The disadvantage of a floor-mounted spectrograph is the loss of light in the near ultraviolet due to absorption and scattering in the fibers. The light loss in 5 meters of QSF-ASW fiber might be 60% at the atmospheric cutoff, but is less than 20% from 400 nm to 900 nm. Focal ratio degradation does not increase with length in the lengths of interest (1 - 100 m). Focal ratio degradation can be induced by increased stress applied to the longer fiber. One scientific possibility which the floor-mounted spectrograph precludes is conventional long slit spectroscopy. I believe the ability of the fibers to record spectra of large areas of the field will more than compensate for this loss. Projects requiring spatial and spectral resolution over a small area of the field should still be done with a long slit spectrograph or a Fabry-Perot imaging spectrometer.

Data Reduction

A series of programs and CLIs (macros) designated MARS = Multi Aperture Reduction System have been written by J. Eisenhamer, D. Silva, and M. Wenz, under the guidance of J. Hill with occasional assistance by A. Koski. The major features of MARS not seen in other spectral reduction systems include: a program that locates the individual spectra on a CCD frame and extracts them into a one-dimensional format, and a program that automatically fits dispersion curves to a series of similar HeAr spectra when supplied with an initial guess at the dispersion curve and a catalog of measurable lines. The MARS driver routines and all 1-D spectra manipulations run on the Data General Eclipse (S-250) computer under AOS. The two-dimensional data manipulations such as flat fields, frame alignment and defect removal are presently being implemented on a VICOM image processing system recently purchased by Steward Observatory. The VICOM is based on a Motorola 68000 microcomputer, running under Versados, which is combined with hardware image processing for increased speed, a high resolution video display, and image memory to hold up to 8 CCD frames. The VICOM can perform pipeline arithmetic and lookup table operations at 8 MHz pixel rates to process an entire image in one video frame time. A simple array processor can be used to operate at video rates on an image with a 3 x 3 small generating kernel.

After collection of the spectral and calibration CCD frames described in Table 2, each frame must be corrected for the flat field response and bias of the CCD detector. These operations will be done on the VICOM image processing system after we have modified it to retain 16 bit data for all operations. Because it was designed for visual image

processing, the standard mode of VICOM operation uses 12 bit planes of memory for the image and 4 bit planes for eight-color graphics. Eleven bit signed integers (±4K) are fine for picture processing but are not adequate for astronomical data reduction involving multiple frame spectral images. Present Medusa data requires frame alignment of individual CCD exposures to remove flexure in the detector chain before further processing can occur. Individual frames are shifted by integer and fractional pixel amounts with the pipeline processor, so that the interlaced HeAr spectra between the galaxy spectra all coincide. Fractional pixel shifts in two dimensions can be performed by operation on the images with a 3 x 3 small generating kernel (SGK). The kernel performs bilinear interpolation of the pixels onto a displaced grid. Larger kernels could be used for more complicated interpolation schemes, but the linear term preserves most of the information in the sampled spectral image, while minimizing the blurring which occurs. We have not yet approached the problem of cosmic ray removal in a serious fashion, but it will ultimately be necessary to remove them from the data at this stage of the reduction processing.

After the individual frames have been refined and aligned, they are coadded to form the final spectral and calibration lamp images. To locate the individual spectra on the CCD frame, a copy of the coaddition result is filtered on the VICOM with a 5 x 5 kernel to smooth the data on pixel to pixel scales and to enhance features with the characteristic size of the spectra. This smooth frame is then searched for local maxima at the interfiber spacing to identify the individual spectra. Ten cuts are made transverse to the dispersion direction and a parabolic

fit is used to locate the maximum position of each spectrum across the chip. These data points are then used to generate second-order polynomials which describe the locations of the spectra on the image frame. This set of polynomials is used as a map to direct the program which extracts the individual spectra from the original, not smoothed, data frames into one-dimensional files. Other parameters for the extraction process such as the width of spectrum to extract are entered by the user.

The one-dimensional files can be formatted to work on either of the spectral reduction systems now in use at Steward: IRS by C. Foltz, or CZWT by W. Tifft. In order to avoid the tedium of measuring the positions of thousands of helium and argon lines by hand, we have written an automatic routine to find dispersion curves for all of the comparison spectra on a given calibration frame. The program uses a rough dispersion curve of the first fiber spectrum on a frame to predict line positions on the next spectrum. The process continues across the entire length of the slit. With an accurate prediction, the program is able to find the center of the emission lines by fitting a parabola to the local maxima in the spectra. This program has been quite successful and usually produces a better dispersion curve than manual measurement while taking only 5% of the time previously required. I should point out that this routine is fast and efficient but not magic. If the calibration frame is of poor quality it will produce meaningless dispersion curves. Care must be taken to be sure that the data and the wavelength catalog are similar enough to prevent the prediction algorithm from becoming unstable.

Measurement of lines in galaxy spectra is currently done manually with IRS. Figure 21 shows one of 30 spectra extracted from a series of exposures in Abell 993B. Both the raw sum and the sky-subtracted sum of nine 20-minute exposures are shown. The raw extraction of a single 20-minute exposure is also shown. No flat field correction has been applied in this preliminary reduction. Large cosmic ray events were removed manually. The redshift measured from six absorption lines in galaxy 255 is 11720 km s^{-1}. At some time in the future we expect to use a cross correlation routine to automate the galaxy measurement process. When combined with manual verification, the cross correlation procedure should be faster and more reliable than manually measuring line positions. The major problems are expected to be creating templates, and removing cosmic rays and emission lines which would give false correlation peaks.

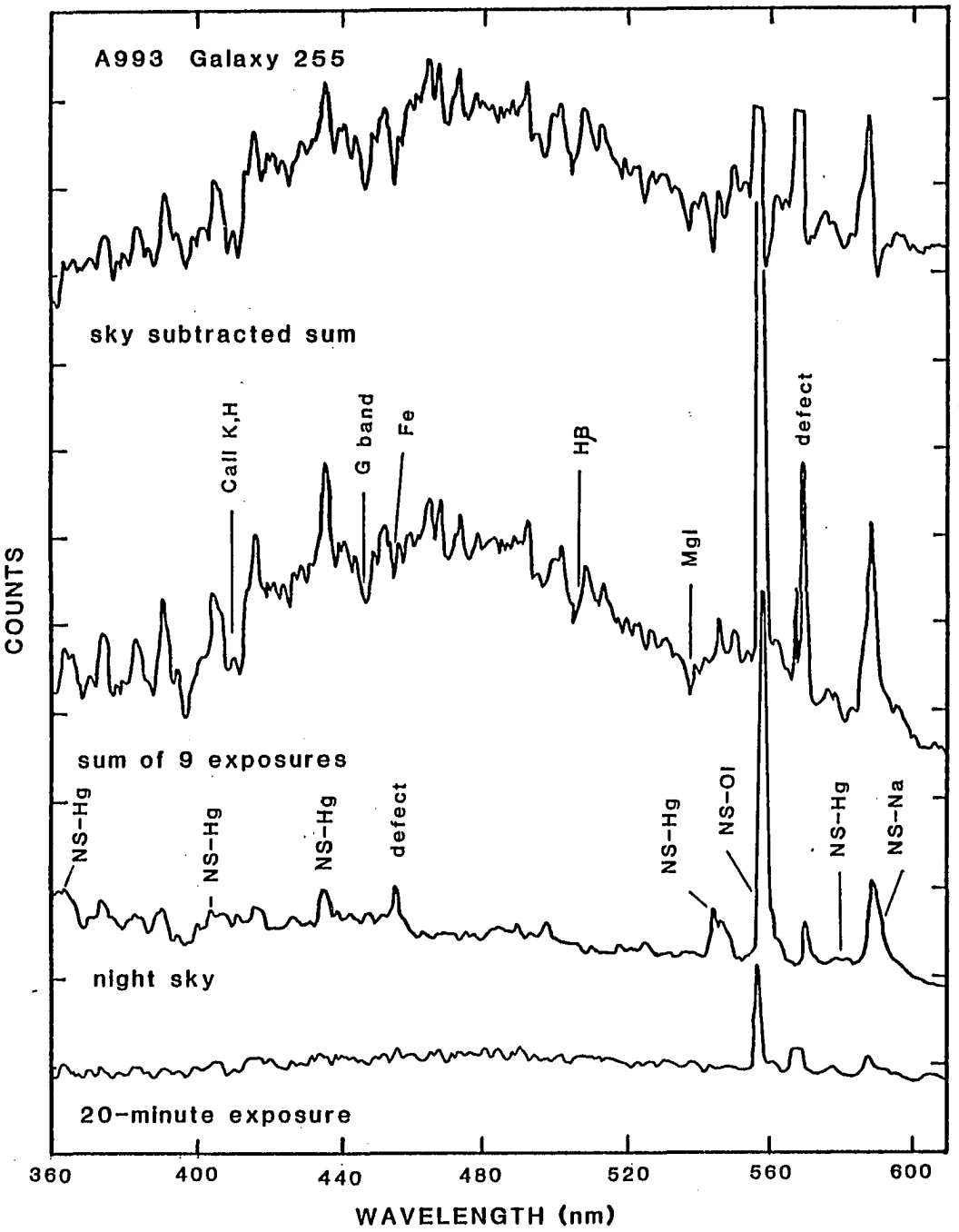

Figure 21. Spectrum of A993B.2.G255

This figure shows the spectrum of galaxy 255 in the cluster A993. The Medusa spectrograph with an intensified CCD detector was used on the 2.3m telescope. A single 20-minute exposure is plotted at the same scale as the raw and sky-subtracted sum of nine 20-minute frames. The spectral resolution is 12 Å.

CHAPTER 8

LENSES FOR MATCHING OPTICAL FIBERS

Hill, Angel, and Richardson (1983) present a detailed discussion of "Optical Matching for Fiber Optic Spectroscopy". The major portion of this chapter is extracted from a draft of that paper. Roger Angel and Harvey Richardson deserve the credit for originally thinking of the pupil-imaged fiber matching technique.

The Need for Matching

In a spectroscopic system with an optical fiber optimally coupled to the telescope and spectrograph, the transmission losses introduced by the fiber should be negligible. The dominant loss is from dielectric reflection, at the ends of the fiber, which can be suppressed by antireflection coating. The most serious light loss in the Medusa system arises from the f/9 input beam being degraded by the fiber to f/4.5. Roughly half of the light is then lost because it misses the spectrograph collimator. A faster collimator could be used at the expense of lost spectral resolution. The best currently available fibers will degrade a slow beam to f/8 in the stress of the telescope environment. Therefore, if the incoming beam is f/4 it will experience relatively little degradation. At the other extreme, beams faster than f/3 start to show transmission losses at the blue end of the spectrum (Barden, 1983). If the correct telescope or spectrograph combination is unavailable, there are four ways to change the speed of

the optical system to match the characteristics of the fiber: 1) build a new telescope or spectrograph (very expensive); 2) use a normal transfer lens as a telecompressor to provide a fast (f/4) focus with smaller images; 3) a microlens may be mounted at the end of the fiber to form an image with the appropriate f/ratio on the fiber core; 4) a microlens may be mounted at the end of the fiber to form an image of the telescope pupil on the fiber core. If a similar lens is placed at the output end of the fiber, the pupil-imaging optics will convert the effects of focal ratio degradation in the fiber into an increased image size at the output lens. In the absence of focal ratio degradation, pupil-imaging will preserve seeing disks smaller than the entrance aperture at the expense of perfect image scrambling. In the absence of an output lens, the pupil-imaged input lens provides optimum coupling of the marginal ray bundles when a significant change in f/ratio is required.

Focal Ratio Degradation

The one bad quality of commercial fibers is focal ratio degradation. Focal ratio degradation is always present at some level in real optical fibers and its causes are rather obscure. The light propagates down the fiber waveguide in modes which correspond to the angles the light makes with the optical axis. Higher-order modes make steeper rays inside the fiber. Modes higher than f/2 in air outside the fiber are lost because the angle of attack at the core-cladding interface is too high for total internal reflection to occur. The angle where this occurs depends on the refractive indices of the core and

cladding materials. Plastic-clad fibers have a slightly larger index difference than all-silica fibers, and therefore can propagate slightly faster beams. If no interaction of modes took place, then all rays would exit the fiber with exactly the same angle at which they entered, and the focal ratio of the resulting beam would be preserved. Stresses on the fiber and irregularities at the core-cladding interface called "microbends" cause imperfections in the propagation characteristics of the fiber. These intrinsic or induced imperfections in the fiber make its waveguide properties slightly nonlinear. The nonlinearity causes coupling between modes travelling at different angles in the fiber. The mode coupling causes a spreading of the beam that propagates through the fiber. Thus parallel or nearly parallel light entering the fiber may exit in an f/6 or faster cone. Some measurements of this effect have been published by Powell (1983), by Barden, Ramsey, and Truax (1981) and by Angel, et al. (1977). See Gambling, Payne, and Matsumura (1975), and Jeunhomme and Pocholle (1975) for a discussion of mode coupling in fibers. This degradation of focal ratio, regardless of its precise cause is a significant obstacle to spectroscopy of faint sources. Unfortunately, some mode mixing is desirable for telecommunications fiber, since it causes monochromatic photons to travel at the same average angle and therefore the same average speed in the fiber. This averaging minimizes pulse dispersion and increases the useable bandwidth. Herskowitz, Kobrinski, and Levy (1983) discuss Angular Division Multiplexing, a technique which transmits several signals through the same step index fiber simultaneously at different angles. This allows step index fiber to have a bandwidth comparable to graded

index fiber. This technique relies on low mode coupling in the fiber, and could lead to the development of fibers with very low focal ratio degradation. The following sections will discuss optical coupling to fibers and methods to minimize the effects of focal ratio degradation. Figure 22 reproduced with permission from Powell (1983) shows integrated output profiles of fibers to illustrate the effects of focal ratio degradation at various input focal ratios. 70% absolute transmission including end reflections and focal ratio degradation can be achieved in visible light.

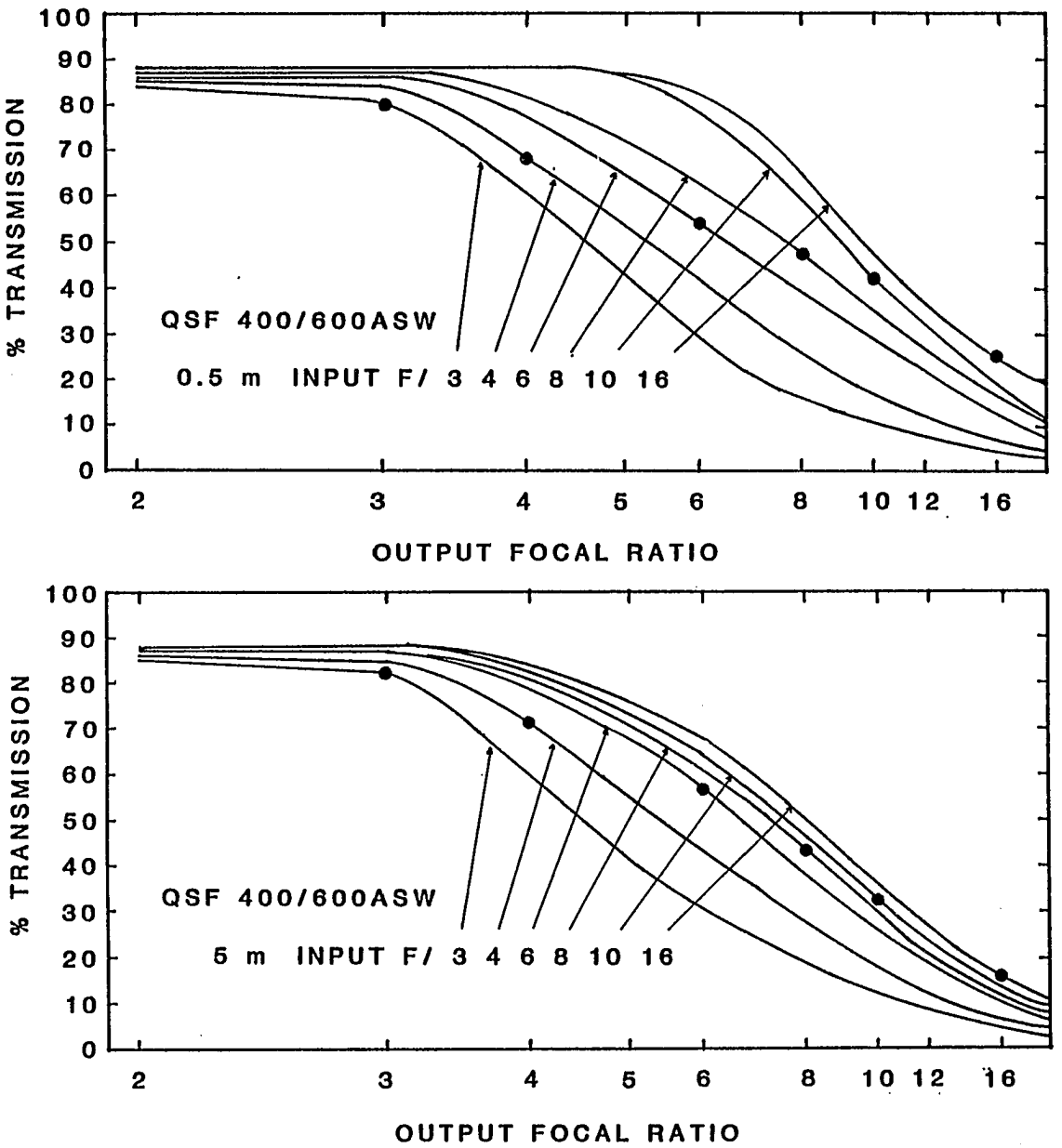

Figure 22. Effects of Focal Ratio Degradation on Transmission

This figure reproduced from Powell (1983) shows measured integral profiles of the output of 400 micron core all-silica fibers. Absolute transmission at various input and output focal ratios was measured. The dots indicate the transmission within the input focal ratio.

Optical Matching Considerations

The major objectives in using optical fibers efficiently for astronomical spectroscopy are: first, matching the fiber diameter to the size of the image or seeing disk; and second, obtaining a fiber or fiber - lens combination that doesn't degrade the focal ratio of the propagated beam and thereby destroy the Lagrange invariant of the telescope. The Lagrange invariant, $ny\theta = n'y'\theta'$, must hold paraxially throughout the unaberrated telescope system. n is the refractive index, y is the marginal ray height or pupil diameter, and θ is the ray angle. This is sometimes expressed as the $A\Omega$ product, where A is the area of the beam or entrance pupil, and Ω is the solid angle subtended by a source or the spectrometer entrance aperture on the sky. These products must remain invariant through the telescope-spectrometer system in order to preserve the photometric intensity (radiance) of the source being observed. In an astronomical spectrograph this product can never be reduced below the value $A_t\Omega_s$, the product of the area, A_t, of the telescope primary, and the solid angle on the sky, Ω_s, of the light to be accepted by the spectrograph. Any optical aberrations, focal ratio degradation, or image-aperture mismatch will lower the intensity and degrade the system throughput (see Meaburn, 1970). The $A\Omega$ product is related to the slit-limited resolving power, R, of a grating spectrograph in or near the Littrow condition as follows:

$$R = 2 \tan \beta \, (sA_g/A_t\Omega_s)^{1/2} \qquad (8.1)$$

where β is the grating blaze angle, s is the shape factor, or the aspect ratio of the beam at the grating, and A_g is the area of the grating. $A\Omega$

is also directly related to the area, A_p, of an image or spectral resolution element at the detector. The solid angle of light converging to the focus is proportional to $1/F^2$, where F is the camera focal ratio, thus:

$$A_p = F^2 A_t \Omega_s \tag{8.2}$$

When a fiber is introduced into the optical train, the product $A\Omega$ is in general increased. Ω is increased because of focal ratio degradation, and A will be increased if the light entering the fiber does not fill the fiber entrance. An important goal in using fibers for spectroscopy is to minimize the increase in $A\Omega$, since this will reduce the spectral resolution and increase the detector size needed. The aspect ratio of a single round fiber is unity, so reformatting an image for increased resolution can only be done by using multiple fibers, or an image slicer after transmission by one or more fibers.

The range of values of $A\Omega$ that can be effectively transmitted by any given fiber is quite limited. At the output, A is fixed by the core diameter. Ω can only range between a minimum of around 0.01 (f/9), set by the amount of focal ratio degradation in the fiber, and a maximum of around 0.20 (f/2), set by losses into the cladding. The fact that single fibers can be used efficiently for stellar or near-stellar object spectroscopy depends on a coincidence between $A\Omega$ found for large telescopes in reasonable seeing, and the small range of the $A\Omega$ product characteristic of communications fibers. Fibers have an area around 10^{-9} that of telescope aperture, but the solid angle they transmit efficiently is about 10^9 times larger than that of atmospheric seeing.

Coupling into Fibers

There are several ways to minimize the impact of fiber focal ratio degradation on the optical system. The most straightforward solution is to look for fibers with weaker mode coupling. Minor variations in jacketing and manufacturing technique can have significant effects on fiber performance. Care should also be taken to mount the fiber at the telescope with minimum stress and bending. Heacox (1983) has reported measurements of a 15 m length of 50 micron diameter fiber from Fujikura which suffers only 4% focal ratio degradation at f/5. A second way to avoid the degradation problem is to use fast beams (f/2.5-f/4) which are altered significantly less than slow (f/10) beams. This cannot be carried to the extreme, since for beams faster than f/2.5 transmission losses begin to show up due to imperfect total internal reflection. For beams slower than f/6, degradation of the focal ratio widens the beam to a faster one in greater relative proportion. Measurements of all-silica fibers (QSF-AS) by Powell (1983) show that 82% of the light in a f/4 input beam remains inside f/4 while only 48% of an f/10 beam remains inside f/10 for the same fiber at 550 nm. This driver to a f/3 beam makes prime focus mounting of fibers most convenient. The use of a fiber in a focal plane at a fast focus is the simplest form of fiber coupling. The fiber area should then be given by equation (8.2). At the f/2.7 prime focus of a 4m telescope, for example, a fiber with 100 micron core diameter is needed. For those cases where the telescope does not offer the appropriate f/ratio, coupling can be made at a slower focus, such as Cassegrain or Ritchey-Chrétien. The change in speed can be accomplished in three ways with

lenses or mirrors used to reimage onto the fiber. In making the coupling into a fiber, we need to choose a point in the optical system where $A\Omega$ is equal to its minimum value $A_t\Omega_s$. Minima are reached in the focal planes, and at images of the entrance pupil. Care must be taken to ensure that $A\Omega$ is not increased in the imaging process. Of course a suitable lens arrangement must be made at the output end of each fiber for coupling with the spectrograph. The details of the coupling schemes are discussed in the following sections.

Macrolens Coupling

A macro- or normal-size lens acts as a telecompressor to reimage a slow focus to give the telescope a fast focus with small images. There is no problem preserving $A\Omega$ if macroscopic scale optics are used. The lens forms a large image of the pupil, and the chief rays remain effectively parallel over the scale of the fiber. This approach is most practical with a narrow field-of-view. In the case of very large fields to be covered with many fibers, the costs of large, high-quality optics make it desirable to use microscopic lenses to couple each fiber individually.

Microlens Coupling - Direct

In the most straightforward application of a microlens for fiber matching, the lens is used to alter the focal ratio of the beam before the image is formed on the fiber end. A microlens mounted directly at the end of each fiber will form a small, fast image on the fiber tip. "Microlens" is used here as a general term to describe several types of optical focusing elements with dimensions comparable to those of the

fiber itself. The fast beam (f/4) can then propagate through the fiber without suffering serious focal ratio degradation. The fiber entrance aperture must now be smaller than the unlensed stellar image to compensate for the demagnification of a faster focal ratio. Figure 23 shows the "direct" microlens schematically. The principle advantage of this direct microlens or telecompressor scheme is that the image scrambling properties of the fiber are preserved while minimizing focal ratio degradation. However, when a single microscopic lens images a small pupil near the focus, then Ω will be increased over its minimum value by a fraction equal to the ratio of the fiber area to the pupil area. This effect can be eliminated through the use of two microscopic lenses or two surfaces of a thick lens which are together afocal. The pupil is then kept distant from the fiber end, but increases its angular diameter.

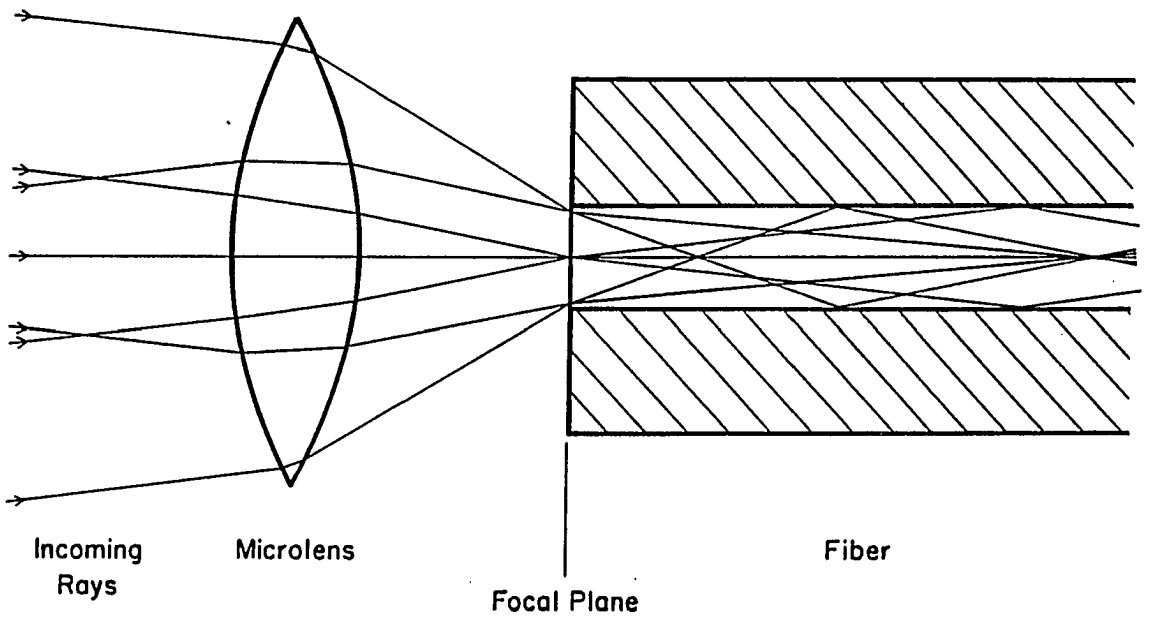

Figure 23. Schematic View of Direct Microlens Coupling

This figure shows the simplest approach to changing the f/ratio of light entering an optical fiber. The microlens reimages a small area of the focal plane to a more compact plate scale.

Microlens Coupling - Pupil

I wish to point out a new alternative approach to microlens coupling. A microlens on each fiber is used to image the telescope pupil rather than the star image on the fiber core. A pupil-imaging microlens is shown schematically in Figure 24. In this case the microlens acts somewhat like a field lens or a Fabry lens. The star image is focused at the front focal point of the lens and emerges from the rear surface of the lens as a parallel bundle. Off-axis points in the front focal plane emerge as parallel bundles which intersect the axial bundle to form the image of the telescope entrance pupil at the rear focal plane. Depending on the type of lens used, the front and rear surfaces of the lens may or may not correspond to the focal planes. If a pupil is to be formed at the rear focal plane of the microlens, the stellar image must be placed at the front focal plane of the microlens. The size of the pupil image on the fiber core is determined by the f/number of the incoming beam and the focal length of the microlens. This holds promise for better matching, for now the fixed circular area of the fiber can be exactly matched to the fixed circular telescope pupil. The focal length of the lens and the diameter of the fiber are chosen so the telescope pupil fills the fiber core while the propagating beam has a focal ratio suitable for minimum degradation. When the telescope pupil is imaged on the end of the fiber in this manner, the range of angles or number of modes propagating in the fiber is determined by the original image size and its position relative to the fiber axis. The condition that $A\Omega$ entering the fiber be at the minimum value is now met by the star image being distant as seen from the fiber.

If a second lens is used at the output end of the fiber, focal ratio degradation will cause an increase in the image size while retaining a constant angular diameter output cone. A pair of pupil-imaging lenses at each end of a fiber work in a fashion similar to a two-element symmetrical transfer lens. In addition to not overfilling the spectrograph optics with a fast beam, this lens scheme potentially preserves the seeing disk incident on the input lens. Neglecting the effects of focal ratio degradation, an image centered on the input lens will be reimaged as an azimuthally-scrambled image of the same size by the output lens. Output image size is now independent of the fiber core diameter. An off-axis image will be scrambled into a ring with radius equal to its distance off-axis and width equal to the original image diameter. Imaging of the telescope pupil allows preservation of good seeing at the expense of losing better image scrambling previously obtained. Figure 25 shows predicted images for various sizes and positions of the input image. The azimuthal scrambling of the pupil-imaged fiber and microlens combination should eliminate color effects caused by atmospheric dispersion. Thus images of all colors at the spectrograph entrance aperture will have the same centroid, provided they fall within the entrance aperture of the fiber at the telescope focal plane. The useful size of the entrance aperture stop is still determined by the uncorrected atmospheric dispersion or seeing disk, whichever is larger. By placing adjustable slit jaws after a pupil-imaged fiber or set of fibers at the entrance aperture of the spectrograph, it is possible to adjust the resolution in the direction of the dispersion to match the seeing. A better solution which is not

very practical would be to place a tiny adjustable aperture in front of each fiber in the focal plane. A set of slicing optics could be added to the slit assembly to reimage the round pupils into narrow rectangles entering the spectrograph. Image slicing at the fiber slit requires a larger spectrograph field to accomodate the space used between the individual fibers.

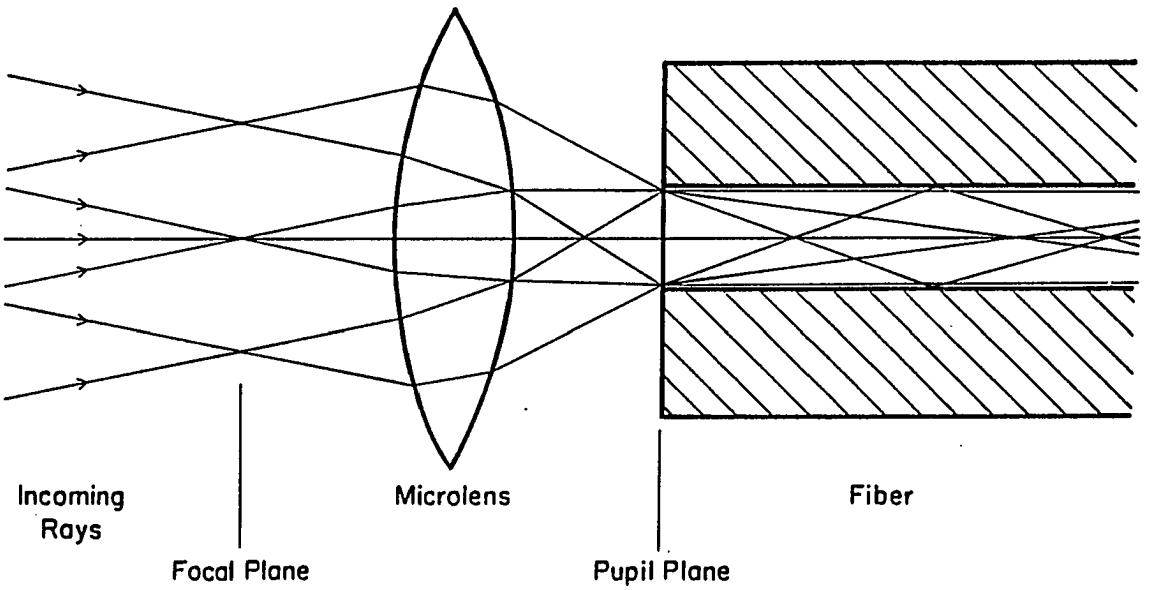

Figure 24. Schematic View of Pupil Microlens Coupling

This figure shows the alternate method of modifying the f/ratio of light entering a fiber. The microlens forms an image of the telescope entrance pupil on the end of the fiber rather than the usual star image.

Types of Microlenses

Nicia (1981) discusses lens coupling in fiber optic devices from a communications point-of-view, ie. a two-lens connector coupling the ends of two lengths of fiber. We wish to consider the astronomical point of view where two optical systems, ie. telescope and spectrograph, are each coupled to the ends of a single fiber with lenses. Among the various microlens varieties available for this purpose, we find the following types:

1) the simple lens, a single refracting surface, or two curved surfaces with glass in between. In fact, this thin lens version of the microlens is not practical because of the short focal lengths involved.

2) a pair of thin lenses acting as a telescope. This makes an afocal system which changes the speed of the incoming beam, but does not appear practical in very small sizes.

3) the spherical lens, a complete sphere of glass. The focal length is determined by the radius of the sphere and the index of refraction of the glass. A sphere of refractive index 2 has the interesting property that the focal length is equal to the diameter. Sapphire (n=1.78) and ruby spherical lenses are available from the Adolf Meller Co., Providence, RI in a variety of sizes.

4) the rod lens, a cylinder of glass with a hemispherical curve on one end. Rod length and curvature are adjusted for desired imaging properties. Because all of the optical power is in a single surface, rod lenses are not as useful as spheres at very short focal lengths where total internal reflection limits performance. Rod lenses could possibly be made from short lengths of large diameter fiber.

5) the graded index (GRIN) lens, known commercially as SELFOC, a cylindrical glass rod with optical power derived from a radial refractive index gradient. A 1/4-pitch lens has focal length effectively equal to the lens length. SELFOC lenses are manufactured in several sizes by Nippon Sheet Glass Co..

6) the distributed-index planar microlens, similar to a GRIN lens but with a three-dimensional index gradient. These lenses are described by Iga, Oikawa, and Banno (1982), but are not yet in commercial production.

7) lenses built into a fiber. A lens can be formed on the end of a fiber by heating or by etching. The fiber can also have a tapered diameter to change the beam f/ratio gradually along the fiber. Tapered fibers appear attractive for matching to a particular spectrograph format, but are not readily available.

In this chapter I will deal with the spherical, rod, and GRIN lenses as the most readily available examples of microlenses. Versions of these lenses, which form a pupil image at the back surface when the star image is at the front focal plane, are quite useful, because optical coupling directly onto the fiber can eliminate reflections from a pair of air-glass surfaces. While 1/4-pitch SELFOC lenses and rod lenses have this property, no glass of refractive index 2.0 exists to make a suitable spherical lens at visible wavelengths. Optical coupling of a spherical lens with an index matching fluid would remove some of the power of the second surface of the lens.

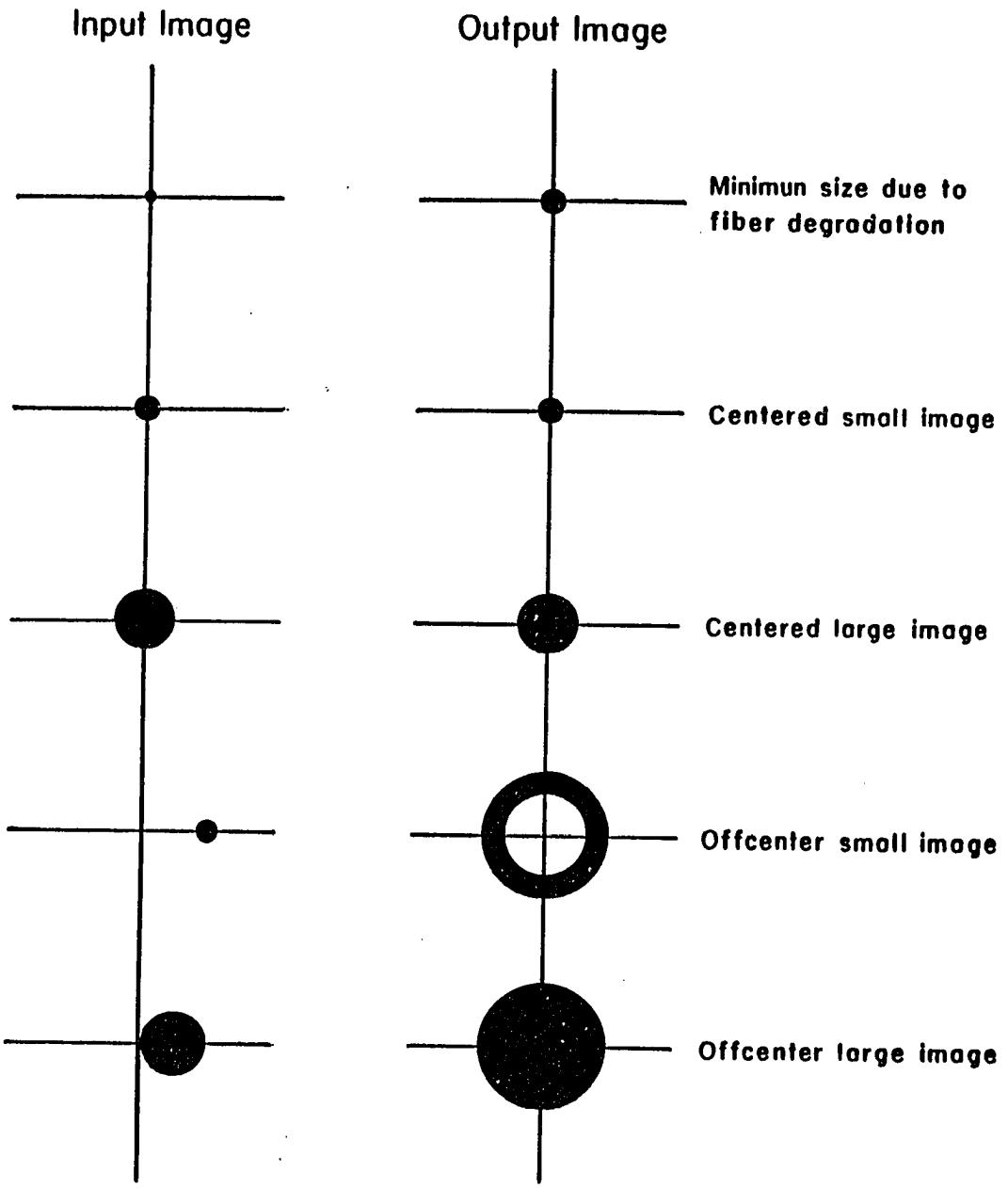

Figure 25. Predicted Images for Pupil-Lensed Fibers

This figure shows the predicted images transmitted by pupil-lensed fibers for a variety of inputs. The left side of the figure shows the image at the telescope focal plane seen relative to the optical axis in front of the input lens. The right side shows the azimuthally scrambled image at the spectrograph entrance aperture after transmission through the fiber and output lens.

Specific Lens Properties

Ray Traces

We (Angel, Hill) have performed ray traces to verify the properties of pupil-imaging onto fibers described in the previous section. Paraxial ray traces were carried out for spherical, rod, and SELFOC lenses. Thomlinson (1980) discusses ray tracing in graded index lenses. As an example, I present here a ray trace of spherical microlenses used in the pupil-imaging mode. This is surely not an exhaustive treatment of the subject. The input conditions of an f/9 beam and a 300 micron image spot are pupil-imaged with a sapphire ball onto a 133 micron core silica fiber propagating light at f/3.8. The focal length (f) of a spherical lens of radius (r) and refractive index (n) in air is given by:

$$f = {}^{nr}/_{2(n-1)} \tag{8.3}$$

A 2 mm sapphire ball (n=1.78) has a focal length of 1.14 mm. Table 12 shows the results of the ray trace. The marginal and chief rays were traced simultaneously at all surfaces using the equations of refraction and transfer:

$$w'_j = w_j - y_j \phi_j \tag{8.4}$$

$$y_{j+1} = y_j + t_j w_j$$

where y is the ray height, w is the product of the ray angle and the refractive index, t = d/n is the optical path length, and ϕ is the power of the refracting surface. A bar indicates the corresponding chief ray variable. The lens reimaging preserved AΩ at the 0.4% level, although the slightly oversized fiber accounted for a 9% degradation.

Table 12. Ray Trace Results

This table lists the results of a paraxial ray trace of a pupil-imaging lens and fiber system. w is the product of the ray angle and refractive index. y is the ray height of the marginal ray. The bar indicates the corresponding values for the chief ray. n is the refractive index between surfaces. t is the optical path length between surfaces. Ø is the refractive power of the surface. AΩ is the area - solid angle product. All units are in millimeters. The input beam is f/9 with a 300 micron image. The sapphire lens is 2 mm in diameter with a 1.14 mm focal length. The output beam is f/3.8 into a 133 micron fiber. The transfer equations are shown in 7.4.

Surface	$\frac{w}{y}$	$\frac{\bar{w}}{\bar{y}}$	n	t	Ø	AΩ
	0.0000	0.0555				
focal plane						6.85E-03
	0.1500	0.0000				
			1.00	0.000		
	0.0000	0.0555				
1st surface					0.78	
	0.1500	0.0000				
			1.78	1.124		
	-0.1170	0.0555				
2nd surface					0.78	
	0.0185	0.0624				
			1.00	0.140		
	-0.1310	0.0068				
fiber surface						6.88E-03
	0.0002	0.0634				
			1.45			

Lens Aberrations

Because of the size and simplicity of these lens systems, spherical and chromatic aberration dominate. Nicia (1981) compares the magnitude of the aberrations for graded index, ball, and rod lenses. His results are applicable with minor modifications to fiber-coupled spectroscopy, as well as communications. Spotsize due to spherical aberration in a microlens depends on the focal length of the lens, the refractive index, the type of microlens, and the third power of the numerical aperture of the fiber or cone of light entering the fiber. The rms spotsize due to third-order spherical aberration in the spherical lens raytraced above was 0.2 microns. Spherical aberration becomes significant when matching fibers to optical systems faster than f/2. Chromatic aberration is dominated by the change in focal length due to the variations of refractive index with wavelength in glass. For the sapphire lens described above, the focal length varied by 1%, giving a spotsize of 1 micron between 486 and 656 nm, for a focal length of 1.14 mm.

Lens Transmission and AR Coatings

In the visible region of the spectrum, lens transmission is not a serious problem as a wide variety of glasses are available. Lenses made of doped glasses, such as SELFOC microlenses, should be checked carefully before use in the infrared or ultraviolet. A much more serious problem is Fresnel reflection from the glass surfaces. A fiber with a microlens at each end has six air-glass surfaces before the light reaches the spectrograph optics. The amount of reflection increases

with higher index glasses such as sapphire. Four sapphire surfaces with n=1.78 would reflect 28% of the incident light. Most microlens suppliers have an antireflection (AR) coating available (typically MgF_2). Four of the six air-glass surfaces can be combined into a pair of glass-glass surfaces by optically coupling the microlenses to the ends of the fiber when the optical design permits. In practice, both AR coatings and optical coupling can be used to reduce reflection losses to the 4% level.

Summary of Tests of Sapphire Balls and Optical Fiber

The tests described here were performed to verify the imaging properties of a sapphire ball imaging the telescope pupil on the end of a fiber. The spherical lenses used were 2 mm diameter, uncoated, sapphire (n=1.78) balls with focal length 1.14 mm. The fibers were QSF200AS, 133 micron core with doped-silica cladding, silicone resin buffer, and teftzel plastic jacket in 60 cm lengths. The fibers were previously polished flat to one wavelength by hand polishing on Moyco Ultralap abrasive film. The balls and fibers were mounted in 6 mm thick aluminum plates for testing as shown in Figure 26. The fiber was focused by tuning the sharpness of the output cone as the glue hardened. A special clamping and testing fixture would be needed to do this efficiently in the future.

Tests of the bare (unlensed) 200AS fiber showed potential for propagation at f/9 when the fiber was held straight and unstressed. When mounted in position similar to that used in a fiber optic spectrograph, the output beam was f/6 - f/7 with a f/3 halo ring. The

halo appears to be caused by peculiar mode coupling caused by the refractive index distribution of the cladding layers in the all-silica type of fiber. . Sharp bending stresses could degrade the image to f/2.5, but these glass-on-glass fibers are generally more resistant to pressure induced degradation than are plastic-coated silica (PCS) fibers. The test setup is shown in Figure 27. A 45 micron test image was formed by reimaging and minifying a laser-illuminated 133 micron core fiber through a 55 mm focal length El Nikkor lens with an adjustable aperture stop. The tests were performed at f/9, but the results were insensitive to the input focal ratio. The source and target fibers were mounted on translation stages for focus and alignment adjustments.

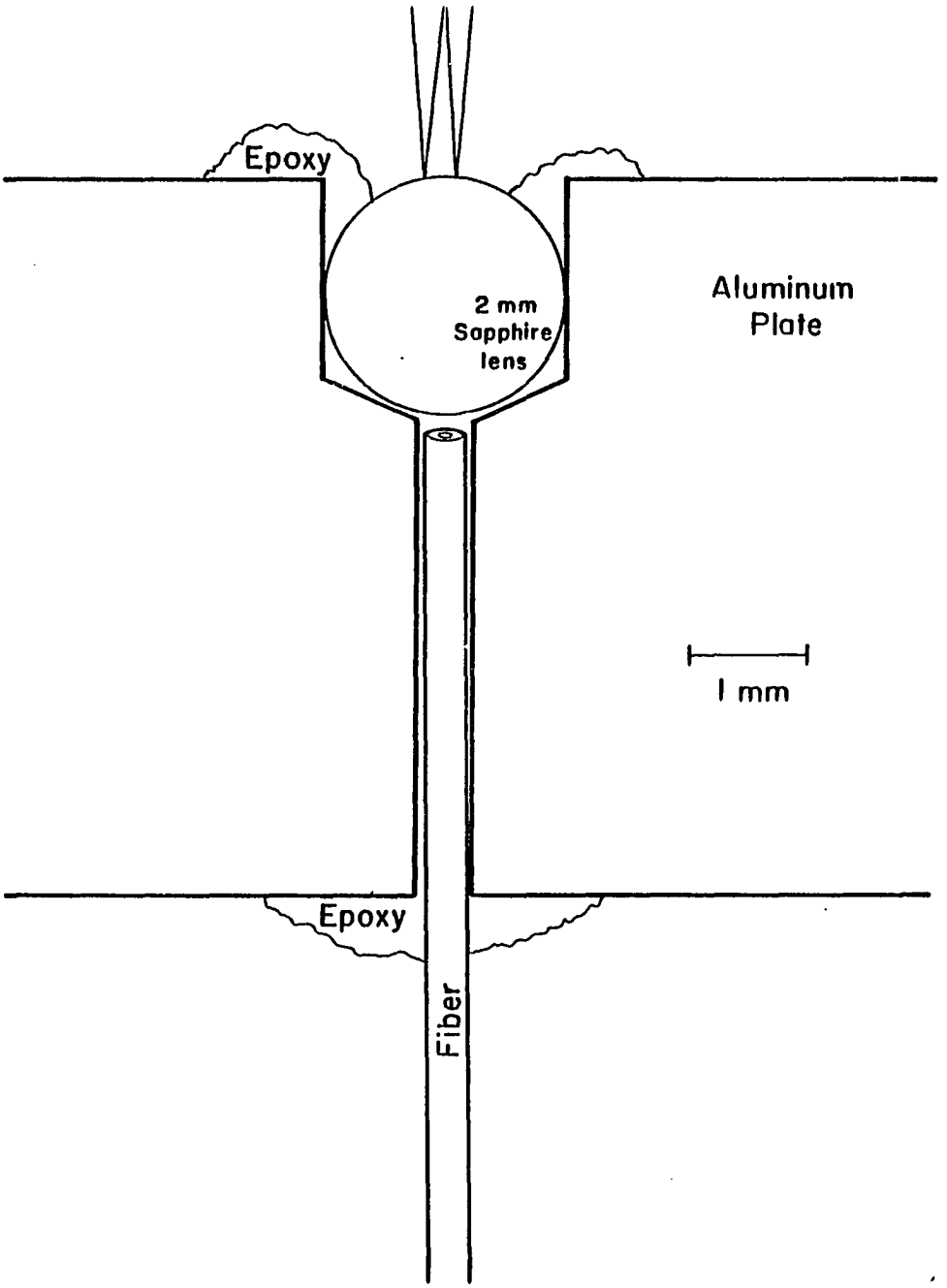

Figure 26. Lens and Fiber Mounting for Testing

This figure shows the method used to mount the optical fibers and sapphire microlenses for testing.

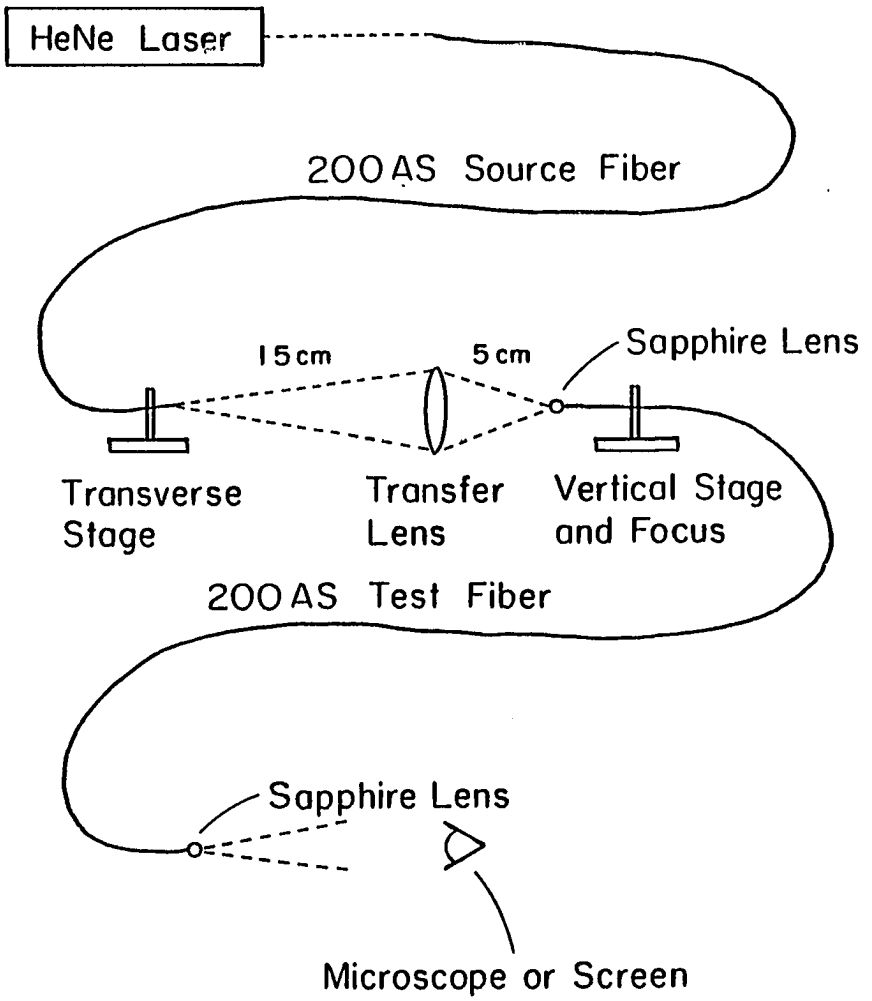

Figure 27. Fiber Test Setup for Observing Pupil-Lensed Images

This figure shows the optical test setup used for evaluating the pupil-imaging of optical fibers. A bare fiber illuminated with a laser was reimaged to form a test spot. 2 mm sapphire microlenses and 133 micron core silica fiber were used.

The image shown in Figure 28 was observed with best focus and alignment. This structure is expected with a point source image and the known amount of focal ratio degradation within the fiber. The same core-halo structure is observed in the output cone (pupil) of a bare 200AS fiber. The following calculations provide crude quantitative verification that the observed image would be expected from bare fiber characteristics.

$$F/\# = (2*\tan u)^{-1} \qquad (8.5)$$

where, u = ray angle, tan u = N.A. = numerical aperture

$$\phi = 1/f$$

where, ϕ = power (phi), f = focal length of lens

$$\phi * y = u$$

where, y = image radius

Thus for a f/3 halo the expected image diameter is 380 microns, and for a f/6 core the expected image diameter is 166 microns. The observed image diameters were 400 microns and 175 microns respectively. The observed output cone angle of the lensed fiber is about f/8. This is slightly faster than the predicted value of f/8.5, but may be due to poor lens focus. The cone is uniformly illuminated and shows no pressure induced effects except intensity changes. In summary, these tests verified the predicted performance of the lens - fiber combination with the pupil-imaged onto the fiber end.

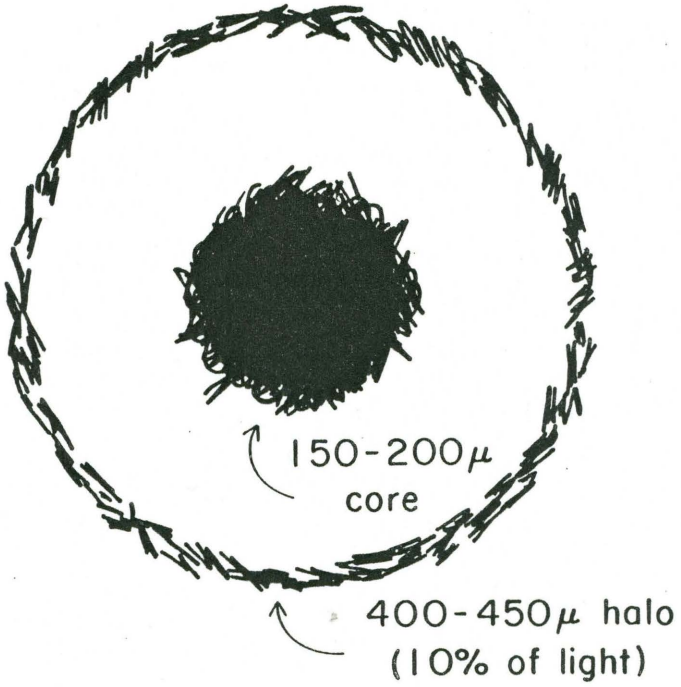

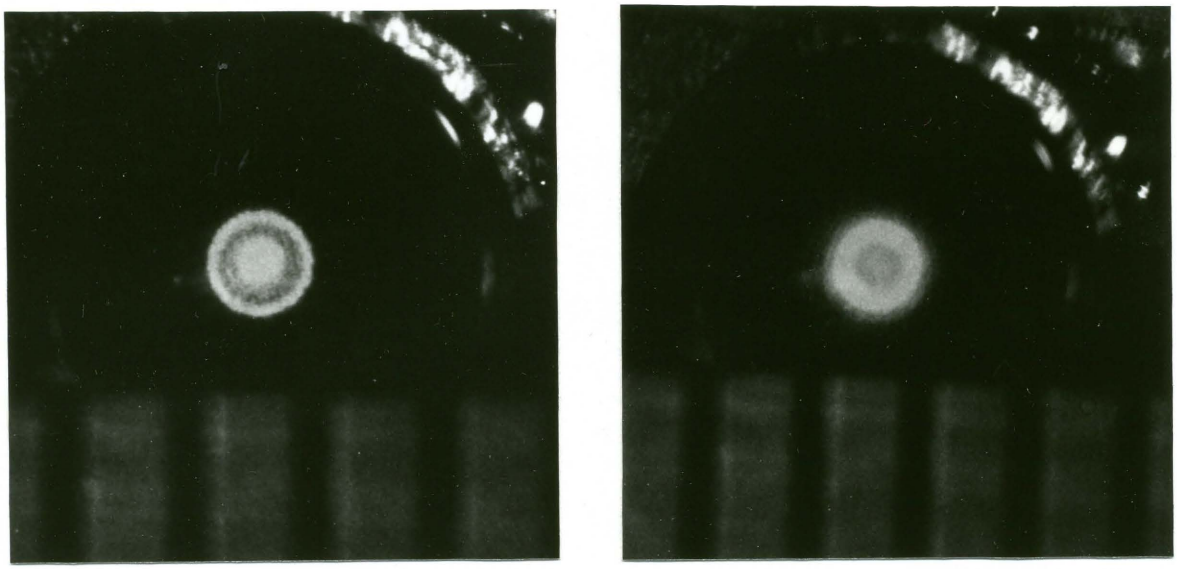

Figure 28. Observed Image through Fiber and Sapphire Balls

This figure shows the image observed through a fiber with sapphire ball lenses in the pupil-imaged configuration. The sketch at the top shows the structure of the best focus image. The halo is due to a peculiar defect of the QSF-AS fiber. The photomicrographs (overexposed) show the output image with the input image centered (left) and offcenter (right). The ruler divisions are 0.5 mm.

Implications for the MX Spectrometer and Other Systems

"To lens or not to lens"

The previously described tests of spherical lenses used to image the telescope pupil through optical fibers have revealed several disadvantages to accompany the previously known advantages of this type of optical matching scheme. I consider these advantages and disadvantages for the MX mobile fiber spectrometer which is now under construction. The principal merits of using a spherical microlens or Selfoc lens to image the telescope pupil on the fiber end are:

1) easy optical matching to any f/ratio system by proper choice of fiber diameter and lens focal length.

2) optimum preservation of the $A\Omega$ product or seeing size despite the image scrambling characteristics of the fiber.

3) fixed f/ratio output regardless of the focal ratio degradation in the fiber.

The corresponding disadvantages or problems with this scheme include:

1) the presence of a minimum output image size caused by focal ratio degradation in the fiber.

2) nonstable image geometry to introduce possible second-order radial velocity errors.

3) difficulty in mounting and aligning tiny lenses, fibers and field stops.

The details and implications of these problems and tradeoffs will be discussed in the following sections.

Image Size

Image size at the output end of a lensed fiber system is determined by three factors for a given optical configuration, specifically with the telescope pupil-imaged onto the fiber end with a microlens. The output image is an azimuthally scrambled version of the input image within certain size limits. This is because the ray angles or modes, but not positions, are preserved as the light travels through the fibers. The spherical lens then reimages each ray angle to a specified image radius, but no particular angle. Focal ratio degradation via mode coupling causes light to be scattered out of the low angle modes which form the axial image and into higher angle modes which are imaged at a larger radius. For the MX Spectrometer configuration of 2 mm balls and QSF200AS fiber, the minimum image size, even with perfect seeing, is limited to 150 microns due to the f/6 focal ratio degradation in the fiber. This effectively eliminates any large gains that would otherwise be made with sub-arcsecond seeing if the aperture size was not changed. Image size is also degraded by offcenter input images. The scrambling properties of the fiber introduce azimuthal scrambling in the lensed image. An offcenter star image appears as a ring with a radius equal to the distance of the input image from the fiber axis. This makes excellent guiding essential for obtaining small images at the fiber output.

Velocity Effects

Variable image size and geometry caused by the effects described above have the potential to introduce radial velocity errors via

"second-order slit effects". The azimuthal scrambling prevents the centroid of the output image from moving with the input image. The second moment of the image changes with input motion and is different for comparison and stellar images. This allows for small random and systematic errors in the radial velocity determination. The severity of the problem is a strong function of image sampling and non-uniformity of detector response (i.e. CCD pixels). The QSF-AS fibers also produce the f/3 halo which causes similar problems by imaging as a ring around the output image core. Bare fibers, in contrast, produce circular, fixed-size, well-scrambled images while their output cones may vary in focal ratio. The varying angle of spectrograph illumination in combination with vignetting and focus errors can also effect velocity determinations. The velocity errors may or may not be significant depending on the application. I should point out that these errors will be significantly smaller than first-order slit effect velocity errors introduced by uneven guiding on a conventional slit spectrometer. Therefore, while fibers do not remove all the problems of high resolution spectroscopy, they certainly improve the situation.

Mounting and Handling

The final problem involves the difficulty of actually aligning and centering the fiber, the ball lens and a field stop on the end of a thin positioning probe and maintaining this alignment in the telescope environment. In principle this is possible, but in practice may prove very difficult, or at least time consuming. The problem is demonstrated by trying to pick up a 1/32-inch diameter sapphire ball while keeping

its optical surface clean. Fortunately 1 - 2 mm diameter balls will do for many applications. With all microlens methods, there may be a crowding problem if many multiple lensed fibers are used at the spectrograph slit. The solution to the slit crowding problem is to use several parallel rows of fibers to produce interlaced spectra. The diameter of the microlenses also causes crowding for closely spaced objects in the focal plane as discussed in chapter 5. These lens reimaging techniques were not practical with the Medusa aperture plate spectrograph, because the fibers were constantly being changed from one aperture plate to the next. The MX and other permanently mounted fiber systems can take advantage of more complicated lens reimaging techniques. King (1955) describes an interesting historical precedent, where William Herschel used a 1/45-inch glass bead in a high power eyepiece for his 40-foot telescope.

It appears that the MX multiobject spectrometer may use 2 - 3 arcsecond apertures with bare fibers during its initial operation since it will be observing faint galaxies with an f/9 spectrograph. Focal ratio degradation may limit the speed gains with current spectrograph optics, but this may be offset by earlier scientific results at the telescope. The MX and other fiber systems must keep their options open for future lensed fibers and for the option of having multiple sets of fibers and slit assemblies to allow aperture choice to match observing conditions. This is reasonable because fibers and microlenses are very much less expensive than other parts of the telescope-spectrograph-detector combination. Seeing matching will also become more important as fiber quality and telescope images improve. Lenses are still highly

useful for matching systems where a suitable bare fiber is unavailable. A compromise between the two microlens matching schemes may involve using a lens to image the pupil on the input end of the fiber with no output lens. This allows optimum input matching to preserve the $A\Omega$ product while retaining the perfect image scrambling of the bare fiber. The spectrograph f/ratio and fiber diameter are now chosen for efficient coupling and the lens focal length is chosen for optimum f/ratio in the fiber. A prime focus coupled fiber may conversely only require a pupil-imaging lens at the output of the fiber into the spectrograph. In cases where a fast beam must be slowed before entering the fiber or made faster on exiting the fiber, the pupil-imaging technique is the only practical microlens solution.

CHAPTER 9

CONCLUSION

The Medusa fiber optic spectrograph and its descendants have started a major revolution in astronomical spectroscopy. Spectroscopic observations of less than a dozen objects simultaneously will soon be considered wasteful of telescope time. Medusa was not an operationally or optically optimized system and can be improved in many ways. A major improvement which the MX Spectrometer will make over Medusa is the transition from a prototype instrument, with its attendant masses of duct tape, 5-minute epoxy, cereal boxes, and baling wire; to a versatile, high quality, research instrument available to the general user.

Completion of MX

Better quality optical fibers with less focal ratio degradation will roughly double the optical throughput of the spectrometer. Additional optical gains will be made by MX with improvements to the spectrograph camera and detector system. Aside from optical throughput, the single most important factor for MX performance is the development of the mobile fiber positioner probes. The mobility of the probes provides greater flexibility of the observing program and more rapid changeover between target fields than Medusa offered. The rapid change between target fields allows better use of observing time since the program can be changed to suit prevailing sky conditions. The probes

under computer control can be reconfigured to the the next target field in less time than an aperture plate could be exchanged. Change of target fields will usually be completed while the telescope is slewing to the next position. Motions of individual probes also allow fine tuning of positions of target objects while observing. Construction of the positioner probes and the associated electronics is now in progress. When the MX Spectrometer is completed, in late 1984, it will demonstrate that the mechanical, optical, and computer problems encountered in multiple object spectroscopy are tractable. I have shown that fiber positioning probes can be economically constructed to meet the desired position tolerances for fibers in the focal plane. The computer problems involved in controlling MX, collecting the data, and reducing the data look smaller each year as computer technology advances. I expect similar multiple fiber devices to be constructed at all major optical telescopes. Indeed, "galaxy fishing" may become a very popular sport in America and around the world. The benefit or penalty of building an instrument 20 times more efficient than its predecessors is that enormous quantities of data are produced. Work must continue on the data reduction process to make it as streamlined as the collection of the data with MX.

Observational Challenges

There are many problems in astronomy well-suited to study by multiple object spectroscopy. In the next year or so, I plan to begin an extensive survey of clusters of galaxies and their environment. The program will involve measuring hundreds of redshifts in selected

clusters. This large sample of cluster redshifts can help answer questions regarding cluster dynamics. Specifically, it will give accurate cluster redshifts and velocity dispersions. We will also get a first look at gradients in the line-of-sight velocity dispersion and at the correlation of the dispersion with x-ray luminosity and other features. If the dispersion of galaxies in clumps inside rich clusters is different from the clusters as a whole, the size scale of the missing mass may be pinned down. Measurements around cD galaxies may provide insight into their formation. Many redshifts in rich clusters and in the "field" will provide data on supercluster structure and dynamics. In retrospect, the mistake we made with Medusa was spending a lot of time studying faint clusters while assuming that nearby clusters were "well studied". Finally, it appears that using MX to survey "everything" to a given limiting magnitude in selected fields would be useful. This study will probably coincide with part of the CTI Survey strip around the sky. Only in recent years have galaxy surveys begun to use both projected positions and velocities to study the large scale structure of the universe. Stellar spectra which would be collected in such a survey should contribute to our knowledge of the halo of our Galaxy with respect to its extent and its chemical composition. Quasar spectra from such a survey would provide information on selection effects in other optical surveys. The ability to collect 32 spectra simultaneously should serve MX well in carrying out such a survey.

Future Fiber Instruments

Given the enormous increase in data-taking efficiency that a multiple fiber spectrograph provides, it seems clear that nearly every large telescope will have one sooner or later. This influences the design of new telescopes by placing added importance on having a wide-field (1 degree) focus with excellent image quality. Spectroscopic throughput on non-clustered objects like QSOs goes up directly with the area of the field of view on the sky. Multiple object spectroscopy has in fact been listed as the first scientific priority by the committee studying the possible designs for the National New Technology Telescope (NNTT) (Gehrtz, et al., 1984). A multiple fiber spectrograph can be operated at a number of foci, depending primarily on the local mechanical and optical constraints. Some likely candidates are: 1) a Ritchey-Chrètien or other wide-field setup at a Cassegrain or Nasmyth position; 2) a corrected prime focus, currently used for direct imaging on most 4m class telescopes; 3) a Paul-Baker two-mirror corrector which can be used as a module dedicated to wide-field imaging and spectroscopy. See Woolf, et al. (1982) and Angel, Woolf, and Epps (1982) for a possible Paul-Baker setup in a 15m MMT. The f/ratio of a telescope is not critical because microlenses can be used on each fiber to give the f/ratio needed for optimum propagation. Fibers will also eliminate the need for Coudè optics for all but a few specialized systems working in the ultraviolet. The high transmission of fibers allows single or multiple object feeds to all kinds of instruments from low dispersion spectrographs to massive Coudè spectrographs. It is important to note that fibers do not eliminate the need for large high

resolution spectrographs, they just make getting there easier. It is possible that future telescopes will not require a conventional single-slit Cassegrain spectrograph at all since nearly all optical spectroscopic problems can be handled by fiber coupled floor-mounted spectrographs or by two-dimensional imaging spectrometers based on a Fabry-Perot etalon. The TAURUS and CIGALE instruments have demonstrated the capability of high throughput - high resolution spectroscopy with a scanning Fabry-Perot spectrophotometer. Astronomers who really like data reduction may wish to imagine a multiple fiber feed on a large telescope linked to an array of 25 or so echelle spectrographs, each with its own two-dimensional detector! Because of the high transmission and therefore low emissivity of fibers, multiple object spectroscopy in the near infrared, 0.7 - 2 microns, should be possible once two-dimensional infrared arrays become available (see McCreight and Goebel, 1982). The dominant problem at the long wavelength end of the near infrared appears to be proper cold baffling at the input and output ends of the fibers. High resolution spectroscopy in the thermal infrared (longward of 2.5 microns) may still require a Nasmyth spectrograph. Fiber-coupled spectrographs may also be used in space, although the lack of ultraviolet transmission becomes an impairment in the general purpose spectrograph because the atmosphere no longer provides a natural cutoff just below that of the fiber. More exotic possibilities for fiber spectroscopy include having tracking fibers in the focal plane of a very large transit instrument. See Angel (1982b), McGraw, et al. (1982), and Shectman (1983a) for a description of this type of instrument. These fibers would collect spectra from an object

for up to an hour as it crossed the meridian. An extension of this concept to give engineers nightmares would have clusters of fibers in an MX-like configuration tracking clusters of very faint galaxies in the focal plane of a 20+ meter spherical mirror (MIRV'd fibers?).

In summary, I see single and multiple object fiber optic spectroscopy growing into an important observational tool. Development programs involving fibers have started at almost every major optical observatory. The multiplex advantage of fiber spectroscopy adds enormous capability to the data collecting potential of present and future large telescopes.

LIST OF REFERENCES

Aaronson, M. 1983, Ap.J.Lett., **266**, L11.

Adams, M. T. 1981, Ph.D. Dissertation, University of Arizona.

Allen, C. W. 1976, Astrophysical Quantities (London: Athlone Press), p126.

Allen, R. G., Cromwell, R. H., Liebert, J. W., Macklin, R. H., and Stockman, H. S. 1983, Proc. S.P.I.E., **445**, 168.

Angel, J. R. P. 1982a, Nature, **295**, 651.

_____ 1982b, IAU Coll. #67, Instrumentation with Large Optical Telescopes, ed. C. M. Humphries, p117.

Angel, J. R. P. 1983, IAU Coll. #83, Astronomy with Schmidt-Type Telescopes, in press.

Angel, J. R. P., Adams, M. T., Boroson, T. A., and Moore, R. L. 1977, Ap.J., **218**, 776.

Angel, J. R. P., and Hill, J. M. 1982, Proc. S.P.I.E., **332**, 298.

Angel, J. R. P., and Hill, J. M. 1983, Proc. S.P.I.E., **444**, 184.

Angel, J. R. P., and Woolf, N. J. 1983, Proc. XI Texas Symposium on Relativistic Astrophysics, D. Evans, ed., in press.

Angel, J. R. P., Woolf, N. J., and Epps, H. W. 1982, Proc. S.P.I.E., **332**, 134.

Arganbright, D. 1984, (Steward Observatory) in preparation.

Bahcall, N. A. 1977, Ann.Rev.Astr.Ap., **15**, 305.

Bahcall, N. A. 1984, Bull.AAS (abstract), **15**, 946.

Barden, S. C. 1983, Master's Thesis, Penn State University

Barden, S. C., Ramsey, L. W., and Truax, R. J. 1981, Pub.A.S.P., **93**, 154.

Barden, S. C., Staver, R. P., and Ramsey, L. W. 1984, in preparation.

Barr, L. D., and Mack, B., eds. 1983, Advanced Technology Optical Telescopes II, Proc. S.P.I.E., **444**.

Batuski, D. J., and Burns, J. O. 1984, Bull.AAS (abstract), **15**, 946.

Beckers, J. M., Hege, E. K., and Murphy, H. P. 1983, Proc. S.P.I.E., **445**, 462.

Beers, T. C., and Geller, M. J. 1983, Ap.J., **274**, 491.

Beers, T. C., Geller, M. J., and Huchra, J. P. 1982, Ap.J., **257**, 23.

Beers, T. C., Huchra, J. P., and Geller, M. J. 1983, Ap.J., **264**, 356.

Bessel, M. S. 1979, Pub.A.S.P., **91**, 603.

Bingham, R. G. 1979, Quart.J.R.A.S., **20**, 395.

_____ 1983a, private communication.

_____ 1983b, Proc. S.P.I.E., **369**, 303.

Birkinshaw, M. 1979, M.N.R.A.S., **187**, 847.

Birkinshaw, M., and Gull, S. F. 1984, M.N.R.A.S., **206**, 359.

Birkinshaw, M., Gull, S., and Northover, K. 1978, M.N.R.A.S., **185**, 245.

Bothun, G. D. 1981, Thesis, University of Washington.

Bothun, G. D., Geller, M. J., Beers, T. C., and Huchra, J. P. 1983, Ap.J., **268**, 47.

Brodie, J. P., and Hanes, D. A. 1981, IAU Coll. #68, Astrophysical Parameters for Globular Clusters, eds. A. G. D. Philip and D. S. Hayes, p381.

Burbidge, G., and Barr, L. D., eds. 1982, Advanced Technology Optical Telescopes I, Proc. S.P.I.E., **332**.

Butcher, H. 1982, Proc. S.P.I.E., **331**, 296.

Butcher, H. and Oemler, A. 1978, Ap.J., **219**, 18.

_____ 1984, Ap.J., submitted.

Capelato, H. V., Gerbal, D., Mathez, G., Mazure, A., and Salvador-Solè, E. 1982, Ap.J., **252**, 433.

Chincarini, G. 1983, IAU Symp. #104, Early Evolution of the Universe..., eds. G. O. Abell and G. Chincarini, p159.

Ciardullo, R., Ford, H., Bartko, F., and Harms, R. 1983, Ap.J., **273**, 24.

Cohen, J. G. 1983, Ap.J.Lett., **270**, L41.

Cook, K., Schecter, P., and Aaronson, M. 1984, Bull.AAS (abstract), **15**, 907.

Cromwell, R. H. 1984, private communication.

Danese, L., DeZotti, G., and diTullio, G. 1980, Astr.Ap., **82**, 322.

Davis, M., Huchra, J., Latham, D. W., and Tonry, J. 1982, Ap.J., **253**, 423.

Dressler, A. 1980a, Ap.J., **236**, 351.

_____ 1980b, Ap.J.Suppl., **42**, 565.

_____ 1984, Astr.Ap., in press.

Dressler, A., and Gunn, J. E. 1983, Ap.J., **270**, 7.

Eisenhardt, P. R. M. 1982, Proc. S.P.I.E., **331**, 434.

Eisenhardt, P. R. M. 1984, Ph.D. Dissertation, University of Arizona, in preparation.

Ellis, R. S. 1983, IAU Symp. #104, Early Evolution of the Universe..., eds. G. O. Abell and G. Chincarini, p87.

Ellis, R. S, Gray, P. M., Carter, D., and Godwin, J. 1984, M.N.R.A.S., **206**, 285.

Ellis, R. S., and Parry, I. 1983, private communication.

Enard, D. 1983, Proc. of the Workshop on ESO's Very Large Telescope, (Caragèse), p89.

Faber, S. M., and Gallagher, J. S. 1979, Ann.Rev.Astr.Ap., **17**, 135.

Forman, W., Bechtold, J., Blair, W., Giacconi, R., Van Speybroeck, L., Jones, C. 1981, Ap.J.Lett., **243**, L133.

Forman, W., and Jones, C. 1982, Ann.Rev.Astr.Ap., **20**, 547.

Fuchs, B., and Materne, J. 1982, Astr.Ap., **113**, 85.

Gambling, W. A., Payne, D. N., and Matsumura, H. 1975, Appl. Optics, **14**, 1538.

Gehrtz, R., et al. 1984, Report of NNTT Scientific Advisory Comm., in preparation.

Grainger, J. F.. 1981, Observatory, **101**, 140.

Gray, P. M. 1983a, Proc. S.P.I.E., **374**, in press.

Gray, P. M. 1983b, Proc. S.P.I.E., **445**, 57.

Gregory, S. A., and Thompson, L. A. 1982, Scientific American, **246**, #3, p106.

Griffiths, R. E., et al. 1983, Ap.J., **269**, 375.

Gunn, J. E., and Griffin, R. F. 1979, A.J., **84**, 752.

Gustafsson, B. 1983, Highlights Astr., **Vol.** 6, ed. R. M. West (IAU - D.Reidel) p. 101.

Hall, D. N. B., ed. 1982, IAU Commission 44, The Space Telescope Observatory (NASA, CP-2244).

Hanes, D., and Madore, B., eds. 1978, Proc. NATO Adv. Study Inst. on Globular Clusters (Cambridge Univ. Press).

Harris, H. C., and McClure, R. D. 1983, Ap.J.Lett., **265**, L77.

Heacox, W. 1980, Optical and Infrared Telescopes of the 1990's, ed. A. Hewitt (Tucson: KPNO), p702.

_____ 1983, private communication.

Henry, J. P., Henricksen, M. J., Charles, P. A., and Thorstensen, J. R. 1981, Ap.J.Lett., **243**, L137.

Herskowitz, G. J., Kobrinski, H., and Levy, U. 1983, Laser Focus, **Feb.**, p83.

Hesser, J. E., ed. 1979, IAU Symp. #85, Star Clusters (IAU - D. Reidel).

Hewitt, A., ed. 1980, Optical and Infrared Telescopes for the 1990's (Tucson: KPNO).

Hill, J. M., and Angel, J. R. P. 1983, Proc. S.P.I.E., **380**, 100.

Hill, J. M., Angel, J. R. P., and Richardson, E. H. 1983, Proc. S.P.I.E., **445**, 85.

Hill, J. M., Angel, J. R. P., and Scott, J. S. 1983, Proc. S.P.I.E., **380**, 354.

Hill, J. M., Angel, J. R. P., Scott, J. S., Lindley, D., and Hintzen, P. 1980a, Optical and Infrared Telescopes of the 1990's, ed. A. Hewitt (Tucson: KPNO), p370.

Hill, J. M., Angel, J. R. P., Scott, J. S., Lindley, D., and Hintzen, P. 1980b, Ap.J.Lett., **242**, L69.

Hill, J. M., Angel, J. R. P., Scott, J. S., Lindley, D., and Hintzen, P. 1982, Proc. S.P.I.E., **331**, 279.

Hill, J. M., Eisenhamer, J., Silva, D. R., and Wenz, M. 1984, in preparation.

Hintzen, P. 1984, Ap.J.Suppl., in press.

Hintzen, P., Hill, J. M., Lindley, D., Scott, J. S., and Angel, J. R. P. 1982, A.J., **87**, 1656.

Hintzen, P., and Scott, J. S. 1979, Ap.J.Lett., **232**, L145.

Hubbard, E. N., Angel, J. R. P., and Gresham, M. S. 1979, Ap.J., **229**, 1074.

Huchra, J., Davis, M., Latham, D., and Tonry, J. 1983, Ap.J.Suppl., **52**, 89.

Hunter, G. M., and Steiglitz, K. 1979, IEEE Trans. on Pattern Anal. and Mach. Intelligence, **PAMI-1**, 45.

Iga, K., Oikawa, M., and Banno, J. 1982, Appl. Optics, **21**, 3451.

Jeunhomme, L., and Pocholle, J. P. 1975, Electronics Lett., **11**, 425.

Johnson, H. L. 1966, Ann.Rev.Astr.Ap., **4**, 193.

Jones, C., and Forman, W. 1984, Ap.J., **276**, 38.

Kibblewhite, E. 1983, Automated Photographic Measuring System (SERC).

King, H. C. 1955, History of the Telescope (New York: Dover), p139.

Kirshner, R. P., Oemler, A., Schecter, P. L., and Shectman, S. A. 1981, Ap.J.Lett., **248**, L57.

_____ 1983, A.J., **88**, 1285.

Koo, D. 1983, IAU Symp. #104, Early Evolution of the Universe..., eds. G. O. Abell and G. Chincarini, p105.

Labeyrie, A. 1970, Astr.Ap., **6**, 85.

_____ 1978, Ann.Rev.Astr.Ap., **16**, 77.

Lasenby, A. N., and Davies, R. D. 1982, M.N.R.A.S., **203**, 1137.

Lesser, M. 1983, private communication.

Lindley, D. A. 1983, (Steward Observatory), unpublished.

Longair, M. S., and Warner, J. W., eds. 1979, IAU Colloquium #54, Scientific Research with the Space Telescope (USGPO).

Lund, G., and Enard, D. 1983, Proc. S.P.I.E., **445**, 65.

Marcuse, D. 1981, Principles of Optical Fiber Measurements (New York: Academic Press).

Malumuth, E. M., and Richstone, D. O. 1984, Ap.J., **276**, 413.

Materne, J., and Fuchs, B. 1982, European Colloquium on Clusters of Galaxies (Meudon, Oct 1982).

McCreight, C. R., and Goebel, J. H. 1982, Proc. S.P.I.E., **331**, 9.

McGraw, J. T., Stockman, H. S., Angel, J. R. P., Epps, H., and Williams, J. T. 1982, Proc. S.P.I.E., **331**, 137.

McKee, J. D., Mushotsky, R. F., Boldt, E. A., Holt, S. S., Marshall, F., Pravdo, S. H., and Serlemitsos, P. J. 1980, Ap.J., **242**, 843.

McMillan, R., et al. 1984, J.Opt.Soc.Am., **74**, in press.

Meaburn, J. 1970, J.Ap.Space Sci., **9**, 206.

Meinel, A. B. 1979, Proc. S.P.I.E., **172**, 2.

Melnick, J., and Sargent, W. L. W. 1977, Ap.J., **215**, 401.

Merritt, D. 1984, Ap.J., **276**, 26.

Midwinter, J. E. 1979, Optical Fibers for Transmission (New York: John Wiley & Sons).

Miller, R. H. 1983, Ap.J., **270**, 390.

Miller, S. E., and Chynoweth, A. G. 1979, Optical Fiber Telecommunications (New York: Academic Press).

Mould, J. R. 1983, Highlights Astr., **Vol. 6**, ed. R. M. West (IAU - D. Reidel), p179.

Nicia, A. 1981, Appl. Optics, **20**, 3136.

Noonan, T. W. 1981, Ap.J.Suppl., **45**, 613.

Oemler, A. 1974, Ap.J., **194**, 1.

Oort, J. H. 1983, Ann.Rev.Astr.Ap., **21**, 373.

Osmer, P. S., and Smith, M. G. 1980, Ap.J.Suppl., **42**, 333.

Pagrazio, M. 1983, Return of the Jedi magazine, official collector's edition (Newtown, CT: Lucasfilm - Paradise Press), p57.

Philip, A. G. D., and Hayes, D. S., eds. 1981, IAU Coll. #68, Astrophysical Parameters for Globular Clusters (Schenectady: L. Davis Press Inc.).

Pilachowski, C. A., Bothun, G. D., Olszewski, E. W., and Odell, A. 1983, Ap.J., **273**, 187.

Postman, M., and Geller, M. J. 1984, Ap.J., submitted.

Powell, J. R. 1983, Proc. S.P.I.E., **445**, 77.

Pravdo, S. H., Boldt, E. A., Marshall, F. E., McKee, J., Mushotzky, R. F., Smith, B. W., and Reichert, G. 1979, Ap.J., **234**, 1.

Quintana, H., and Melnick, J. 1982, A.J., **87**, 972.

Rivolo, A. R., and Yahil, A. 1983, Ap.J., **274**, 474.

Ritchey, G. W. 1928, J.R.A.S.Canada, **22**, 303.

Robson, E. I., and Grainger, J. F. 1983, J.Brit.Astr.Assn., **93**, 75.

Rothenflug, R., Vigroux, L., Mushotzky, R. F., and Holt, S. S. 1983, ApJ., (NASA tech memo #85103), in press.

Sarazin, C. L., Rood, H. J., and Struble, M. F. 1982, Astr.Ap., **108**, L7.

Schiffer, J. G. V. 1983, Proc. S.P.I.E., **445**, 52.

Schiffer, J. G., Appenzeller, I., and Ostreicher, R. 1982, Mitt. Astron. Ges., **57**, 323.

Schmidt, M., and Green, R. F. 1983, Ap.J., **269**, 352.

Shanks, T., Bean, A. J., Efstathiou, G., Ellis, R. S., Fong, R., and Peterson, B. A. 1983, Ap.J., **274**, 529.

Shectman, S. A. 1983a, Proc. S.P.I.E., **444**, 106.

_____ 1983b, Proc. S.P.I.E., **445**, 128.

Silk, J., and Wilson, M. L. 1979a, Ap.J., **228**, 641.

_____ 1979b, Ap.J., **233**, 769.

Smith, H., Hintzen, P., Holman, G., Oegerle, W., Scott, J., and Sofia, S. 1980, Ap.J.Lett., **234**, L97.

Slipher, V. M. 1921, New York Times, January 19.

Spinrad, H., Stauffer, J., and Butcher, H. 1981, Ap.J., **244**, 382.

Stauffer, J. R., Hartmann, L., Soderblom, D. R., and Burnham, N. 1983, CFA preprint.

Stobie, R. S., and McInnes, B., eds. 1982, Occ. Rep. R.O.E., Proc. Wkshp. Astr. Measuring Mach..

Stocke, J. T., Liebert, J., Gioia, I. M., Griffiths, R. E., Maccacaro, T., Danziger, I. J., Kunth, D., and Lub, J. 1983, Ap.J., **273**, 458.

Struble, M. F., and Rood, H. J. 1981, Ap.J., **251**, 471.

Tarenghi, M., Tifft, W. G., Chincarini, G., Rood, H. J., and Thompson, L. A. 1979, Ap.J., **234**, 793.

Tifft, W. G., and Gregory, S. A. 1976, Ap.J., **205**, 696.

Thomlinson, W. J. 1980, Appl. Optics, **19**, 1117,1127.

Thompson, L. A., and Gregory, S. A. 1983, IAU Symp. #104, Early Evolution of the Universe..., eds. G. O. Abell and G. Chincarini, p291.

Timothy, J. G. 1983, Pub.A.S.P., **95**, 810.

Tubbs, E. F., Goss, W. C., and Cohen, J. C. 1982, Proc. S.P.I.E., **331**, 289.

Van den Bergh, S. 1977, Vistas in Astronomy, **21**, 77.

Watson, F. G. 1984, M.N.R.A.S, **206**, 661.

White, S. D. M. 1976, M.N.R.A.S., **177**, 717.

White, S. D. M., and Silk, J. 1980, Ap.J., **241**, 864.

Woolf, N. J. 1982, Ann.Rev.Astr.Ap., **20**, 367.

Woolf, N. J., and Angel, J. R. P. 1980, Optical and Infrared Telescopes for the 1990's, ed. A. Hewitt (Tucson: KPNO), p1062.

Woolf, N. J., Angel, J. R. P., Antebi, J., Carleton, N., and Barr, L. D. 1982, Proc. S.P.I.E., **332**, 79.

Young, E. et al. 1984, Ap.J.Lett., **278**, L75.